Spring 2018

Laser foil printing and surface polishing processes

Chen Chen

Department: Mechanical and Aerospace Engineering

LASER FOIL PRINTING AND SURFACE POLISHING PROCESSES

by

CHEN CHEN

A DISSERTATION

Presented to the Faculty of the Graduate School of the

MISSOURI UNIVERSITY OF SCIENCE AND TECHNOLOGY

In Partial Fulfillment of the Requirements for the Degree

DOCTOR OF PHILOSOPHY

in

MECHANICAL ENGINEERING

2018

Approved by:

Dr. Hai-Lung Tsai, Advisor

Dr. Kelly Homan

Dr. Edward Kinzel

Dr. Heng Pan

Dr. John G. Story

PUBLICATION DISSERTATION OPTION

This dissertation has been prepared in the style utilized by the Missouri University of Science & Technology in the form of four journal papers. The papers will be referred to by their Roman numerals. The papers are printed as the university format. The list of journal publications appended to this dissertation is given below:

Paper I, on pages 10-34, has been published in *Journal of Manufacturing Science and Technology*.

Paper II, on pages 35-69, has been submitted to *International Journal of Machine Tools and Manufacture*.

Paper III, on pages 70-98, has been submitted to *Journal of Manufacturing Science and Technology*.

Paper IV, on pages 99-129, has been submitted to *Optics and Lasers in Engineering.*

ABSTRACT

A foil-based additive manufacturing technology for fabricating metal parts, called Laser Foil Printing (LFP), was proposed and developed in this dissertation. The manufacturing sub-processes comprising the LFP technology were comprehensively studied, which include the laser spot welding of foil, laser raster-scan welding of foil, laser cutting of foil, and laser polishing processes. The fabricated free-form parts were demonstrated and own better mechanical properties (micro hardness and tensile strength) than the raw material, because of the rapid-cooling process of laser welding. The full and strong bond between layers was formed by the laser welding process, with no micro-cracks or pores observed. The clean and accurate cutting edges were produced by the laser cutting process, with no burr or thermal distortion. The study of laser polishing shows that the width and depth of polished track have significant impacts on the polishing capability. The numerical analysis of laser polishing process shows that the convection flow in the melting pool can deepen the polished track. Three different scan paths were studied to polish the side surface of LFP parts. The finally resulted side surface roughness can be reduced to 0.72 μm in Sa, for both the vertical side surface (with the initial surface roughness of 4.39 μm) and the 45º-inclined side surface (with the initial roughness of 24.22 μm). And the foil bonding defects on the side surface can be completely repaired in the post-processing of laser polishing. Finally, the bulge structure along polished track was noticed in the experiments and studied on Ti-6Al-4V slabs. The spatial spectra analysis shows that the overlapping process of polished tracks can effectively reduce the induced bulge structures.

ACKNOWLEDGMENTS

I would like to thank my advisor, Dr. Hai-Lung Tsai, for providing me with the opportunity to work on this project. I admire his hard work and enthusiasm towards research, which inspired me to pursue a career as a researcher. Further, I thank the Department of Energy's Office of Fossil Fuels, Honeywell Inc., and Intelligent Systems Center (ISC) at Missouri S&T for providing financial support at various stages of my Ph.D. study.

I would like to also thank my committee members, Dr. Kelly Homan, Dr. Edward Kinzel, Dr. Heng Pan, and Dr. John G. Story, for their insightful comments and time commitment. Furthermore, I would also like to thank the Department of Mechanical and Aerospace Engineering for this educational opportunity.

I would like to express my deep thanks to my lab mates, Cheng-Hsiang Lin, Yiyu Shen, Yingqi Li, Chia-Hung Hung, and Chien-Yu Lo, for their support during my Ph.D. study in Rolla.

Finally, I would like to dedicate this work to my parents and my brother, for their emotional support and unconditional love and sacrifices.

TABLE OF CONTENTS

SECTION

LIST OF ILLUSTRATIONS

Page

PAPER I

PAPER II

LIST OF TABLES

Page

PAPER II

PAPER IV

SECTION

1. INTRODUCTION

1.1. ADDITIVE MANUFACTURING FOR METAL PARTS

Additive manufacturing (AM) refers to the processes of building three-dimensional (3D) objects by adding layer-upon-layer of material, and the material forming in each layer is directed by 3D digital model data [1]. Since the commercialization of the first machine for AM in 1987 [2], AM technologies have been developed and improved rapidly in recent 30 years, and received wide attention in both academic and industrial fields [3, 4]. To date, many specific AM technologies have been developed and commercialized, such as stereolithography (SL), laminated object manufacturing (LOM), selective laser sintering (SLS), laser-engineered net shaping (LENS), direct metal deposition (DMD), ultrasonic consolidation (UC), fused deposition modeling (FDM) and selective laser melting (SLM). According to the form of feedstock, most AM processes can fit into three categories: photopolymer-based technologies (SL), powder-based technologies (SLS, LENS, DMD, SLM), foil/sheet-based technologies (LOM, UC) and wire/extrusion-based technologies (FDM).

The above-mentioned AM technologies which are applicable to metal parts, mainly include SLS, SLM, DMD, LENS, LOM, and UC. SLS and SLM are the very popular AM processes of metal parts currently [5], and they are both powder bed fusion processes. During the manufacturing process of each layer, the metallic powder is fed in a powder bed, and the powder of specific regions is sintered or fully fused by the energy from laser beam. This process recurs layer by layer according the design of 3D models. For LENS

and DMD processes [6], a part is fabricated by focusing a high-power laser beam onto a substrate to create a molten pool in which the metal powder particles are injected to build each layer. These processes can be used to repair parts, and the composition of powder can be changed from one location to others during the processing to make products with varied compositions which could lead to the possibility of fabricating functional graded parts. LOM and UC are the foil/sheet-based processes where sheets can be either form-then-bond or bond-then-form [7]. Initially, LOM involves layer-by-layer lamination of paper material sheets, cut using a CO2 laser, each sheet representing one cross-sectional layer of the CAD model of the part. Later, some variants [8-12] of LOM can build metal part through thermal bonding (diffusion bonding, brazing or laser spot-welding process). UC is a hybrid sheet lamination process combining ultrasonic metal seam welding and CNC machining [13, 14].

In this proposed research, a new foil-based AM technology, Laser Foil Printing (LFP), will be developed, which employs the foil laser welding process and the foil laser cutting process. And the reason for choosing metal foils as feedstock instead of metal powders is some inevitable drawbacks from powder particles. The drawbacks in powder based AM processes include:

(1) Micro- or nano-size powder particles have potential health hazards to operators and environments.

(2) The metal particles are quite active, and the cost of equipment and maintenance of power-based AM machines is very high.

(3) Metal powders are much more expensive than metal foils, and many powders are patented and machine-specific.

1.2. LASER POLISHING IN AM PROCESSES

Although foil-based AM processes have some advantages, such as low-cost and flexibility, over powder-based AM processes, they also have some obvious drawbacks such as the difficulty in automation and the interfacial defects [15]. Here we focus on how to reduce and eliminate the interfacial defects. In the layer-bonding process of most AM processes, the resulted top surface of bonded layer cannot be as smooth as the initial substrate. And the rough top-surface could cause interfacial defects for the next-layer bonding process in the foil-based AM, but does not cause problems in powder-based AM processes. For example, in the ultrasonic consolidation process, Janaki [16] and Stucker [17] found that surface roughness is an important factor for inducing interfacial defects or unbounded area and that the surface roughness reduction process can improve the interfacial bonding quality and result in higher-strength end-products.

In the proposed LFP process, the problem of interfacial defects is also concerned. The bonding process in LFP is carried out by the raster-scan laser welding, and the welding process is conducted in the keyhole penetration mode. Generally, there are two different heating modes in laser welding processes, the conduction mode and keyhole mode. And in the keyhole mode [18], the power density is great enough that the metal goes beyond just melting. It evaporates intensely, and the vaporized material creates a rapidly expanding gas-flow that pushes outward. The recoil effect of expanding vapor creates a keyhole down to the depth of the weld, and produces a typically deep and narrow weld. Due to the nature of keyhole mode, the laser welding process applied in LFP can withstand some micro gaps between the fresh foil and the bonded foil and achieve a decent bonding quality.

However, the top surface of keyhole-mode welds is not very smooth, and the overlap of weld tracks in the raster-scan process further increases the surface roughness.

And the surface roughness is measured around 4 μm in Ra (arithmetic mean roughness). And it is found in experiments that the surface quality and bonding quality gradually get worse in the welding process of subsequent layers if no additional measure of surface roughness reduction was applied. Finally, the raster-scan welding process would get unstable and fail in some area after several layers. Therefore, in the proposed research, the laser macro polishing process should be studied and applied in order to suppress and control the roughness of the raster-scan weld surface in LFP.

Laser polishing (LP) is a relatively new method used for eliminating surface roughness and polishing surfaces for materials including glass, lens, fiber, diamond, and metals [19-24]. During a laser polishing process, a thin surface layer is molten and the surface tension leads to a material flow from peaks to valleys. As a result, the surface asperities are evened out, surface peak-valley heights are reduced, and the surface quality gets improved. Laser polishing has two sub-variants: laser macro polishing and laser micro polishing [25]. Generally, macro polishing is used to remove large surface structures from milling, turning, or EDM, and micro polishing is used to remove the finer micro roughness and leads to a high gloss level [26]. Usually macro polishing is carried out with a continuous-wave (CW) laser, while micro polishing is carried out with a pulsed laser radiation.

In the field of AM, the surface finish of fabricated parts is an important issue that affects the industrial application of AM technologies. However, only a few studies have been reported on laser polishing processes in AM. Ramos et al. [22] polished SLS fabricated metal parts and achieved a roughness reduction up to 37% of the original Ra value with a laser energy density ranged between ~ 250 and 580 J/cm2 (CO2 laser).

Lamikiz et al. [27] polished SLS parts and achieved a surface roughness reduction up to 80%, resulting in polished surfaces of 1.49 μm in Ra. Dadbakhsh et al. [28] polished LENS manufactured parts, and achieved a surface roughness reduction of about 80% with the resulted surface roughness of 2 μm in Ra. Rosa et al. [29] studied the laser polishing of LENS topographies of complex and thin geometries, and achieved a surface roughness reduction up to 62% with a final surface roughness of 5.39 μm in Sa (areal surface roughness). However, most of the previous LP studies are based on statistical models using Design of Experiments (DoE), but did not analyze and discuss the underlying physical processes in LP.

1.3. POST-PROCESSING OF THE SIDE SURFACE OF AM FABRICATED PARTS

Post-processing is an important step in most AM processes after the part building in order to prepare the part for its intended form, fit and function [15]. Depending on the specific AM technology, post-processes may include support material removal, surface texture improvement, property enhancements, etc. For the proposed LFP technology, the post-processes of smoothing the stair-steps and improving the foil bonding quality on side surfaces could be very helpful and necessary to the fabricated parts. Note the stair-stepping is a fundamental issue in layered manufacturing processes, although one can choose a thin layer thickness to minimize error at the expense of build time.

Yasa et al. [30] determined the relationship between stair-step effect and the surface inclination for the nickel-based alloy parts built with direct metal laser sintering. And they found that the laser remelting process can significantly increase the density of SLM parts to almost 100 percent and enhance the surface quality up to 90 percent, but the process

parameters of remelting affect the results significantly [31]. Alfieri et al. [32] evaluated the post-process treating via laser surface modification to process metal parts resulted from SLM in order to improve surface topography. It was shown that the laser-scan strategy of beam wobbling has a better performance than the linear scan, as the heat effects in the base metal are proven to be lower.

1.4. FUNDAMENTAL STUDY OF LASER POLISHING PROCESS

Basically, surface tension plays a major role in laser polishing processes to remove the surface asperities. But laser polishing is a complicated process, and many factors are involved to determine the final polished surface quality, including initial surface condition, workpiece thermal and optical properties, laser power, scan speed, beam spot size, beam shape, overlapping percentage, number of passes, etc.

Ramos [22] defined two surface polishing regimes, shallow surface melting (SSM) and surface over melting (SOM), based on the depth of the molten layer. In the regime of SSM, the thickness of the melted layer is less than the peak-to-valley height of the typical surface asperities, and the molten material flows from the peaks to the local valleys under the capillary pressure. In the regime of SOM, the thickness of the melted layer is greater than the peak-to-valley height of asperities, then the original surface topography may completely disappear and a continuously moving melting pool is created. Similarly, Pfefferkorn et al. [33, 34] studied the laser micro polishing process with pulsed lasers and found two different polishing regimes, capillary and thermos-capillary, depending on the pulse duration used. Besides, the laser polishing process not only reduce the initial surface roughness, but also introduce some new surface microstructures. Nusser [35] et al. studied

the process- and material-induced surface structures during laser macro polishing, which include ripples, undercuts, bulges, step structures and martensitic needles.

In our experimental study of laser polishing, it was found the bulge structure produced along the polished tracks has an important impact on the final resulted surface quality. Therefore, a fundamental study on the bulge structure will be carried out.

1.5. RESEARCH OBJECTIVES

The current research aims at the development of a new AM technology, Laser Foil Printing (LFP), which includes the procedure design, the optimization of processing parameters, the study of the mechanical properties of fabricated parts and the improvement of surface qualities. A combined experimental and numerical research methodology is to be implemented including the basic parametric study of the subprocesses (spot laser welding, raster-scan laser welding, foil laser cutting, and laser polishing processes) in LFP, the numerical analysis of heat transfer and convection flow in laser polishing process, and the study of mechanical properties and surface quality of as-fabricated parts.

The study of the laser macro polishing of raster-scan weld surfaces is to be carried out with the aim of suppressing the surface roughness of raster-scan weld surfaces and preventing the surface roughness accumulation in the manufacturing process of parts. A thermo-fluid model will be developed to analyze the heat transfer and convection flow in the melting pool during laser polishing processes. The post-processing of laser remelting/polishing in LFP will be explored which would reduce or eliminate the stair-steps on the lateral surface of as-fabricated parts and improve the surface mechanical quality. Finally, the study of the laser-polishing-induced bulge structure will be conducted

with the aim of understanding its formation and the reduction process through polished track overlapping.

1.6. ORGANIZATION OF DISSERTATION

The first paper, “A Foil-Based Additive Manufacturing Technology for Metal Parts”, introduces the manufacturing process of Laser-Foil-Printing. The sub-processes of the laser spot welding, laser raster-scan welding and laser cutting of foils are discussed in detail. The four as-fabricated parts are demonstrated and the superior mechanical properties (hardness and tensile strength) of fabricated parts are presented.

The second paper, “Study of the Laser Polishing Process in Laser-Foil-Printing Additive Manufacturing”, presents the parametric study of the laser polishing process on the raster-scan laser weld surface. The polished track width and depth were analyzed and the temperature field and convection flow in the melting pool were analyzed through a validated numerical model. Finally, the overlap percentage of polished tracks was studied and the surface roughness could be polished to 0.578 μm from the initial surface roughness of 3.77 μm.

The third paper, “Surface Enhancement of the Laser-Foil-Printing Fabricated Parts by the Laser Polishing Process”, studied the laser polishing process on two typical side surfaces of LFP parts, the vertical and 45º-inclined side surfaces. Three different laser scan paths were investigated for the single-track laser polishing process, which are the straight-line, sine-wave and grinding scan paths. With the multi-step polishing process of the grinding-scan and linear-scan polishing steps, the final side surface can be polished to 0.72 μm in Sa. And the foil bonding defects on the side surface can be completely repaired.

The fourth paper, “Fundamental Study of The Bulge Structure Generated in Laser Polishing Process”, studied the bulge structure produced by the laser macro polishing process on Ti-6Al-4V slabs. The bulge formation should be mainly due to the mass transport and phase transition during the polishing process. The influences of laser power, scan speed and focal offset on the bulge structure were studied. The reduction of bulge structure through the overlapping process of polished tracks was studied with the spatial spectrum analysis.

The last section of this dissertation presents a brief summary of the research, the major conclusions drawn from these studies, and some recommendations for future work.

PAPER

I. A FOIL-BASED ADDITIVE MANUFACTURING TECHNOLOGY FOR METAL PARTS

Chen Chen **Yiyu Shen** **Hai-Lung Tsai**

Department of Mechanical and Aerospace Engineering

Missouri University of Science and Technology, Rolla, MO, 65409, U.S.A.

ABSTRACT

In this paper, the method, system setup, and procedure of a new additive manufacturing (AM) technology for manufacturing three-dimensional (3D) metal parts are introduced. Instead of using metal powders as in most commercial AM technologies, the new method uses metal foils as feed stock. The procedure consists of two alternating processes: foil-welding by a high-power continuous-wave (CW) laser and foil-cutting by a Q-switched ultraviolet (UV) laser. The foil-welding process involves two sub- processes: laser spot welding and laser raster-scan welding. The reason for using two lasers is to achieve simultaneously the high- speed and high-precision manufacturing. The results on laser foil- welding and foil-cutting show that complete and strong welding bonds can be achieved with determined parameters, and that clean and no-burr/distortion cut of foil can be obtained. Several 3D AISI 1010 steel parts fabricated by the proposed AM technology are presented, and the microhardness and tensile strength of the as-fabricated parts are both significantly greater than those of the original foil.

1. INTRODUCTION

Since the commercialization of the first machine for AM or 3D printing in 1987 [1], many new AM processing technologies have been proposed and commercialized [2–6]. Over 30 years into its development, AM is expected to be one of the mainstream manufacturing processes [7]. Recently, AM is welcomed in some industrial fields like medical, aerospace, and automotive, and its application scope keeps expanding. The reported AM technologies include stereolithography (U.S. Patent No. 4,575,330), fused deposition modeling (U.S. Patent No. 5,121,329), laminated object manufacturing (LOM) (U.S. Patent No. 4,752,352), inkjet printing (U.S. Patent No. 2,566,443), laser-engineered net shaping (LENS) (U.S. Patent No. 6,046,426), selective laser sintering (SLS) (U.S. Patent No. 4,863,538), selective laser melting (SLM) (DE Patent No. 19,649,865), electron beam melting, ultrasonic consolidation (U.S. Patent No. 6,519,500), etc. AM is applicable to all classes of materials including metals, ceramics, polymers, composites, and biological systems [8]. In this study, we focus on the AM of metal parts with anticipations that the as-fabricated parts could have the mechanical properties of their bulk materials and could be directly used without additional machining or post-processing.

Many of the aforementioned AM techniques are applicable to metal parts, and the significant and representative among them are: selective laser sintering/melting (SLS/SLM), LENS, and LOM including ultrasonic consolidation. SLS/SLM and LENS are powder-based processes. In SLS/SLM, the powder is fed in a powder-bed, and the powder of a specific region is sintered or fully fused by a laser beam; this process recurs layer-by-layer according to the design of 3D models. The main advantage of SLS/SLM is that a wide range of materials (polymers, metals, or ceramics) can be used, and the disadvantages

are that the manufacturing accuracy is limited by the size of material particles and the material changeover is difficult [7]. In LENS process, a part is fabricated by focusing a high-power laser beam onto a substrate to create a molten pool in which the metal pow- der particles are injected to build each layer. LENS can be used to repair parts, and the composition of powder can be changed from one location to others during the processing to make products with varied compositions which could lead to the possibility of fabricating functional graded parts [9]. However, the parts built by LENS usually have rough surface finish which may require additional milling or polishing process. LOM is a foil- based AM technique. In the LOM process, initially papers were used and they were bonded together by glues/binders with pressure and/or heat. This technology was later extended to the material of metal foils and the use of ultrasonic solid-state welding for foil fusion. Then, a milling tool was used to cut or trim the foil to the desired shape [10]. The LOM process is inexpensive and has the possibility of building large parts. The disadvantages are that the subtracted material cannot be reused, and the fabricated parts are usually directionally dependent of mechanical properties [11]. In summary, among the above- described processes, powder-based technologies (SLS/SLM and LENS) are much more researched and applied, but there are very fewer studies on foil-based AM technologies of metal parts (e.g., LOM), and the potential of foil-based technologies needs to be fully explored.

In this paper, a foil-based AM process is proposed and studied. The raw material used is metal foils of various thicknesses ranging from a few 10 s of microns to a few 100 s of microns. The rea- sons for choosing foils instead of powders are: (1) micro- or nano- size powder particles have potential health hazards to opera- tors and environments; (2) the

cost of equipment and maintenance of powder-based AM technology is very high; and (3) powders are more expensive than foils, and many powders are patented and machine-specific.

In 2001, Hardjadinata and Doumanidis [12] reported a rapid prototyping method by using laser metal foil bonding and cutting. In their method, thin metal foils are successively joined by a recurring sequence of laser spot welding and laser cutting of each layer contour. The weld spots are laid on a square grid and centered 3mm apart from each other. Obviously, the mechanical and thermal properties of the as-fabricated parts are insufficient for most practical applications. In order to enhance the mechanical properties of as-fabricated parts, Prechtl et al. [13] added an additional process, diffusion welding (bonding), after the whole recurring processes of laser spot welding and cutting. In the diffusion welding process, the foil stack is pressed at a high temperature and protected with an inert atmosphere for a defined time. The mechanical properties of final parts mainly depend on the final diffusion welding process. The achieved tensile strength was still not good enough, the integration lines between layers can be seen on the cross section under the microscope, and the geometry of parts could not be preserved well. In the proposed processing method of this paper, laser raster-scan welding is applied to bond foils in a specified area which can achieve fully fused and high-strength bonding between foils, and no post-processing (e.g., diffusion welding) is needed to improve the interlayer bonding. And another Q-switched laser is used for foil-cutting.

In this paper, the system setup and procedure of the proposed AM technology are described first. Then, the processes of laser foil-welding (including spot welding and raster-scan welding) and foil laser cutting are presented and discussed, respectively. Some 3D

parts were fabricated by the proposed technology with the raw material of AISI 1010 steel foils. The mechanical properties of microhardness and tensile strength of the as-fabricated parts were examined.

2. APPARATUS SETUP AND PROCEDURE

The schematic diagram of the apparatus setup for the proposed foil-based AM process is shown in Figure 2.1. The welding laser is a high-power CW fiber laser (IPG Lasers, Model: YLR-1000-MM- WC-Y11) with a wavelength of 1070nm and a maximum power of 1000W. The cutting laser is a Q-switched UV laser (Coherent Lasers, Model: 1053565 AVIA 355-X) with a 355nm wavelength, a 30 ns pulse duration, and a 10Wmaximum power. The welding laser beam comes out of the laser head, passes through a beam expander and a beam collimator, becoming an expanded parallel beam, then enters the scanner (SCANLAB, HurryScan 30 mm), and finally is focused on the working plane by an F-theta lens with a focus length of 30 cm. The beam spot diameter on the focal plane is about 160 lm. The workpiece (foil and substrate) is placed in a shielding gas chamber with a top opening which allows the laser beam to pass through and with a bottom inlet for argon shielding gas. The shielding gas chamber is fixed on an X–Y (horizontal) motion stage (Aerotech Model: ATS 10060-H-M-80P-NC). Once the laser welding process is done in one layer, the workpiece is translated by the motion stage for the laser cutting process. The cutting laser beam passes through a turning mirror and is focused by a focusing lens with a 10 cm focal length. A coaxial com- pressed inert gas nozzle mounted under the focusing lens is used to protect and clean the cutting edge. The cutting laser beam diameter on the focal plane is about 40lm. Note that the optical delivery system (the scan head, beam expander, beam collimator, focusing lens of UV laser, and the gas nozzle) is mounted on the Z (vertical) motion stage which is not shown in the schematic diagram. After the welding and cutting processes for one layer are done, the Z-motion stage moves up a distance of one-layer thick- ness for processing another layer. The foil used in this study is

AISI 1010 steel with a thickness of 150lm (Precision Brand, UPC No. 16850), and the substrate is a thick (6.35mm) common low-carbon steel plate. The two lasers, scanner, and three-axis motion stage are integrated logically through a control program to a computer which is not shown in the schematic diagram.

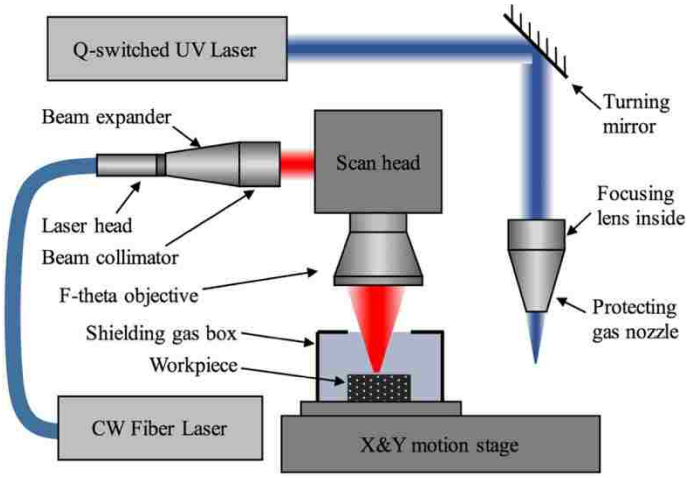

Figure 2.1. Apparatus setup for the foil-based laser AM process

Like most of other AM technologies, the procedure starts with a 3D CAD model (StereoLithography format) of a part. Then, the 3D model is transferred to a set of layer data by slicing software. The set of layer data is then translated by the control program into machine instructions and executed layer-by-layer. In the manufacturing process of each layer, a metal foil is fixed upon a flat substrate by laser spot-welding, and then, a laser raster-scan welding process is done to achieve the full fusion and bonding of foil in selected regions. After the laser welding processes are done, the scanner and the fiber laser stop working temporarily, and the workpiece is translated to the location under the UV laser beam. Then, the control program controls the X–Y motion stage and UV laser to cut the welded foil along the contour of the welding region. After the laser cutting is completed,

the redundant foil is removed and another fresh foil is placed on the top of the work- piece for the process of next layer. This manufacturing procedure is repeated until the desired 3D part is built. Note that the mechanical properties of the as-fabricated parts are dominated by the laser welding processes, especially laser raster-scan welding, and the laser cutting process has an important influence on the surface quality of the as-fabricated parts.

3. LASER WELDING OF FOILS

3.1. LASER SPOT-WELDING

Laser spot-welding is applied in the proposed technique to “anchor” the unprocessed foil on the substrate or the semi-finished part which would prevent the foil from possible thermal distortion. The spot welds are laid on a square grid and centered 2–3mm apart from each other. For a good laser spot-welding process, all the weld spots penetrate into the substrate or the top surface layer of the semi-finished part, and stable and strong bonds are formed between the foil and the substrate or the semi-finished part. Thus, the negative influence of possible thermal distortion of foil in the process of laser raster-scan welding would be eliminated effectively.

The major control parameters in laser spot-welding include laser power, irradiation time, and the distance between spots. After some parametric study, the process parameters for laser spot-welding in the present study are determined as 390Wof laser power, 6ms of irradiation time, and 2 mm of the spots distance. Note that the irradiation time here is equivalent to the pulse duration of a pulsed laser, since a CW fiber laser is used in both the processes of spot welding and raster-scan welding. The top sur- face and the cross section of a spot weld under this set of parameters are shown in Figure 3.1.

From Figure 3.1, it is seen the top surface of the spot weld is roughly circular, the weld penetrates into the substrate deeply, no thermal distortion is observed around the weld spot, and the melting zone diameter in foil is much larger than that in substrate, which is due to the contact thermal resistance between the foil and the substrate. Through the measurement of ten spot- welds under the same processing condition, the average diameter at the surface of the spot-weld is about 621 μm, the average melting depth of the spot weld

is about 527 μm, and the average diameter of the bonding between the foil and the substrate is about 315 μm.

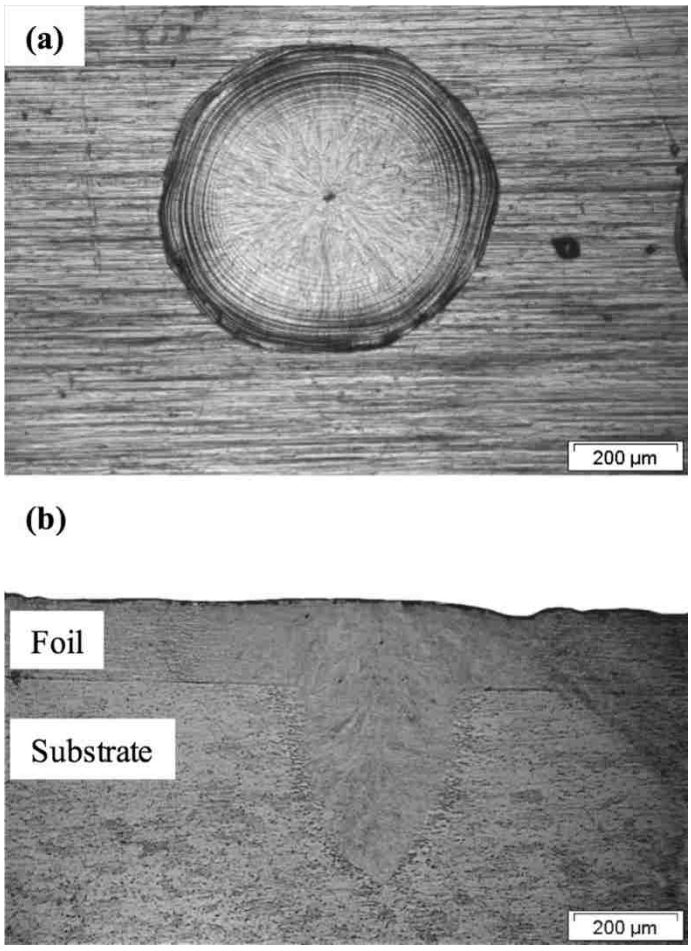

Figure 3.1. (a) The top surface and (b) the cross section of a spot weld under the condition of 390W of laser power and 6ms of irradiation time

Considering the physical process of laser spot-welding, when the laser power density is low and cannot cause significant evaporation of material, a conduction-limited welding [14] occurs and the weld pool is shallow. When the laser power density is high and the evaporation of material is significant, the spot welding enters the keyhole mode [14], where a hole is generated in the melting pool leading to a deep weld. If the laser power

density increases further, the evaporation becomes very strong and the melt can be pushed out and solidifies around the melt pool. The ejection of the melt could occur if the power density is too high and the process approaches laser drilling. In our experiments, when the laser power is higher than 270W, the spot welding can be roughly seen as a keyhole welding, and when laser power is about 500Wor higher, the phenomenon of melt spatter (recast) is observed on the surface of the foil.

3.2. LASER RASTER-SCAN WELDING

Laser raster-scan welding is employed to fully weld the foil onto the substrate or the semi-finished part after the process of laser spot-welding and it has the dominant influence on the mechanical properties of the as-fabricated part by the proposed AM technology. The ideal result of the laser raster-scan welding would be that foils are fully fused and bonded onto the substrate or the semi-finished part and that the weld surface is smooth. A high-power CW fiber laser is employed for the foil raster-scan welding.

Although some literature reported on the studies of metal foil/sheet welding [15–22], we have not found any study related to the laser foil-welding onto a thick metal substrate, so the feasibility and quality of laser foil-welding onto a steel substrate were conducted in the experiment. After some parametric studies on the welding parameters (laser power, scanning speed, and welding track interspace), some welds of good quality were obtained. In this paper, the selected processing parameters are 390W of laser power, 200 mm/s of scanning speed, and 100 μm of welding track interspace. The resultant weld surface and cross sections are presented in Figure 3.2.

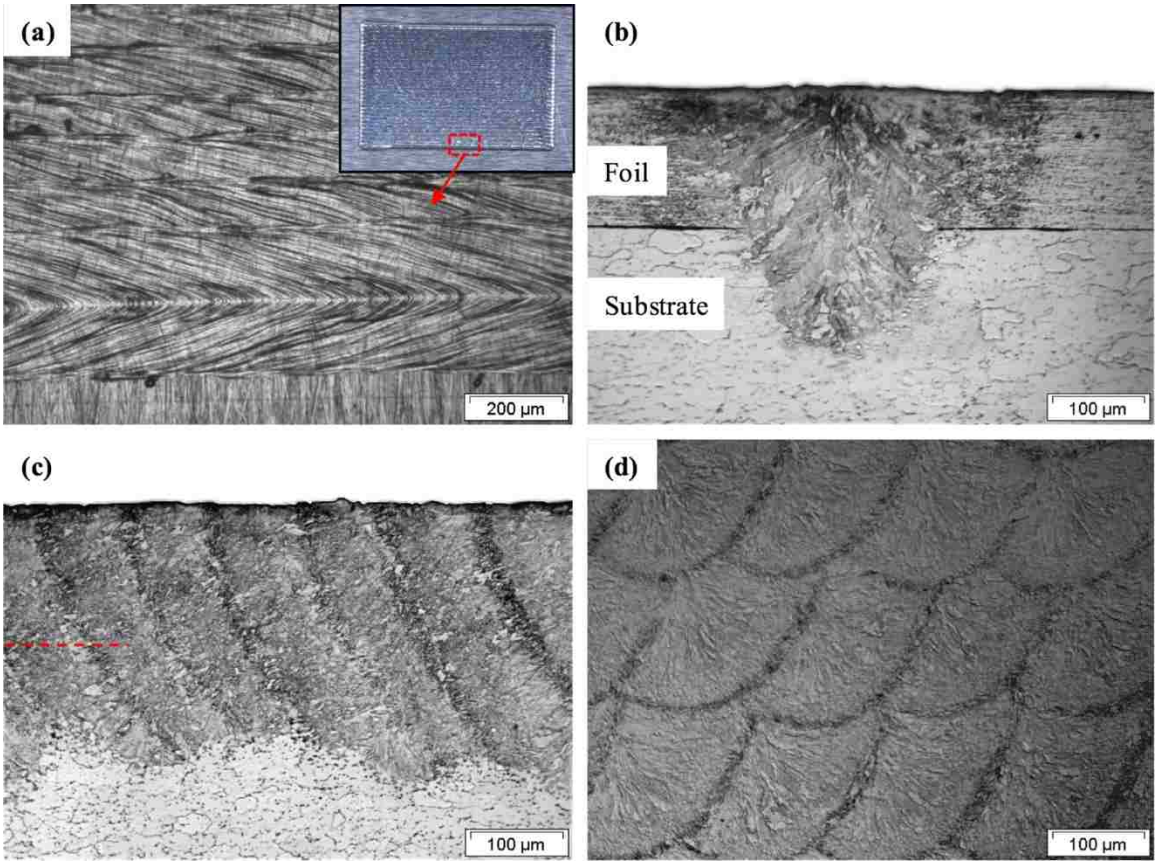

Figure 3.2. (a) The surface morphology of the raster-scan weld, (b) the cross section of a single-line laser foil-welding onto a substrate, (c) the cross section of the raster- scan weld of one-layer foil onto a substrate, and (d) the cross section of a multi- layer raster-scan weld

Figure 3.2(a) shows the surface morphology of a raster-scan weld in which the welding tracks are overlapped one-by-one with an interspace of 100 µm; the bottom welding track is the last one and has the welding direction from right to left and the weld width of about 310 µm. The inset in Figure 3.2(a) shows the overall raster-scan weld surface of the size 10mm × 7mm; the raster-scan weld surface looks quite uniform and has an average roughness Ra of about 10 µm. Figure 3.2(b) shows the cross section (the surface perpendicular to the welding direction) of a single-line foil weld with the determined laser parameters. The melt depth of the weld is about 275 µm, and the bonding width at the

interface between the foil and the substrate is about 200 μm. From the geometry of the fusion zone, the laser welding regime should be of the keyhole mode. Figure 3.2(c) shows the cross section of the raster-scan weld of one-layer foil (i.e., the sample in Figure 3.2(a)), where the average melt depth of raster-scan weld is about 270 μm and the welding sequence is from left to right. Figure 3.2(d) shows the cross section of a multilayer foil weld, where different welding tracks can be clearly recognized by the dark-color curves which should be the heat-affected zone (HAZ) of each weld track. Note that all the cross sections shown in Figure 3.2 were etched by 5% of HNO_3 solutions for about 5 s.

From the cross section result of multilayer foil raster-scan welding, complete fusions are formed between foils and the original separation lines between foils disappear in the final weld cross section (Figure 3.2(d)). Examining the whole cross section of the multilayer foil weld, there is no micro-cracks and very few micro-pores which could be caused by the initial impurities between foils or the instability of raster-scan welding. Note that the overlap of a certain extent between the raster-scan welding tracks is important to the repeatability of raster-scan welding. In our experiments, with the determined laser power and welding speed, the bonding width at the interface between the foil and the substrate/semi-finished part is about 200 μm under a good contact condition. During the process of multi-layer foil-welding, the top surface of the semi-finished part is usually not in perfect flat and there exist some micro-gaps between the next added foil and the semi-finished part. Besides, although the spot welding process restrains possible thermal distortion of the foil, there still exists some thermal distortion of the un-welded foil between two weld spots which could be generated during the raster-scan welding. These two factors are thought to affect the repeatability of raster-scan welding, which is embodied by unequal

weld depths. Unequal weld depth also implies possible variation of bonding strength between the foil and the semi-finished part. When the welding track interspace of 150 μm was used in the experiment, some intermittent and short separation lines can be observed from the cross section of multilayer weld, which implies incomplete bonding between foils, especially for higher layers. However, when the welding track interspace of 100 μm was applied, no separation line was observed.

4. LASER CUTTING OF FOILS

After the laser raster-scan welding is done on one layer, the laser cutting process is used to cut along the inner and outer circumferences of the welding region to remove the redundant foil. For a good laser cutting process, the following cut qualities can be obtained [23]: (1) the cut edge can be square and not rounded as occurs with some thermal cutting techniques; (2) the cut edge can be smooth and clean; (3) there is no edge burr or dross adhesion around cut edges; and (4) there is a very narrow HAZ and negligible distortion. To this end, a Q-switched UV laser with 355 nm wavelength was applied in the current experimental setup. The parameters of the cutting process were determined as 115 μJ pulse energy, 10,000 Hz pulse rate, and 30 mm/min cutting speed. Besides, the foil surface is placed on the focal plane, and the beam spot diameter is about 40 μm.

The resultant front and rear surfaces of the foil cut edge are shown in Figure 4.1. The cut edges shown are quite clean and straight, no edge burr or dross adhesion was generated, and no significant HAZ and thermal distortion are observed. The taper of the cut edge can be recognized by the dark band along the cut line from the front surface image, see Figure 4.1(a). The taper distance is about 20lm, which is much less than the foil thickness of 150lm. Also, no edge burr or melt dropout was generated on the rear surface, see Figure 4.1(b).

The 30-ns pulse duration of the Q-switched UV laser, combined with the determined pulse energy and beam size, results in a laser intensity of 3×10^{8} W/cm^{2}. With such high laser intensity, the foil material is removed mainly through evaporation [23]; consequently, the melting layer is very thin. Generally, the more melt there is, the poorer

the quality of the cutting edge. Also, a very small fraction of energy is spent on generating the HAZ and distortion in this case.

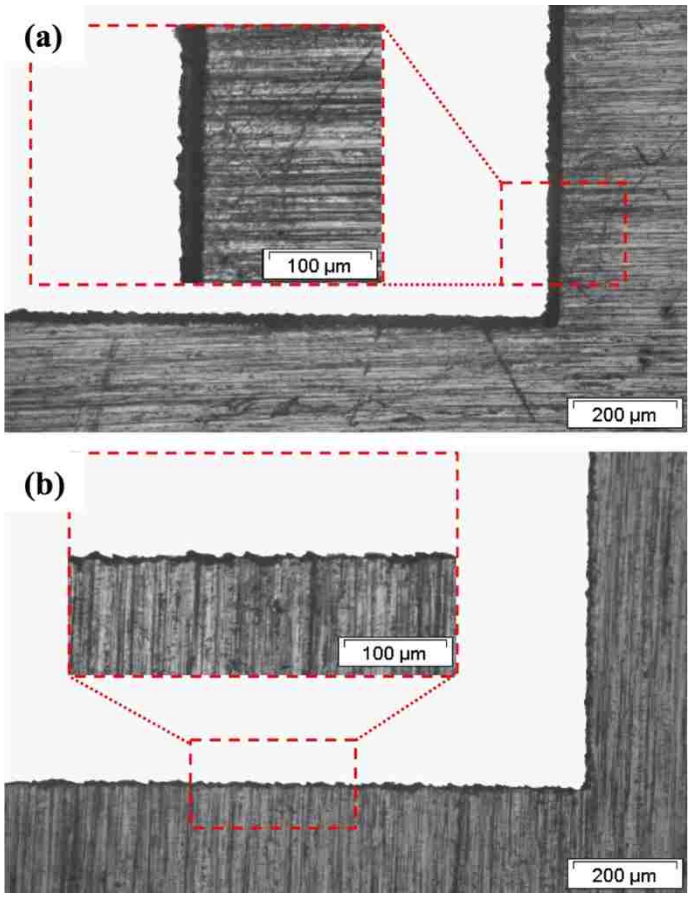

Figure 4.1. (a) The front surface and (b) the rear surface of a cutting edge with laser parameters of 115 µJ pulse energy, 10,000 Hz pulse rate, and 30 mm/min cutting speed

Different laser cutting environments were tried in the experiments, including ambient air, compressed air flow, ambient argon, and compressed argon flow. Through the experiment, it is concluded that the overall cutting performance (efficiency and quality) in ambient air is the best, and the sample in Figure 4.1 is cut in ambient air.

5. AS-FABRICATED 3D PARTS

With the processing parameters obtained from the previous experimental studies, some 3D steel parts, as shown in Figure 5.1, were fabricated by the new foil-based AM procedure. Figure 5.1(a) shows a proportionally scaled model of the Gateway Arch in St. Louis, with 90mm for both of the height and width. Figure 5.1(b) shows an S&T logo of the Missouri University of Science and Technology, Rolla, MO, with dimensions of 24 × 14 × 2 mm. Figure 5.1(c) shows a cylinder with special gradient lateral surfaces; the top and bottom surfaces are two orthogonally oriented ellipses with major and minor diameters of 12 and 7 mm, respectively, and the height of the cylinder is 7 mm. Figure 5.1(d) shows the demonstration of a sensor-embedded part, where the main component is a cylinder with rotating gradient lateral surfaces at a height of 11 mm, and the horizontal cross section of the cylinder is an ellipse of the size 15 × 9 mm. Three U channels with the cross-section diameter of 1 mm were designed in the main cylinder, and three partially cutoff paperclips to simulate sensors were embedded in the part during the fabrication process.

Full automation control has not yet been realized in our current setup, especially the control of removing the redundant foils and of loading the fresh foils. In our current fabricating process of each layer, we need to take the semi-finished part off to remove the redundant foil and examine the weld surface and reload a new foil. The position of the semi-finished part is locked by two alignment pins. However, the alignment unit in the current setup is not very accurate, so the lateral surfaces of as-fabricated parts are not as good as we expected. To achieve a perfect lateral surface, the automation of the redundant foil removing should be implemented and the semi-finished part should be fixed on the

motion stage until the whole process is completed. If the foil is supplied in a roll for- mat, a roll-to-roll loading mechanism of the foil can be easily accomplished.

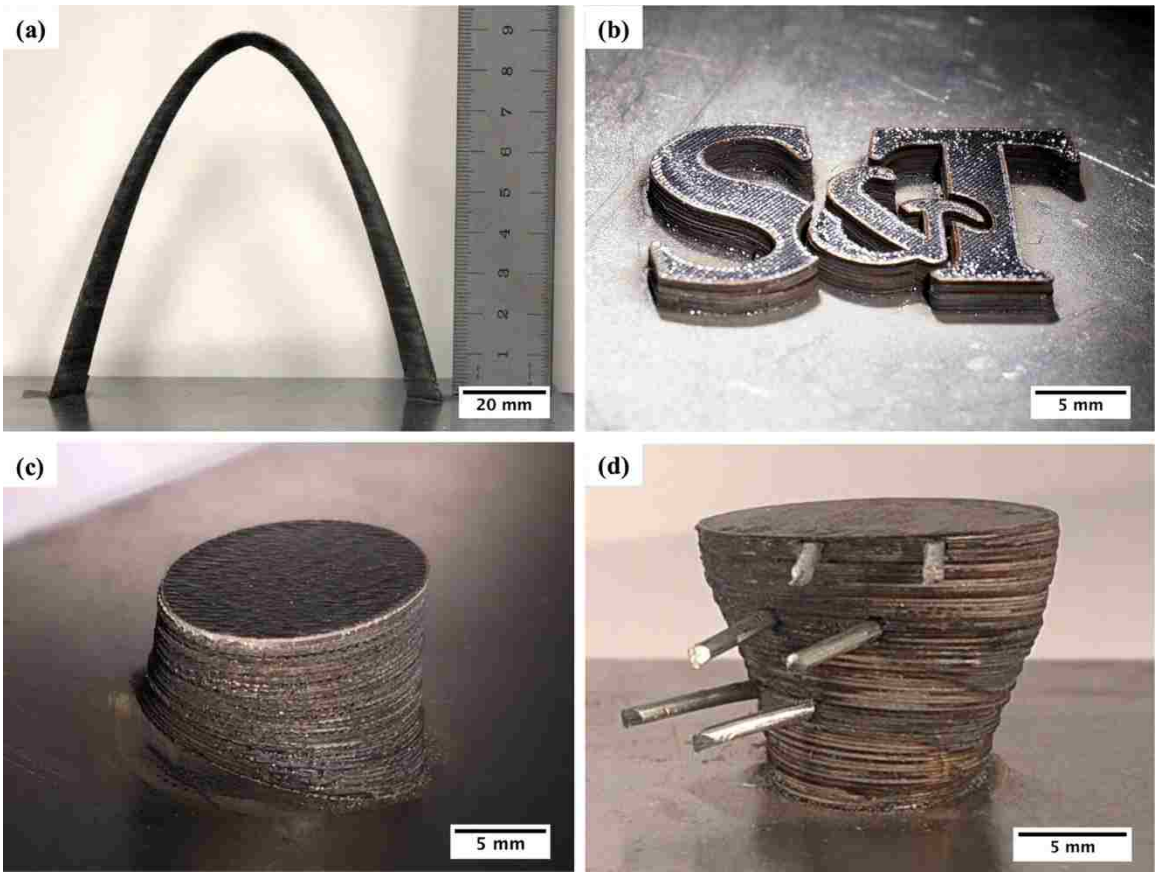

Figure 5.1. As-fabricated samples by the proposed AM technology: (a) a model of St. Louis arch, (b) a logo of Missouri University of Science and Technology, (c) a cylinder with gradient lateral surfaces, and (d) a sensor-embedded cylinder with rotating gradient lateral surfaces

Note that the parts have no significant temperature rise during the whole fabrication processes, because of the low heat input from the laser irradiations for both welding and cutting.

6. MECHANICAL PROPERTIES EXAMINATION

The micro-hardness and tensile strength of the parts fabricated by the proposed technology were examined. The micro-hardness was measured at 50 spots on the cross section of an as-fabricated part and at ten spots on the cross section of an original foil. The average micro-hardness of the as-fabricated part is about 382.2 kg f/mm^2 (Vickers hardness, Hv 0.1/5) with a standard deviation of 35.7 kg f/mm^2, while the average micro-hardness of the original foil is about 240.0 kg f/mm^2 with a standard deviation of 5.2 kg f/mm^2. Hence, the material micro-hardness has increased about 60% in the fabrication process, which may be caused by the fast-cooling rate of laser welding and the subsequent refinement of material grains.

Figure 6.1 shows the tensile test results of two dog-bone samples. For the sample in Figure 6.1(a), the tension direction is along the foil direction (i.e., horizontal direction), while the tension direction in the sample of Figure 6.1(b) is normal to the foil layers (i.e., vertical direction). The ultimate tensile strength in the horizontal direction is about 1015MPa and in the vertical direction is about 744 MPa. Both of these ultimate tensile strengths are much higher than that of the original AISI 1010 steel which is 551 MPa. Note that the tensile strength in the horizontal direction is still much higher than that in the vertical direction, and there is no significant plastic strain in the vertical direction. The possible reason for less tensile strength in the vertical direction as compared to that in the horizontal direction could be caused by bonding defects between foils due to the two factors discussed above related to the laser raster-scan welding and/or the orientation of crystallization in weld zones.

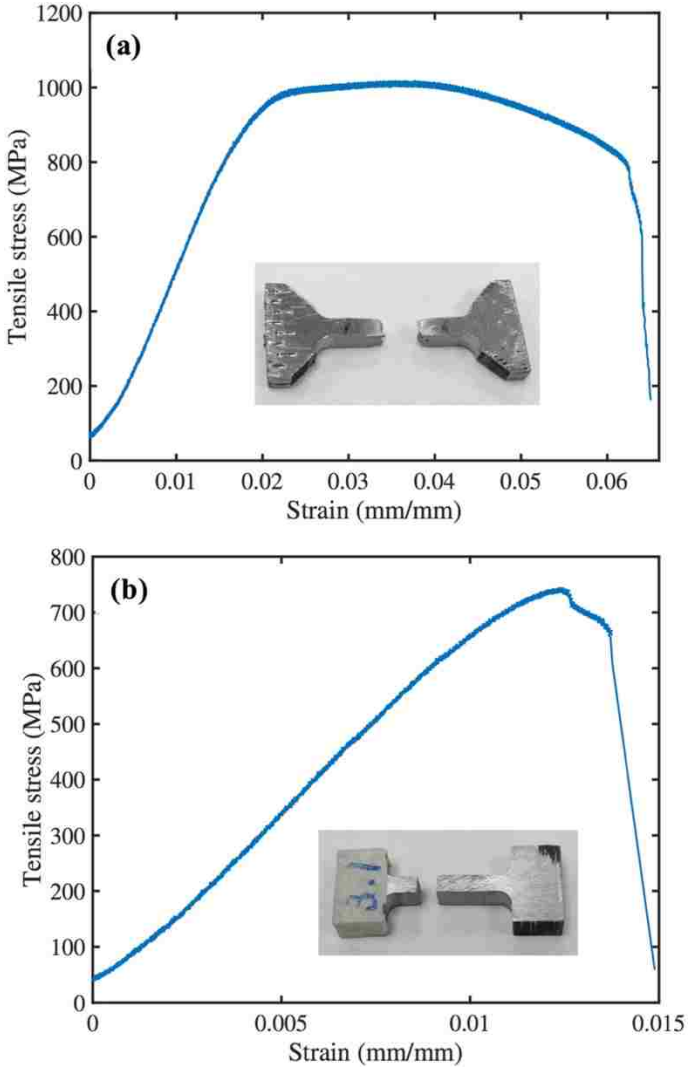

Figure 6.1. Stress–strain curves of as-fabricated parts with tension exerted in the (a) horizontal and (b) vertical directions

7. CONCLUSIONS

A new foil-based AM technology was proposed and implemented. The main manufacturing procedure consists of two alternating steps: the laser foil-welding process and the laser foil- cutting process. The foil-welding process was carried out with a high-power CW laser and a high-speed scanner and includes two sub-processes: laser spot welding and laser raster-scan welding. The foil-cutting process was carried out with a high-energy Q-switched UV laser and a high-accuracy motion stage.

A firm fixture of the foil onto the substrate or semi-finished part can be achieved by laser spot-welding with the parameters of 390 W laser power and 6ms pulse duration. A full and strong welding bond between the foil and the substrate or the semi-finished part can be obtained by the laser raster-scan welding with the parameters of 390 W laser power, 200 mm/s scanning speed, and 100 μm weld track interspace. A clean and no-burr/distortion cut of foils can be accomplished by laser cutting with the parameters of 115 μJ pulse energy, 10,000 Hz pulse rate, and 30 mm/min cutting speed. Note that the processing performance could be further improved with more rigorous parametric studies. Four metal structures were fabricated with the proposed AM technology. The micro-hardness and tensile strength of the as-fabricated parts are both significantly higher than those of the original foil.

The proposed AM technology has two important advantages: low cost and high flexibility. With the further improvement and addition of automation control and process monitoring [24,25], the proposed foil-based AM technology would have a wide application in industry to manufacture complex, large-scale, or sensor-embedded structures.

ACKNOWLEDGMENTS

The authors gratefully acknowledge the financial support from the Department of Energy (Grant No. DE-FE0012272) and the Intelligent System Center at Missouri S&T.

BIBLIOGRAPHY

[1] Wohlers, T. T., and Gornet, T., 2012, "History of Additive Manufacturing," Wohlers Associates, Fort Collins, CO.

[2] Atzeni, E., and Salmi, A., 2012, "Economics of Additive Manufacturing for End-Usable Metal Parts," Int. J. Adv. Manuf. Tech., **62**(9-12), pp. 1147-1155.

[3] Gu, D. D., Meiners, W., Wissenbach, K., and Poprawe, R., 2012, "Laser Additive Manufacturing of Metallic Components: Materials, Processes and Mechanisms," Int. Mater. Rev., **57**(3), pp. 133-164.

[4] Uriondo, A., Esperon-Miguez, M., and Perinpanayagam, S., 2015, "The Present and Future of Additive Manufacturing in the Aerospace Sector: A Review of Important Aspects," Proc. Insti. Mech. Eng. G: J. Aero. Eng., **229**(11), pp. 2132-2147.

[5] Vaezi, M., Seitz, H., and Yang, S. F., 2013, "A Review on 3D Micro-Additive Manufacturing Technologies," Int. J. Adv. Manuf. Tech., **67**(5-8), pp. 1721-1754.

[6] Huang, Y., Leu, M. C., Mazumder, J., and Donmez, A., 2015, "Additive Manufacturing: Current State, Future Potential, Gaps and Needs, and Recommendations," ASME J. Manuf. Sci. Eng., **137**(1), p. 014001.

[7] Huang, S. H., Liu, P., Mokasdar, A., and Hou, L., 2013, "Additive Manufacturing and Its Societal Impact: A Literature Review," Int. J. Adv. Manuf. Tech., **67**(5-8), pp. 1191-1203.

[8] Frazier, W. E., 2014, "Metal Additive Manufacturing: A Review," J. Mater. Eng. Perform., **23**(6), pp. 1917-1928.

[9] Kumar, S., and Pityana, S., 2011, "Laser-Based Additive Manufacturing of Metals," AIP Conf. Proc., **227**, pp. 92-95.

[10] Ghariblu, H., and Rahmati, S., 2014, "New Process and Machine for Layered Manufacturing of Metal Parts," ASME J. Manuf. Sci. Eng., **136**(4), p. 041004.

[11] Wong, K. V., and Hernandez, A., 2012, "A Review of Additive Manufacturing," ISRN Mech. Eng., **2012**, p. 208760.

[12] Hardjadinata, G., and Doumanidis, C. C., 2001, "Rapid Prototyping by Laser Foil Bonding and Cutting: Thermomechanical Modeling and Process Optimization," J. Manuf. Process., **3**(2), pp. 108-119.

[13] Prechtl, M., Otto, A., and Geiger, M., 2005, "Rapid Tooling by Laminated Object Manufacturing of Metal Foil," Adv. Mater. Res., **6-8**, pp. 303-312.

[14] Steen, M. W., and Mazumder, J., 2010, *Laser Material Processing*, Springer, London, Chap. 4.

[15] Xie, J., and Kar, A., 1999, "Laser Welding of Thin Sheet Steel with Surface Oxidation," Weld. J., **78**(10), pp. 343-348.

[16] Okamoto, Y., Gillner, A., Olowinsky, A., Gedicke, J., and Uno, Y., 2008, "Fine Micro-Welding of Thin Stainless Steel Sheet by High Speed Laser Scanning," J. Laser Micro Nanoen., **3**(2), pp. 95-99.

[17] Abe, N., Funada, Y., and Ishide, M., 2003, "Micro-Welding of Thin Foil with Direct Diode Laser," Proc. SPIE 5063, Fourth International Symposium on Laser Precision Microfabrication, **5063**, pp. 287-291.

[18] Liao, Y. C., and Yu, M. H., 2007, "Effects of Laser Beam Energy and Incident Angle on the Pulse Laser Welding of Stainless Steel Thin Sheet," J. Mater. Process. Tech., **190**(1-3), pp. 102-108.

[19] Krasnoperov, M. Y., Pieters, R. R. G. M., and Richardson, I. M., 2004, "Weld Pool Geometry During Keyhole Laser Welding of Thin Steel Sheets," Sci. Tech. Weld. Joi. J., 9(6), pp. 501-506.

[20] Kralj, S., Bauer, B., and Kozuh, Z., 2003, "Laser Welding of Thin Sheet Heat-Treatable Steel," Annals of DAAAM for 2003 & Proceedings of the 14th International DAAAM Symposium, B. Sarajevo, eds., Katalinic, BOSNIA & HERCEG, pp. 245-246.

[21] Kah, P., Suoranta, R., and Martikainen, J., 2011, "Joining of Sheet Metals Using Different Welding Processes," Mechanika 2011: Proceedings of the 16th International Conference, Kaunas University of Technology, Lithuania, pp. 158-163.

[22] Farid, M., and Molian, P. A., 2000, "High-Brightness Laser Welding of Thin-Sheet 316 Stainless Steel," J. Mater. Sci., **35**(15), pp. 3817-3826.

[23] Steen, M. W., and Mazumder, J., 2010, *Laser Material Processing*, Springer, London, Chap. 3.

[24] Rao, P. K., Liu, J., Roberson, D., Kong, Z., and Williams, C., 2015, "Online Real-Time Quality Monitoring in Additive Manufacturing Processes Using Heterogeneous Sensors," ASME J. Manuf. Sci. Eng., **137**(6), p. 061007.

[25] Tapia, G. and Elwany, A., 2014, "A Review on Process Monitoring and Control in Metal-Based Additive Manufacturing," ASME J. Manuf. Sci. Eng., **136**(6), p. 060801.

II. STUDY OF THE LASER POLISHING PROCESS IN LASER-FOIL-PRINTING ADDITIVE MANUFACTURING

Chen Chen Yiyu Shen Yingqi Li Hai-Lung Tsai

Department of Mechanical and Aerospace Engineering

Missouri University of Science and Technology, Rolla, MO, 65409, U.S.A.

ABSTRACT

Laser polishing is an innovative part-finishing process to reduce the surface roughness by melting a thin layer of material on the part surface. In this paper, the laser polishing process is studied for the Laser Foil Printing (LFP) technology, a new additive manufacturing process, to suppress the roughness of the laser weld surface. In the LFP process, the surface roughness produced by the laser welding process is 3.77 μm in Sa. In the single-line laser polishing tests, two polishing modes are found as the incident laser energy increases, and the polished track quality is considered to be related to the polished track width and the melted depth. The polished track width relates to the range of spatial frequency of surface asperities that can be effectively removed, and the melted depth relates to the range of the vertical magnitude of asperities that can be effectively removed. The parametric study about the polished tracks shows that the laser power and scan speed have significant influences on the polished track width and the melted depth. The numerical study of the laser polishing process shows that the thermocapillary-driven convection flow can enhance the melted depth, and the maximum speed of the convection flow has a limit of about 2.5 m/s. The multi-line polishing tests show that the final surface roughness

decreases as the overlap percentage increases. The final surface polishing parameters are determined as the laser power of 390 W, the scan speed of 200 mm/s and the overlap percentage of 85%, and the surface roughness is reduced to 0.578 μm in Sa.

1. INTRODUCTION

Laser polishing is an innovative part-finishing process, and widely used to improve the surface quality of various materials including glass, lens, fibers, diamond, and metals [1-12]. Compared with the traditional polishing methods (e.g., abrasive, chemical and electro polishing), laser polishing has some obvious advantages, such as the high level of automation, non-direct contact, less processing time, no pollutive impact, and user-definable or localized polishing [13]. During the laser polishing process, a thin surface layer is molten and the surface tension drives the material flowing from the peaks to valleys. As a result, the surface asperities are evened out, the surface peak-valley heights are reduced, and the surface quality gets improved. Laser polishing has two sub-variants: the macro polishing and the micro polishing [14]. Generally, the macro polishing is used to remove the relatively large surface structures from milling, turning, or EDM, but the micro polishing process is used to remove the fine micro roughness and achieves a high gloss level [13]. Usually the macro polishing is carried out with a continuous wave (CW) laser, while a pulsed laser is used for the micro polishing.

Since the first additive manufacturing (AM) machine was commercialized in 1987, several AM technologies have been reported particularly for producing metal parts, including selective laser sintering (SLS), selective laser melting (SLM), laser engineered net shaping (LENS), direct metal deposition (DMD), electron beam melting (EBM), etc. These AM technologies usually use metal powders of different sizes and their mixings and, hence, the surfaces of the as-fabricated parts exhibit some degree of roughness (10s of microns) that is usually proportional to the sizes of the powders. The surface roughness not only has a bad cosmetic appearance, but may affect the function or performance of the

parts. Hence, additional machining or polishing processes on the surface of as-fabricated parts by AM are usually necessary [2,15-17]. However, only a few studies have been reported on the laser polishing of AM metal parts. Ramos et al. [18] polished the SLS fabricated metal parts with a CO2 laser and achieved a roughness reduction up to 37% of the original arithmetical mean height of a line (Ra) with the laser energy density ranging from about 250 to 580 J/cm^2. Two laser macro polishing regimes were identified by Ramos: the shallow surface melting (SSM) and surface over-melting (SOM), based on the depth of the molten layer. Lamikiz et al. [19] polished the SLS parts and achieved a surface roughness reduction up to 80%, resulting in polished surfaces of 1.49 μm in Ra. Dadbakhsh et al. [20] polished LENS manufactured parts and achieved a surface roughness reduction of about 80% with the resulted surface roughness of 2 μm in Ra. Rosa et al. [21] studied the laser polishing of the LENS parts with complex and thin geometries, and achieved a surface roughness reduction up to 62% with a final surface roughness of 5.39 μm in the arithmetical mean height of a surface (Sa). The above studies mainly are based on the statistical Design of Experiment method using various laser processing parameters.

Recently, a new AM technology, laser foil printing (LFP), was developed by the authors [22]. In LFP, the metal foils, instead of powders, of different thicknesses are welded by laser, layer-by-layer, upon a substrate. The laser welding process in LFP operates in the keyhole-penetration mode which can achieve a good bonding quality. However, because of the inherent instability of the laser keyhole welding process, the top surface of the weld track is not very smooth, and the overlap between weld tracks may worsen the smoothness of the top surface.

The present work studies the laser polishing process of the metal parts during the LFP process, with both the experimental and the numerical means. The objective of this work is to parametrically study the polished tracks, to analyze the related physical processes of the laser macro polishing, and finally to determine appropriate processing parameters which could effectively suppress the surface roughness induced by the process of laser welding of foils. To this end, the single-line laser polished tracks were parametrically studied in the experiment, the temperature and fluid flow in melt pools were analyzed with a numerical model, which was validated by the experimental data of the melt pool widths and depths, and then the different overlap percentages of polished tracks were studied in the experiment. Finally, the decent result of large-area polished surfaces is presented with the determined polishing parameters of laser power, scan speed and overlap percentage.

2. EXPERIMENTAL PROCEDURE

2.1. MATERIAL AND EXPERIMENTAL SETUP

The AISI 1010 steel foils of thickness 150 μm (Precision Brand, UPC No. 16850) were used in this study, and the substrate is a common low-carbon steel plate of the thickness 6 mm.

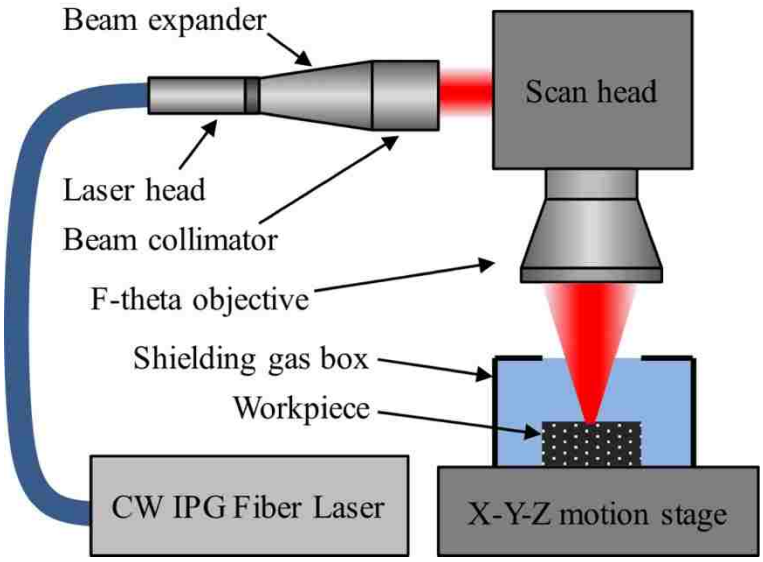

Figure 2.1. The experimental setup for the laser polishing process

The experimental setup is illustrated in Figure 2.1. The laser applied is a 1070-nm 1000-W continuous wave (CW) fiber laser (IPG Lasers, Model: YLR-1000-MM-WC-T11). The CW laser beam is directed into a scan head (ScanLab, HurryScan 30 mm) allowing for high-speed two-dimensional scanning, and focused by an F-theta lens with a focal length of 300 mm. The workpiece is fixed on an XYZ motion stage (Aerotech, Model: ATS 10060-H-M-80P-NC) which provides a motion resolution of 1 μm in the X and Y

directions and a 0.1 μm resolution in the Z direction. The laser, scanner and motion stage are integrated logically through a control program.

Note the same laser system and setup is used for both the laser welding and laser polishing processes, and the main differences between them are the processing parameters. Generally, a lower laser power, a larger beam size and a higher overlap percentage are used in the polishing process. The laser beam size is adjusted by changing the offset distance between the working plane and lens focal plane. In this study, the beam diameter is 170 μm for the laser welding process and 356 μm for the laser polishing process. During the laser welding and polishing processes, the workpiece is protected from oxidation in a top-open box filled with the argon gas flow.

The sample surface topographies before and after the polishing process were measured with a Wyko NT9100 white light interferometer having a 1 nm height measurement resolution in the VSI mode. And some samples were sectioned, grounded and polished with diamond particles of 3 μm in diameter, cleaned with ethanol, and finally etched with a solution of 2% Nitral for about 15 s. The etched cross-sections were examined under an optical microscope at a magnification of up to 500X.

2.2. RESEARCH METHODOLOGY

Prior to the laser polishing experiments, the samples were prepared with the foil welding process [22]. During the welding process, a steel foil of the thickness 150 μm was anchored on a steel substrate of thickness 6 mm by laser spot welding, and then a full bond between foil and substrate was formed through the raster-scan laser welding process. The spot welds were laid on a square grid and centered 3 mm apart from each other. The laser parameters of spot welding are the laser power of 390 W and the irradiation time of 6

millisecond. The rectangular welding pattern has a dimension of 16 mm × 12 mm, which is generated with the raster-scan lines with an interspace of 100 μm. The processing parameters are the laser power of 500 W and the scan speed of 250 mm/s.

The experimental study of the laser polishing process comprises two steps: the single-line polishing tests and the overlapped-lines areal polishing tests. In the first step, a parametric study of the single-line polished tracks was conducted with different laser powers and scan speeds. And shown in Table 2.1 are the tested parameter values, with totally 20 combinations. The surface morphologies by the single-line polished tracks were examined, and the parametric dependence of the polished track size (width and depth) was analyzed. Meanwhile, the numerical analysis of the single-line polishing process was carried out, which takes into account of the heat transfer and fluid flow behavior in the material. In the second step of the overlapped-lines areal polishing tests, different overlap percentages were studied, with the selected laser power and scan speed from single-line tests. The final polishing parameter combination was determined basing on the final surface topography and the polishing speed.

Table 2.1. Experimental design used for single-line polishing tests

Laser power (W)	170, 225, 280, 335, 390
Scanning speed (mm/s)	100, 200, 400, 800

3. MATHEMATICAL MODEL

In order to examine the temperature distribution and fluid flow in the melting pool during a laser polishing process, a three-dimensional mathematical model of the single-line laser polishing process was developed, taking into account of the physical processes of heat transfer and fluid flow in material. The computing domain is a rectangular block of workpiece. A laser beam radiation moves along a straight line and provides an incident flux of thermal energy at the top surface of workpiece. The metal is heated, melted and re-solidified. Different than the laser welding process [23−26], there is no significant keyhole-penetration phenomenon occurring in the laser polishing process. So, the melting pool surface is assumed flat in the model, and the effort of tracking the free surface of melting pool can be saved in the simulation. However, the fluid flow in melting pool must be taken into account because the convection in melting pool have profound impacts on the melting pool size, especially on the penetration depth. In the melting pool of a laser polishing process, the main driving forces of convection include buoyancy (or gravity) force and thermal capillary (or surface tension gradient) force. Besides, the heat loss due to the evaporation effect is considered in the model but the influence of recoil pressure is ignored.

3.1. GOVERNING EQUATIONS

From the above considerations, the mathematical model describing the laser polishing process is based on three basic partial differential equations: the mass conservation equation, the momentum conservation (or Navier-Stokes) equation, and the energy conservation equation.

Mass Conservation:

$$\vec{\nabla} \cdot \vec{u} = 0, \tag{1}$$

where $\vec{u}$ is the velocity vector field. And the fluid here is considered incompressible.

Momentum Conservation:

$$\rho\left(\frac{\partial \vec{u}}{\partial t} + \vec{u} \cdot \left(\vec{\nabla}\vec{u}\right)\right) = \vec{\nabla} \cdot \left[-pI + \mu\left(\vec{\nabla}\vec{u} + \left(\vec{\nabla}\vec{u}\right)^T\right)\right] - \rho\beta_l\vec{g}\left(T - T_{\text{melting}}\right) - K\vec{u}, \tag{2}$$

where ρ is the fluid density, t the time, p the pressure, I the identity matrix, μ the dynamic viscosity, $(\cdot)^T$ the matrix transpose operation, β_l the coefficient of thermal expansion of the liquid molten metal, $\vec{g}$ the gravity acceleration vector, T_{melting} the melting temperature of material, $K\vec{u}$ the Darcy damping force to cancel the velocity if the temperature is lower than the melting temperature, and K the isotropic permeability in mushy zone. Note that the fluid density is assumed constant in the continuity equation and the inertia of momentum equation, and that buoyance force due to density change is included through the Boussinesq approximation. The thermal capillary force is not added as a volumetric term in the momentum equation, but as a boundary condition on the top surface.

Energy Conservation:

$$\rho c_{\text{p}}^{\text{eq}}\left[\frac{\partial T}{\partial t} + \vec{\nabla} \cdot (\vec{u}T)\right] = \vec{\nabla} \cdot \left(\lambda\vec{\nabla}T\right), \tag{3}$$

where c_{p}^{eq} is the equivalent specific heat, T the temperature, λ the thermal conductivity. Note the heat source and sinks due to laser irradiation, thermal radiation and surface convection were setup as boundary conditions.

In Eq. (2), the isotropic permeability K is defined with the Carman-Kozeny equation:

$$K = -C_l\frac{(1-f_l)^2}{f_l^3+\varepsilon}, \text{ and } C_l = \frac{180}{d^2}, \tag{4}$$

where f_l is the volume fraction of the liquid phase, ε a small constant to avoid the division by zero, d is proportional to the dendrite dimension, which is assumed to be a constant and on the order of 10^{-2} cm. The volume fraction of liquid phase f_l is defined as

$$f_l = \begin{cases} 0 & \text{for} \quad T < T_s \\ \frac{T-T_s}{T_l-T_s} & \text{for} \quad T_s < T < T_l \\ 1 & \text{for} \quad T > T_l \end{cases}, \tag{5}$$

where T_s and T_l are the solidus and liquidus temperatures, respectively.

In Eq. (3), the equivalent specific heat $c_{\mathrm{p}}^{\mathrm{eq}}$ can be defined as:

$$c_{\mathrm{p}}^{\mathrm{eq}} = (1 - f_l)c_{\mathrm{p,\,s}} + f_l c_{\mathrm{p,\,l}} + L_f \frac{\exp\left(-\frac{\left(T-T_{\mathrm{melting}}\right)^2}{\left(T_{\mathrm{l}}-T_{\mathrm{s}}\right)^2}\right)}{\sqrt{\pi\left(T_{\mathrm{l}}-T_{\mathrm{s}}\right)^2}}, \tag{6}$$

where $c_{\mathrm{p,\,s}}$ and $c_{\mathrm{p,\,l}}$ are the specific heat of solid phase and liquid phase respectively, L_f the latent heat of fusion, and the fraction term after L_f is a normalized Gaussian function centered at the melting temperature T_{melting} and with a width of $(T_{\mathrm{l}} - T_{\mathrm{s}})$.

3.2. BOUNDARY CONDITIONS

On the top surface, the boundary conditions for the heat exchange and thermal capillary force are

$$k\frac{\partial T}{\partial z} = Q_{\mathrm{laser}} - Q_{\mathrm{radi}} - Q_{\mathrm{conv}} - Q_{\mathrm{evap}}, \tag{7}$$

$$\mu\frac{\partial \vec{u}_{\mathrm{x,\,y}}}{\partial z} = \tau_s = \frac{\partial \gamma}{\partial T}\nabla_{\mathrm{x,\,y}}T;\ u_z = 0, \tag{8}$$

where Q_{laser}, Q_{radi}, Q_{conv} and Q_{evap} are the heat source or sink at the top surface of metal due to the laser irradiation, thermal radiation, surface convection and material evaporation, respectively. τ_s is the temperature-dependent Marangoni shear stress in the XY plane of top surface, γ is the temperature-dependent surface tension.

The heat source of the laser irradiation, and the heat losses from the thermal radiation, surface convection and material evaporation can be written as:

$$Q_{\text{laser}} = \alpha_s I_{\text{laser}} = \alpha_s \frac{2P_{\text{laser}}}{\pi R_{\text{laser}}^2} \cdot \exp\left\{-\frac{2[(x-x_0-v_s t)^2+(y-y_0)^2]}{R_{\text{laser}}^2}\right\}, \quad (9)$$

$$Q_{\text{radi}} = \varepsilon\sigma(T^4 - T_\infty^4), \quad (10)$$

$$Q_{\text{conv}} = h_c(T - T_\infty), \quad (11)$$

$$Q_{\text{evap}} = L_v \dot{m}_v, \quad (12)$$

where α_s is the surface absorptivity of laser energy, I_{laser} the laser intensity, P_{laser} the laser power, R_{laser} the laser beam radius, x_0 and y_0 the initial coordinates of laser irradiation, v_s the scan speed of laser beam, ε the surface radiation emissivity with the same value as α_s, σ the Stefan-Boltzmann constant, T_∞ the ambient temperature, h_c the convective heat transfer coefficient between metal and the surroundings, L_v the latent heat of evaporation, and $\dot{m}_v$ the mass evaporation rate on the top surface. Here the mass evaporation rate can be deduced from the local temperature and the saturated vapor pressure.

$$\dot{m}_v = \sqrt{\frac{m}{2\pi k_b}} \frac{p_{\text{sat}}(T)}{\sqrt{T}}(1 - \beta_r), \quad (13)$$

$$p_{\text{sat}}(T) = p_a \exp\left[\frac{mL_v}{k_b T_{\text{vap}}}\left(1 - \frac{T_{\text{vap}}}{T}\right)\right], \quad (14)$$

where m is the atomic weight of iron, k_b the Boltzmann constant, p_{sat} the saturated vapor pressure, β_r the retrodiffusion coefficient, and p_a the ambient atmospheric pressure.

The symmetric boundary (y = 0) coincides with the centerline of laser polishing track. Other boundaries (bottom and lateral surfaces) are assumed as the surface heat convection, with the heat transfer coefficient h_c = 60 W/m^2/K, and no slip for fluid flow.

The surface tension is affected not only by temperature, but also by some surface-active elements such as O, S, Se, or Te. Here the pseudo-binary Fe-O system is assumed

in the simulation, and the surface tension, as a function of temperature T and oxygen concentration, f^{α}, is given by [27]

$$\gamma = 1.943 - 4.3\times10^{-4}(T-1700) - RT\times2.03\times10^{-8} \times\ln\left[1+0.0138f^{\alpha}\exp\left(\frac{1.46\times10^{8}}{RT}\right)\right], \quad (15)$$

where R is the ideal gas constant, f^{α} the oxygen concentration. In the laser polishing process of AISI 1010 steel, the oxygen concentration is assumed to be 300 ppm.

Besides, the thermophysical properties of workpiece are listed in Table 3.1. The overall numerical model was built and computed in the COMSOL Multiphysics software.

Table 3.1. Thermophysical properties of workpiece

Property (unit)	**Symbol**	**Value or reference**
Thermal conductivity of solid/liquid (W/m/K)	λ_s/λ_l	$f(T)$[28] / $3.75\times10^{-3}T$+22
Density of solid/liquid (kg/m^3)	ρ_s/ρ_l	7870 / 7870
Specific heat of solid/liquid (J/kg/K)	$c_{p,s}/c_{p,l}$	$f(T)$[28] / 573
Dynamic viscosity of liquid (Pa·s)	μ	6×10^{-3}
Latent heat of fusion (J/kg)	L_f	2.54×10^{5}
Latent heat of vaporization (J/kg)	L_v	6.34×10^{6}
Solidus temperature (K)	T_s	1670
Liquidus temperature (K)	T_l	1730
Melting temperature (K)	T_m	1700
Vaporization temperature (K)	T_{vap}	3100
Thermal expansion coefficient of liquid (1/K)	β_l	4.95×10^{-5}
Atomic mass of iron (kg)	m	9.27×10^{-27}
Retrodiffusion coefficient of vapor atom (1)	β_r	0.1

4. RESULTS AND DISCUSSION

4.1. INITIAL TOPOGRAPHY ANALYSIS

Figure 4.1 shows the microscopic photo and surface topography of the surface of a sample after the foil welding process. In Figure 4.1(a), it can be seen that the surface is covered with the periodic overlapped weld tracks along the horizontal direction and the irregular re-solidified melt spatters/spillages. Presented in Figure 4.1(b) is the surface topography measured from the initial weld surface. The linear surface roughness along the X direction (perpendicular to the weld tracks) is measured as R_a = 3.78 μm, and the areal surface roughness was measured as S_a = 3.77 μm. From the microscopic image and the measured topography, there can be concluded three kinds of surface asperities on the weld surface, which are the weld tracks, the melt spillage aside of weld tracks, and the fine ripples on the weld tracks.

Furthermore, Figure 4.2(a) presents the averaged spatial spectrum in the X direction, which is the average value of the spatial spectra of all parallel linear surface profiles. It can be seen that the major surface roughness is located at the low spatial frequency range, which means that the major roughness components are the relative large surface structures of melt spillages and overlapped weld ridges. Especially, the significant peak at the spatial frequency f = 10 [1/mm] represents the periodic overlap of weld tracks with a successive displacement of 100 μm. Figure 4.2(b) is one of the linear surface profiles in the X direction extracted from Figure 4.1(b), and Figure 4.2(c) is the averaged profile of all linear surface profiles in X direction. The periodic ridge structure of the overlapped weld tracks can be clearly observed, and the amplitude of the periodic ridges is about 4

μm, while the magnitude of the solidified spillage or spatter could reach 15 μm in Figure 4.2(b), where the mean value of the curve is adjusted to zero.

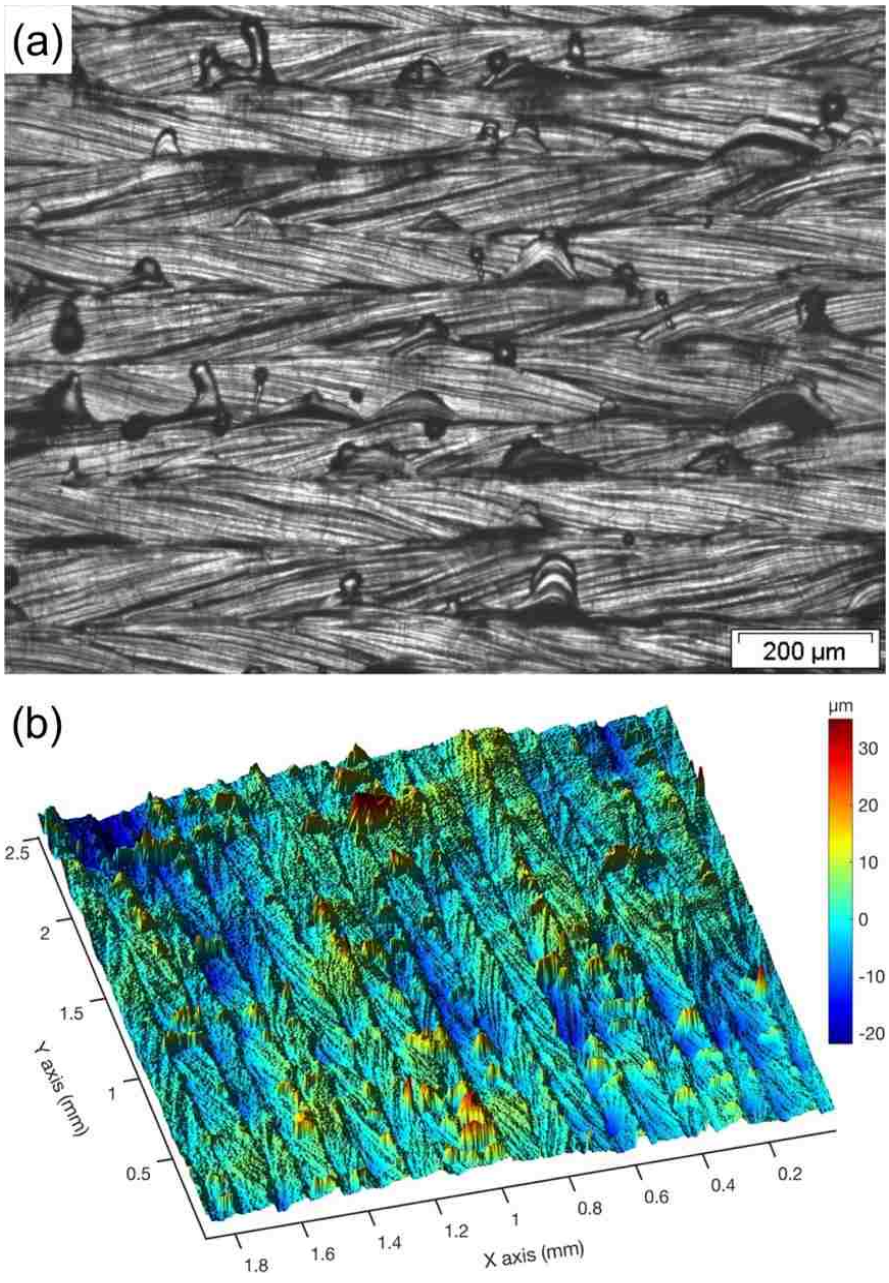

Figure 4.1. The (a) microscopic photo and (b) the 3d topography of the initial surface from the foil welding process

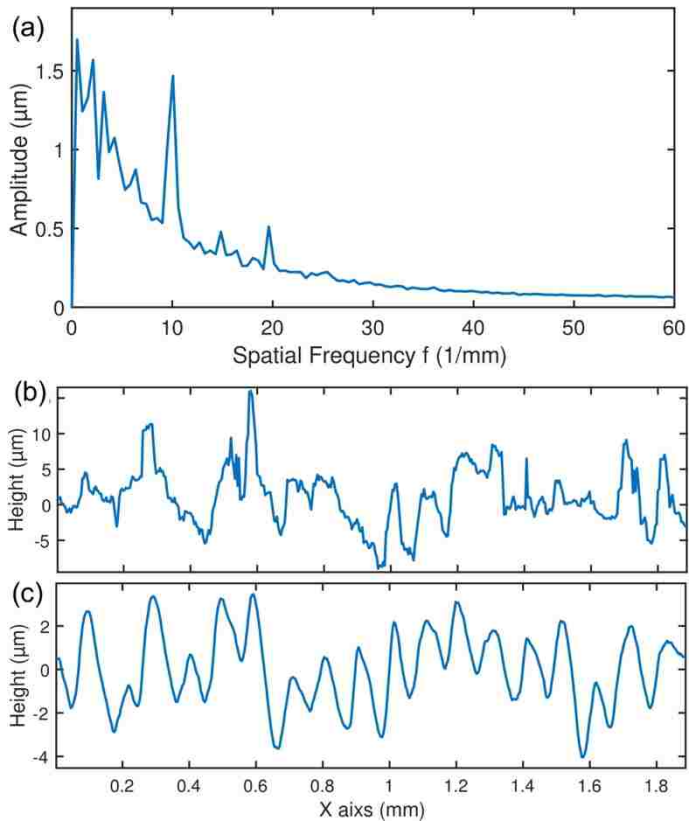

Figure 4.2. (a) A line profile of the initial surface with the direction perpendicular to the laser welding direction. (b) The spatial frequency spectra of 900 line profiles of the initial surfaces

4.2. SINGLE-LINE POLISHING TESTS

The single-line laser polishing tests were conducted with various laser powers (P) and laser scan speeds (V) but a fixed beam spot size of 356 μm in diameter. Some typical results of the top surface and the transverse cross-section of polished tracks are shown in Figure 4.3. The polished tracks are perpendicular to the initial weld tracks. The scale bars in the surface images are 200 μm, and the scale bars in the cross-section images are 100 μm.

The polished track in Figure 4.3(a), by P = 170 W and V = 800 mm/s, is very thin and not continuous, and the melted zone is not obvious in the corresponding cross-section

image. The surface roughness got no improvement in this test, and the incident laser energy is obviously too low. The polished track in Figure 4.3(b), by P = 170 W and V = 400 mm/s, is continuous with a width of 112 μm and the melted zone depth is 14 μm from the cross-section image. The fine ripples covering the weld tracks got removed in this test, but the periodic ridge structure of the overlapped weld tracks was not improved much. The polished track in Figure 4.3(c), by P = 225 W and V = 200 mm/s, has a track width of 218 μm and a melted depth of 33 μm. The surface roughness looks better than that in Figure 4.3(b), but the periodic ridges still leaves some influence on the polished surface. The polished track in Figure 4.3(d), by P = 335 W and V = 200 mm/s, has a track width of 300 μm and a melted depth of 52 μm. The initial surface asperities are completely removed in this case, but the polished track was covered with martensitic needles. According to Ref. [29], the generation of martensitic needles on melted surface is due to the high cooling rate of the laser polishing process. The polished track in Figure 4.3(e), by P = 335 W and V = 100 mm/s, has a polished width of 360 μm and a melted depth of 71 μm. The incident laser energy seems too much, and the melted material gets decarburized, which is accompanied with significant vaporization of material [10,14]. Besides, the polished track gets slightly skewed in this case, because the generated vapor could affect the propagation of the laser beam.

In the previous research of laser polishing [18], two different polishing regimes were identified and discussed, which are the surface shallow melting (SSM) and the surface over melting (SOM) modes. The melting depth in the SSM mode is usually less than the typical peak-to-valley height of the surface asperities, while the melting depth in the SOM mode is greater than the peak-to-valley height, and the initial surface asperities can be

completely eliminated in the SOM mode. In general, the SOM mode is found to be more effective to remove the surface asperities than the SSM mode [30]. For the tests shown above, the polishing processes in Figure 4.3(a, b, c) should work in the SSM mode, and the polishing process of Figure 4.3(d, e) should work in the SOM mode.

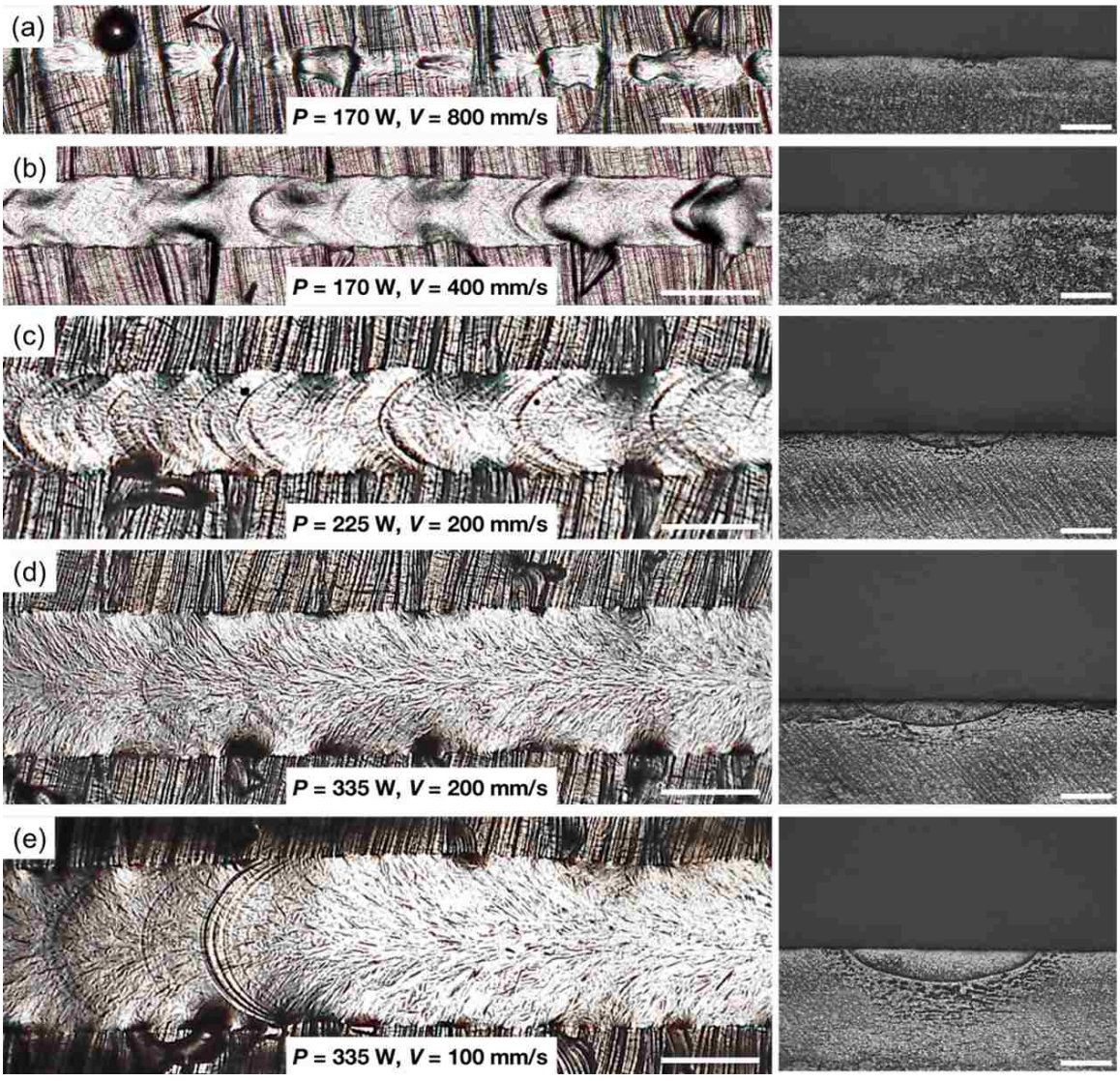

Figure 4.3. The (a - e) top surfaces and corresponding cross-sections of some single-line polishing tracks

For a laser polishing process, the polished surface quality involves a lot of factors including initial surface condition, workpiece thermal and optical properties, laser power, scan speed, beam size, beam shape, overlap ratio, number of passes, etc. Therefore, it is very difficult to study it thoroughly, and many studies are based on the statistical Design of Experiment method, which is very pragmatic but cannot reveal the underlying physical processes.

However, through the single-line laser polishing tests, we think that the polished surface quality should strongly relate to the polished track size, i.e. the track width and the melted depth. Furthermore, the track width should relate to the range of spatial frequency of surface asperities that can be effectively removed, and the melted depth should relate to the range of the vertical magnitude of asperities that can be effectively removed. Therefore, it is necessary to study the relationship between the polished track size and the laser polishing parameters (the laser power and scan speed).

In the parametric study about the polished track size, the selected laser powers and scan speeds are listed in Table 2.1, and there are total 20 parameter combinations. The measurement results (mean value and standard deviation) of the width and depth of polished tracks are presented in Figure 4.4 and 4.5. In the figures, the solid symbols (circle, triangle, square and pentagon) represent experimental data, and the void symbols with the same shapes represent the corresponding simulation results for the model validation.

Shown in Figure 4.4 are the polished track widths produced by all combinations of the laser power and scan speed. It is obvious that the width of polished track increases as the laser power increases, and decreases as the scan speed increases. But the dependence

is not linear. With the laser power increasing, the increasing rate of track width gets slow because of the limit of beam size and the increasing heat conduction loss.

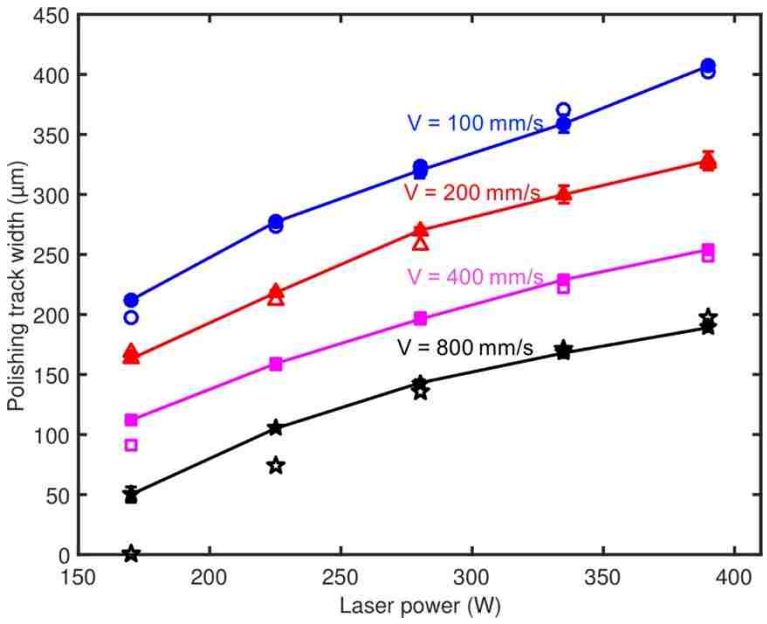

Figure 4.4. The experimental measurements (solid symbols) and the simulation results (void symbols) of the polished track width by the various combinations of the laser power and scan speed

Shown in Figure 4.5 are the melted depths of polished tracks produced by different parameter combinations. The melted depth also increases with the laser power, and decreases as the scan speed increases. Note that, for the scan speed of 800 mm/s, the increasing rate of melted depth increases from the laser power of 170 W to 335 W. This should be due to the effect of fluid convection in the melting pool. When the incident laser energy is very small, the melting pool is too shallow to let the convection flow exists. As the laser power get higher and the melting pool get deeper, the positive impact of the convection flow on the melting depth get significant, because the convection flow can efficiently bring the heat from the surface to the bottom of melting pool and deepen the

depth. Also note that, for the scan speed of 100 mm/s, the increasing rate of melted depth does not get slower when the laser power increases from 225 W to 390 W. This should be due to the influence of vaporization of material. As the incident laser energy get high enough, the vaporization gets significant, and the accompanying recoil pressure could help to deepen the melting pool depth.

4.3. TEMPERATURE DISTRIBUTION AND FLUID FLOW IN THE MELTING POOL

In order to further understand the underlying physical processes during laser polishing, a numerical mode was developed and analyzed, where the temperature distribution and fluid flow in the melting pool is studied. The actual laser absorptivity during laser polishing process is unknown, which depends on the initial surface condition, the material temperature and phase state. In this numerical model, two absorption coefficients are assumed, one (α_s) is for the solid phase and one (α_l) for the liquid phase, since the absorptivity usually has a jump during the melting transition. In order to make the numerical simulation approach the actual experiment as good as possible, the two absorption coefficients were carefully adjusted to make the polished track width and melted depth from the simulations are close to the those from the experiment. Finally, the two absorption coefficients were determined as $\alpha_s = 0.205$ and $\alpha_l = 0.385$.

The polished track width and melted depth from the simulation are also shown in Figure 4.4 and Figure 4.5 (void markers), accompanying the experimental results (solid markers). Generally, the simulation results are in a good agreement with the experiment, except for some deviations of the condition V = 800 mm/s. These deviations should be caused by the simplification of laser radiation absorptivity in the model. For the low laser

powers with the scan speed 800 mm/s, the absorption coefficients could be higher than the setting in the model because of the initial roughness condition.

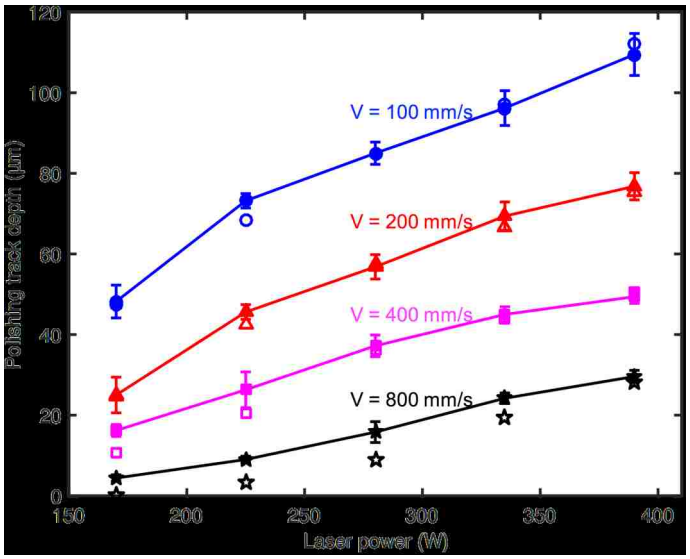

Figure 4.5. The experimental measurements (solid symbols) and the simulation results (void symbols) of the polished track depth by the various combinations of the laser power and scan speed

Shown in Figure 4.6 are the iso-surfaces of temperature field and the streamline of fluid flow in a moving melting pool generated with $P = 390$ W and $V = 200$ mm/s. The iso-surfaces of temperature field have a shape of bowl. The streamlines form a series of vortices near the edge of melting pool, and generate the complex whirlpool convection near the tail part of melting pool. Correspondingly, the temperature distribution and the vector field of fluid flow at the top surface of melting pool are shown in Figure 4.7(a), and the temperature distribution and the fluid flow field of the cross-section along the centerline of polished track are shown in Figure 4.7(b). The maximum temperature in the melting pool is 3009 K, and the maximum flow speed is 2.47 m/s. In Figure 4.7(a), the melting pool has a teardrop shape, and the flow at the melting pool surface is driven by the thermal-capillary

effect. In Figure 4.7(b), two major vortices are formed near the tail of melting pool. The two vortices create a downward flow which brings the surface hot melt downward and improves the depth of melting pool.

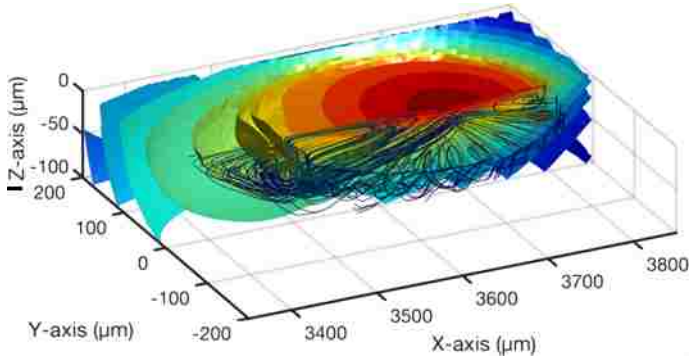

Figure 4.6. The iso-surfaces of temperature field and the streamline of fluid flow in the melting pool during the laser polishing process with P = 390 W and V = 200 mm/s

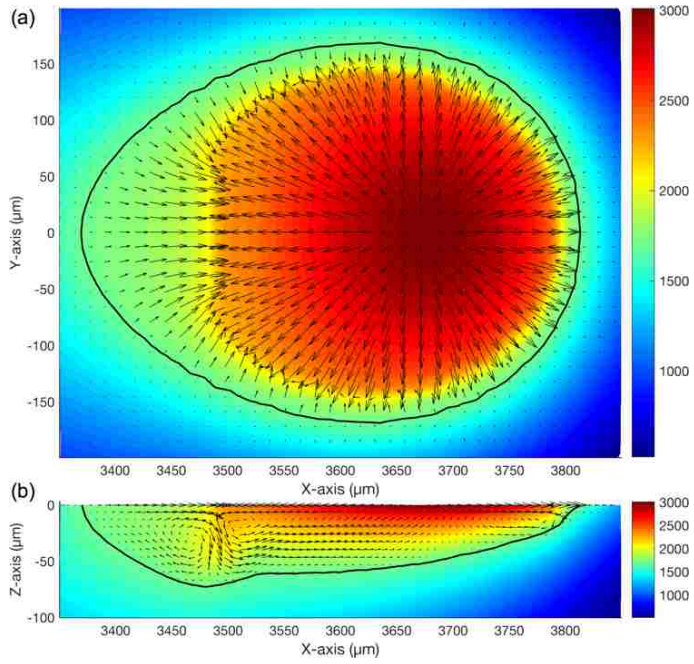

Figure 4.7. The temperature distribution and the vector field of fluid flow at (a) the top surface of melting pool and (b) the cross-section along the centerline of polishing track during the polishing process with P = 390 W and V = 200 mm/s

The maximum values of temperature field produced by different parameter combinations are presented in Figure 4.8. The maximum value of temperature can indicate what state the melting pool is in, not formed, just formed or having significant vaporization. The melting temperature and vaporization temperature are 1700 K and 3100 K, respectively, in the numerical model. In Figure 4.8, the maximum temperature of V = 800 mm/s and P = 170 W is 1595 K, less than the melting temperature. The maximum temperature of V = 100 mm/s and P = 390 W is 3264 K, higher than the vaporization temperature. And the maximum temperature of V = 100 mm/s and P = 335 W power is 3097 K which is roughly equal the vaporization temperature. The maximum temperatures by other parameter combinations are between the melting temperature and evaporation temperature. Note that there are two jumps of the increasing rate of maximum temperature at the (V = 800 mm/s, P = 280 W) and (V = 400 mm/s, P = 225 W), which should be due to the absorptivity change. When the melting pool is not formed or just formed, the overall absorptivity is close to α_s, and as the melting pool expands, the overall absorptivity quickly increases to α_l.

The maximum values of convection flow speed produced by different parameter combinations are presented in Figure 4.9. The maximum value of flow speed indicates the convection strength in the melting pool. When the melting pool is just formed the convection flow is very weak, but as the melting pool expands with the increasing incident laser energy, the convection flow speed increases quickly. Therefore, two increasing-rate jumps of the maximum flow speed can be observed in the at the parameter combinations of (V = 800 mm/s, P = 280 W) and (V = 400 mm/s, P = 225 W). When the melting pool expands to certain extent, the influence of thermal capillary effect on the convection flow

speed has a limit, and in this model, the limit of the maximum flow speed is around 2.5 m/s. In Figure 4.9, as the incident laser energy increases, the maximum flow speed approaches the limit value. However, in the experiment condition, the convection flow speed could be further increased with the increasing incident energy, because of the influence of the recoil pressure from vaporization.

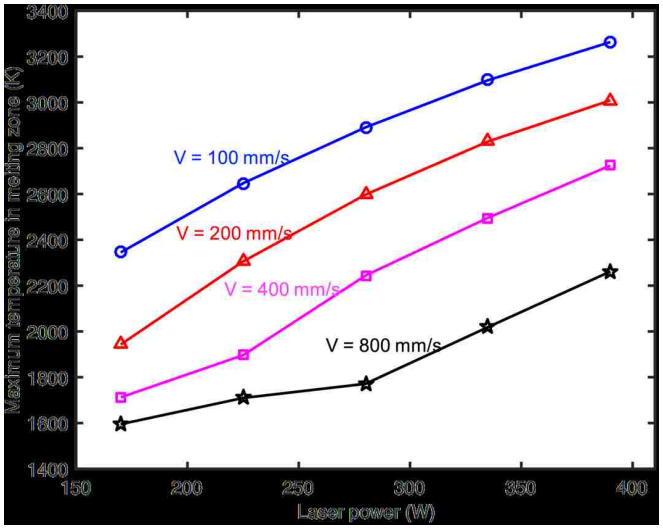

Figure 4.8. The maximum values of temperature field produced by various combinations of the laser power and scan speed

From the above analyses of the experiment and simulation results, the polished tracks are expected to have a large width and a decent melted depth in order to effectively remove the long-wavelength asperities and large-magnitude asperities. However, it is necessary to keep the maximum temperature of the melting pool below the vaporization temperature, because the boiling effect could make the melting pool surface very unstable and decay the resolidified surface. From the aspect of polishing efficiency, a relatively high scan speed is preferred. Besides, the high scan speed can lower the unnecessary heat conduction loss, improve the melting efficiency and reduce the thermal distortion in some

degree. Finally, the laser power of 390 W and scan speed of 200 mm/s are selected for further areal polishing tests, which result in the polished track with of 330 μm and the melted depth of 57 μm.

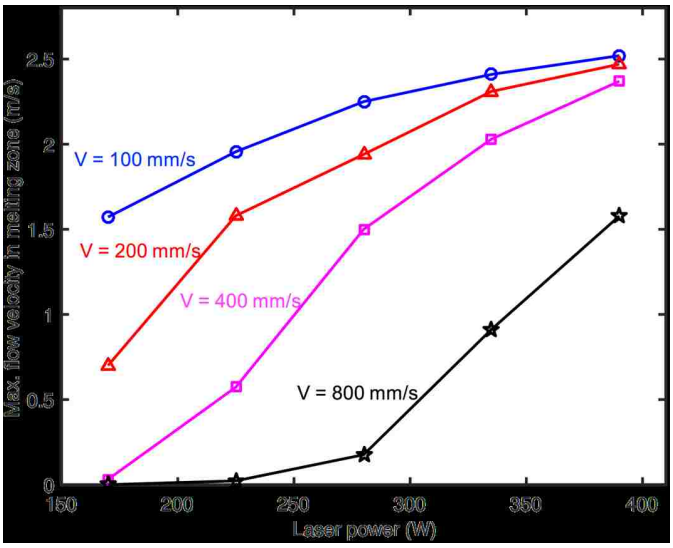

Figure 4.9. The maximum flow speeds in the melting pool for various combinations of the laser power and scan speed

4.4. MULTI-LINES SURFACE POLISHING TESTS

In the actual laser polishing process, the polished surface is composed of many overlapped polished tracks. The overlapping process of polished tracks could effectively reduce or eliminate the roughness or waviness in the transverse direction of polished tracks. And the overlap percentage of polished tracks can have a significant effect on the final surface quality [31]. In this part, the successive track displacements of 150, 100, 50 and 25 μm were tested for the multi-lines areal polishing process, which correspond to the overlap percentage of 55%, 70%, 85% and 92%, respectively.

Shown in Figure 4.10(a) is the microscopic image of multi-line polished surface, where the overlap percentage of polished tracks is 85%. The polished surface looks smooth

and uniform but has a clear periodic stripe pattern from the overlapped tracks. Shown in Figure 4.10(b) is the corresponding three-dimensional topography of the polished surface. The direction of polished tracks coincides with the Y axis. The surface roughness by the periodic stripe pattern of overlapped tracks is insignificant in the topography. And the major surface asperities from the topography measurement are the martensitic structure, which is induced by the rapid cooling process in laser polishing. The final surface roughness of the polished surface is measured as 0.578 μm in both *R*a and *S*a.

Shown in Figure 4.11(a) is a linear surface profile extracted from Figure 4.10(b) in the direction parallel to the X axis. The surface is generally very smooth except for the slight waviness. And the averaged spatial spectrum of the all parallel linear profiles is presented in Figure 4.11(b), accompanied with the average spatial spectrum of the initial surface. Comparing the spatial spectra, the magnitude of surface asperities is significantly reduced by the laser polishing process, especially at the low spatial frequency range. The periodic weld ridges and solidified spatters and spillages are completely removed through the laser polishing process.

In the polishing tests with the overlap percentages of 55%, 70%, 85% and 92%, the resulted surface roughness is 1.33, 0.843, 0.578 and 0.575 μm in *S*a, respectively. It is obvious that the surface roughness is gradually improved with the increasing overlap percentages. As the overlap percentage increases from 85% to 92%, the polished surface quality only gets a slight improvement, because, with the overlap percentage of 85%, the major asperities of initial surface have been completely removed and the periodic overlap pattern does not introduce new roughness significantly, as shown in Figure 4.10(b) and Figure 4.11(b). However, the polishing process time would double as the overlap

percentage increase from 85% to 92%. Therefore, the final polishing parameter set of the laser power of 390 W, scan speed of 200 mm/s and overlap percentage of 85%, was applied to polish the surface roughness from the laser raster-scan welding process. Figure 4.12 shows a comparison of the initial weld surface and the polished surface, where the upper left inset is the photo of sample.

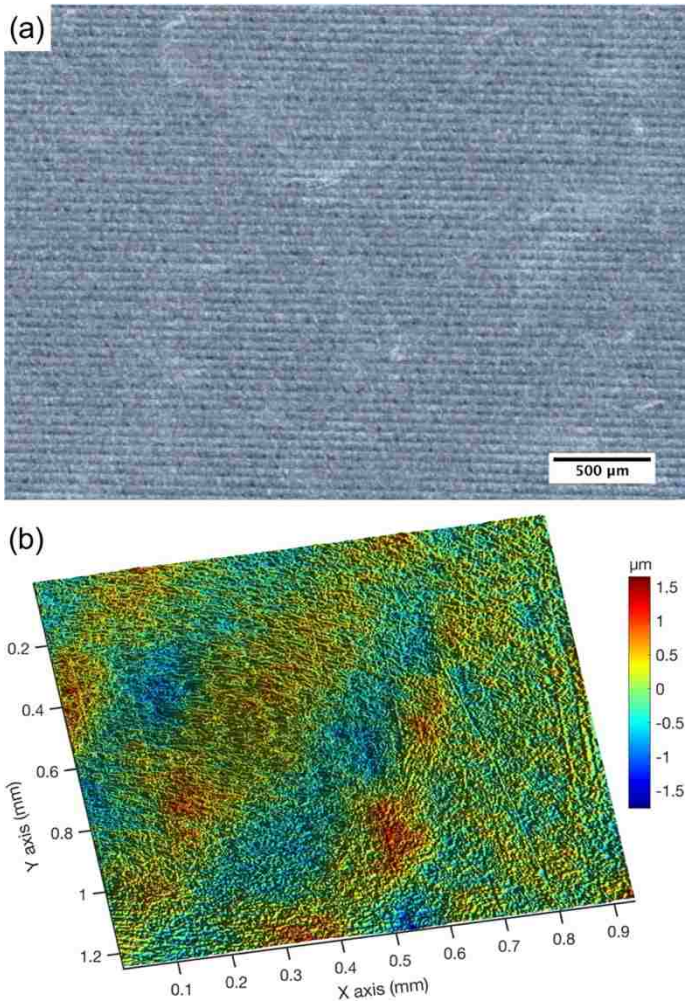

Figure 4.10. The (a) photo and (b) three-dimensional topography of the polished surface produced by the multi-line polishing process with the overlap percentage of 85%

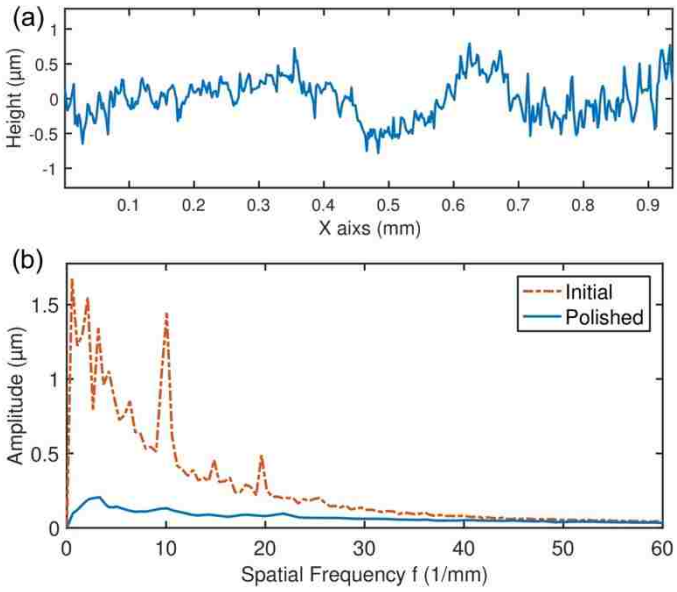

Figure 4.11. (a) A linear surface profile in the transverse direction of polished tracks and (b) the averaged spatial frequency spectra before and after the laser polishing process

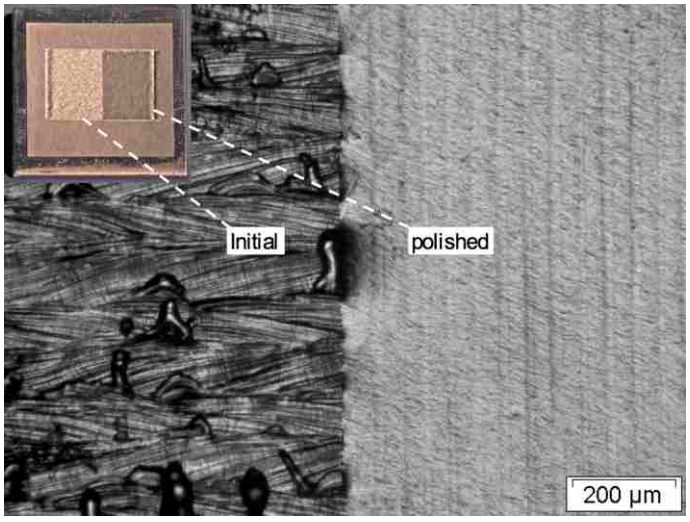

Figure 4.12. Comparison of the initial surface (left half) produced by laser welding and the polished surface (right half)

5. CONCLUSION

The laser polishing process for the Laser Foil Printing technology was studied in this paper, with the objective to suppress or remove the surface roughness produced by the raster-scan laser welding process. The experimental study contains two parts: the single-line laser polishing tests and the multi-line laser polishing tests, with the objective to determine the appropriate polishing parameters of the laser power, scan speed and overlap percentage. Besides, a numerical model was developed to analyze the heat transfer and fluid flow behavior of the moving melting pool in the laser polishing process.

The initial weld surface is covered with the overlapped weld tracks, and the major surface asperities are the periodic weld ridges and the melt spatters and spillages aside of weld tracks. The initial surface roughness is measured as 3.78 μm in *R*a and 3.77 μm in *S*a. In the single-line laser polishing tests, as the incident laser energy increases, the polishing process transits from the SSM mode to the SOM mode. And as the laser energy increase further, the vaporization of material would become significant and the decarburization phenomenon would present. Based on the single-line polishing tests, the polishing quality is considered to be related to the polished track width and the melted depth. In detail, the polished track width should relate to the range of spatial frequency of surface asperities that can be effectively removed, and the melted depth should relate to the range of the vertical magnitude of asperities that can be effectively removed. In the parametric study about the polished track width and the melted depth, the single-line polishing tests of 20 parameter combinations of the laser power and scan speed were conducted. It was found the laser power and scan speed have significant influences on the polished width and the melted depth. In the numerical analysis of the single-line laser polishing process, the

temperature field and convection flow pattern in the melting pool was presented, the melting pool has a water-drop shape on the surface, and the thermocapillary-driven convection flow creates two significant vortices near the tail of melting pool, and the vortices form a downward flow which brings the surface hot melt to the bottom of melting pool, enhancing the melting depth. In the parametric study about the maximum temperature and convection flow speed of melting pools, the different states of melting pool can be recognized, not formed, just formed or having significant vaporization, and the maximum speed of convection flow driven by the thermocapillary effect is found to have a limit of about 2.5 m/s. In the multi-lines surface polishing tests, it is shown that the final surface roughness decreases as the overlap percentage of polished tracks increases. Finally, the polishing parameters selected for the weld surface in LFP are the laser power of 390 W, the scan speed of 200 mm/s and the overlap percentage of 85%. And the surface roughness is reduced from 3.77 μm to 0.578 μm in *S*a.

ACKNOWLEDGEMENTS

The authors would like to acknowledge the financial support by the Department of Energy (Grant No. DE-FE0012272) and the University of Missouri System (Award No. FastTrack-16002R).

BIBLIOGRAPHY

[1] Tokarev, V. N., Wilson, J. I. B., Jubber, M. G., John, P., and Milne, D. K., 1995, "Modelling of self-limiting laser ablation of rough surfaces: application to the polishing of diamond films," Diamond Relat. Mater., **4**(3), pp. 169-176.

[2] Ramos, J. A., Bourell, D. L., and Beaman, J. J., 2002, "Surface over-melt during laser polishing of indirect-SLS metal parts," Mater. Res. Soc. Symp. Proc. 758, LL1.9 (2002).

[3] Kim, Y. G., Ryu, J. K., Kim, D. J., Kim, H. J., Lee, S., Cha, B. H., Cha, H., and Kim, C. J., 2004, "Microroughness reduction of tungsten films by laser polishing technology with a line beam," Jpn. J. Appl. Phys., **43**(4R), pp. 1315.

[4] Mai, T. A., and Lim, G. C., 2004, "Micromelting and its effects on surface topography and properties in laser polishing of stainless steel," J. Laser Appl., **16**(4), pp. 221-228.

[5] Hua, M., Shao, T. M., and Tam, H. Y., 2009, "Surface modification of DF-2 tool steel under the scan of a YAG laser in continuously moving mode," J. Mater. Process. Technol., **209**(10), pp. 4689-4697.

[6] Perry, T. L., Werschmoeller, D., Duffie, N. A., Li, X., and Pfefferkorn, F. E., 2009 "Examination of selective pulsed laser micropolishing on microfabricated nickel samples using spatial frequency analysis," J. Manuf. Sci. Eng., **131**(2), pp. 021002.

[7] Perry, T. L., Werschmoeller, D., Li, X., Pfefferkorn, F. E., and Duffie, N. A., 2009, "The effect of laser pulse duration and feed rate on pulsed laser polishing of microfabricated nickel samples," J. Manuf. Sci. Eng., **131**(3), pp. 031002.

[8] Temmler, A., Graichen, K., and Donath, J., 2010, "Laser polishing in medical engineering," Laser Tech. J., **7**(2), pp. 53-57.

[9] Ukar, E., Lamikiz, A., López de Lacalle, L. N., del Pozo, D., and Arana, J. L., 2010, "Laser polishing of tool steel with CO2 laser and high-power diode laser," Int. J. Mach. Tools Manuf., **50**(1), pp. 115-125.

[10] Ukar, E., Lamikiz, A., Martínez, S., Estalayo, F., and Tabernero, I., 2013, "Laser polishing of GGG70L cast iron with 2D scan-head," Procedia Eng., **63**, pp. 53-59.

[11] Bordatchev, E. V., Hafiz, A. M. K., and Tutunea-Fatan, O. R., 2014, "Performance of laser polishing in finishing of metallic surfaces," Int. J. Adv. Manuf. Technol. 73, pp. 35-52.

[12] Ukar, E., Lamikiz, A., Liébana, F., Martínez, S., and Tabernero, I., 2015, "An industrial approach of laser polishing with different laser sources," Materialwiss. Werkstofftech., **46**(7), pp. 661-667.

[13] Poprawe R., 2011, *Tailored light 2*, Springer, Berlin, Heidelberg, Chap. 11.

[14] Temmler, A., Willenborg, E., and Wissenbach, K., 2012, "Laser polishing," Proc. of SPIE. **8243** pp. 82430W-13.

[15] Kamran, M., and Neil, H., 2009, "Top surface and side roughness of inconel 625 parts processed using selective laser melting," Rapid Prototyping J., **15**(2), pp. 96-103.

[16] Calignano, F., Manfredi, D., Ambrosio, E. P., Iuliano, L., and Fino, P., 2013, "Influence of process parameters on surface roughness of aluminum parts produced by DMLS," Int. J. Adv. Manuf. Technol., **67**(9), pp. 2743-2751.

[17] Strano, G., Hao, L., Everson, R. M., and Evans, K. E., 2013 "Surface roughness analysis, modelling and prediction in selective laser melting," J. Mater. Process. Technol., **213**, pp. 589-597.

[18] Ramos-Grez, J. A., and Bourell, D. L., 2004, "Reducing surface roughness of metallic freeform-fabricated parts using non-tactile finishing methods," Int. J. Mater. Prod. Technol., **21**, pp. 297-316.

[19] Lamikiz, A., Sánchez, J.A., López de Lacalle, L.N., and Arana, J.L., 2007, "Laser polishing of parts built up by selective laser sintering," Int. J. Mach. Tools Manuf., **47**(12–13), pp. 2040-2050.

[20] Dadbakhsh, S., Hao, L., and Kong, C. Y., 2010, "Surface finish improvement of LMD samples using laser polishing," Virtual Phys. Prototyp., **5**(4), pp. 215-221.

[21] Rosa, B., Mognol, P., and Hascoët, J.-y., 2015, "Laser polishing of additive laser manufacturing surfaces," J. Laser Appl., **27**(S2), pp. S29102.

[22] Chen, C., Shen, Y., and Tsai, H.L., 2017, "A foil-based additive manufacturing technology for metal parts," J. Manuf. Sci. Eng., **139**(2), pp. 024501.

[23] Wang, Y., Shi, Q., and Tsai, H. L., 2001, "Modeling of the effects of surface-active elements on flow patterns and weld penetration," Metall. Mater. Trans. B, **32** pp. 145-161.

[24] Zhou, J., Tsai, H. L., and Wang, P.-C., 2006, "Transport phenomena and keyhole dynamics during pulsed laser welding," J. Heat Transfer, **128**(7), pp. 680.

[25] Zhou, J., and Tsai, H. L., 2008, "Modeling of transport phenomena in hybrid laser-MIG keyhole welding," Int. J. Heat Mass Transfer, **51**, pp. 4353-4366.

[26] Rao, Z. H., Zhou, J., Liao, S. M., and Tsai, H. L., 2010, "Three-dimensional modeling of transport phenomena and their effect on the formation of ripples in gas metal arc welding," J. Appl. Phys., **107**, pp. 28-31.

[27] Sahoo, P., Debroy, T., and McNallan, M. J., 1988, "Surface tension of binary metal—surface active solute systems under conditions relevant to welding metallurgy," Metall. Trans. B, **19**(3), pp. 483-491.

[28] Schenk, T., Richardson, I. M., Kraska, M., and Ohnimus, S., 2009, "Modeling buckling distortion of DP600 overlap joints due to gas metal arc welding and the influence of the mesh density," Comput. Mater. Sci., **46**(4), pp. 977-986.

[29] Nüsser, C., Kumstel, J., Kiedrowski, T., Diatlov, A., and Willenborg, E., 2015, "Process- and material-induced surface structures during laser polishing," Adv. Eng. Mater., **17**(3), pp. 268-277.

[30] Chow, M. T. C., Bordatchev, E. V., and Knopf, G. K., 2013, "Experimental study on the effect of varying focal offset distance on laser micropolished surfaces," Int. J. Adv. Manuf. Tech., **67**(9-12), pp. 2607-2617.

[31] Hafiz, A. M. K., Bordatchev, E. V., and Tutunea-Fatan, R. O., 2012, "Influence of overlap between the laser beam tracks on surface quality in laser polishing of AISI H13 tool steel," J. Manuf. Processes, **14**(4), pp. 425-434.

III. SURFACE ENHANCEMENT OF THE LASER-FOIL-PRINTING FABRICATED PARTS BY THE LASER POLISHING PROCESS

Chen Chen **Hai-Lung Tsai**

Department of Mechanical and Aerospace Engineering

Missouri University of Science and Technology, Rolla, MO, 65409, U.S.A.

ABSTRACT

Laser polishing is an innovative part-finishing process to reduce the surface roughness by melting a thin layer of material on the part surface. Laser foil printing (LFP) is a recently developed additive manufacturing technology using metal foils as feedstock. In this paper, the laser polishing process on the side surfaces of LFP fabricated parts was studied, with the objectives of improving the surface finish quality and enhancing the surface mechanical properties. The laser polishing study consists two steps, selecting suitable laser processing parameters for the single-track polishing process and then selecting a decent successive track displacement for the areal multi-track polishing process. Three kinds of scan paths were studied for the single-track polishing process, which are the straight-line, sine-wave and grinding scan paths. In the experimental study, it is found that the polished track should be very wide in order to overcome the discontinuity of thermal property on the surface and the large roughness wavelength. The sine-wave and grinding scan paths could emulate the large-spot-size and uniform-intensity laser beams with the rectangle shape and the disk shape, and thus can generate smooth and stable polished tracks, with a linear roughness in the track direction less than 0.5 μm. Finally, the

polishing procedure is determined as the grinding-scan polishing process with the track displacement of 500 μm and then the linear-scan polishing process with the track displacement of 50 μm. The final surface roughness of 0.72 μm in *S*a can be achieved, and the foil bonding defects on the side surface is completely repaired.

1. INTRODUCTION

In recent years, additive manufacturing (AM) has become more and more popular especially in the aerospace, automotive and medical fields [1, 2]. And various AM technologies has been proposed such as selective laser sintering (SLS), laser engineering net shape (LENS), and fused deposition modeling (FDM). Compared with the traditional subtractive manufacturing processes, the AM processes generally have some significant advantages such as free complexity, no assembly required, little lead time, little-skill manufacturing, less waste and few design constrains [3-5]. However, AM technologies also have a major disadvantage that is the poor surface quality of fabricated parts, which has become a main limitation for the AM applications [6, 7]. The surface quality of fabricated parts not only affects the aesthetic appearance, but also affects the functional performance. Some aerospace components require the surface roughness less than 0.8 μm or better to avoid the premature failure from surface initiated cracking [8], some medical instruments require the surface roughness less than 0.8 μm for sterilization [9], and also some applications have a requirement for surface roughness because of the friction factor [10]. Therefore, the post-processing of fabricated parts is usually very necessary for the most AM processes, and the post-processing methods could include the surface texture improvement, the accuracy improvement, the aesthetic improvement, the mechanical property enhancement, etc.

Generally, there is no standard method to enhance the surface quality of AM fabricated parts due to the complex nature of the process and to the different properties of the materials used. Currently, in many cases the post-finishing is executed by hand due to the shape complexity of the parts produced, which compromises some advantages of AM

processes for industrial production. Grzegorz et al. [11] used the surface treatment solution to process the 3D selective laser melted Ti-6Al-4V open porous structures for bone tissue engineering, to customize the surface porous structure with controlled surface roughness and overall morphological properties. Additionally, some studies [9, 12-15] focus on optimizing the AM fabricating parameters (the laser power, scan speed, hatch interspace, build orientation etc.) to minimize the surface roughness of fabricated parts. In this study, the main attention is focused on the laser polishing processes to improve the surface quality.

In the research of the laser polishing process on AM fabricated parts, a few studies were reported and showed promising results. Ramos et al. [16, 17] polished the SLS fabricated metal parts with a CO_2 laser and achieved a roughness reduction up to 37% of the original arithmetical mean height of a line (*R*a) with the laser energy density ranging from about 250 to 580 J/cm^2. And two laser macro polishing regimes were identified by Ramos: the shallow surface melting (SSM) and surface over-melting (SOM), based on the depth of the molten layer. Lamikiz et al. [18] polished the SLS parts and achieved a surface roughness reduction up to 80%, resulting in polished surfaces of 1.49 μm in *R*a. Dadbakhsh et al. [19] polished LENS manufactured parts and achieved a surface roughness reduction of about 80% with the resulted surface roughness of 2 μm in *R*a. Rosa et al. [20, 21] studied the laser polishing process on the LENS parts with complex and thin geometries, and achieved a surface roughness reduction up to 62% with a final surface roughness of 5.39 μm in the arithmetical mean height of a surface (*S*a).

Recently, an innovative AM method, Laser Foil Printing (LFP) [22], was proposed by the authors, which uses the metal foils as the feedstock instead of the metal powders. In

the manufacturing process of each layer, a metal foil is bonded onto the substrate or unfinished part through the laser welding process, and the redundant foil in the unwelded region is removed through the laser cutting process. The side surface of fabricated parts has significant stair steps with the height of foil thickness, and the foil bonding quality in the region close to the side surface is usually poorer than that in the inner region. Therefore, the objective of this study is to improve the surface finish quality and surface mechanical property, using the laser polishing method. First, the straight-line laser scan path was applied to generate polished tracks, and the track overlap was adjusted to improve the final polished surface quality. Then, two other laser scan paths, called grinding and sine-wave scan paths, were come up with and studied to polish the surfaces of fabricated parts. And these two scan paths could effectively resolve the issues of the straight-line scan path. Finally, the efficient laser polishing procedure for LFP parts was tested and achieved, which combines the grinding/sine-wave polishing strategy and the straight-ling scan strategy.

2. EXPERIMENTAL

The experimental setup is illustrated in Figure 2.1. The laser applied is a 1070-nm 1000-W continuous wave (CW) fiber laser (IPG Lasers, Model: YLR-1000-MM-WC-T11). The CW laser beam is directed into a scan head (ScanLab, HurryScan 30 mm) allowing for high-speed two-dimensional scanning, and focused by an F-theta lens with a focal length of 300 mm. The workpiece is put in a shielding gas chamber filled with argon gas flow, which has a top opening for the incoming laser beam and is fixed on an X-Y-Z motion stage (Aerotech, Model: ATS 10060-H-M-80P-NC), which provides a motion resolution of 1 μm in the X and Y directions and a 0.1 μm resolution in the Z direction.

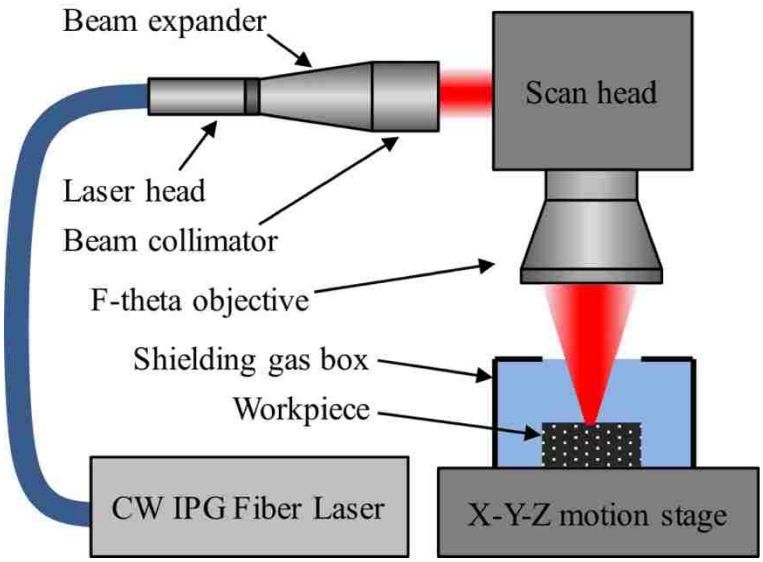

Figure 2.1. The experimental setup for the laser surface polishing study

The sample surface topographies before and after the polishing process were measured with a white light interferometer (Wyko NT9100), which has a height measurement resolution of 1 nm in the VSI mode.

In this paper, the study is focused on the post-processing of the side surface of the parts built by the LFP process, since the foils on side surfaces are not fully fused during the manufacturing process, and the enhancement of the finish quality of side surfaces is very necessary. Two typical kinds of side surfaces were selected and used in this study, which are the vertical side surfaces and the inclined side surface with an inclination angle of 45 deg.

Similar to the laser polishing method of reported studies, the surface is processed by the successive polished tracks with a specific displacement between the successive tracks. Differently, the laser scan path for the single polishing track not only is a straight line, but also can be the sine-wave scan path and the grinding scan path, as shown in Figure 2.2.

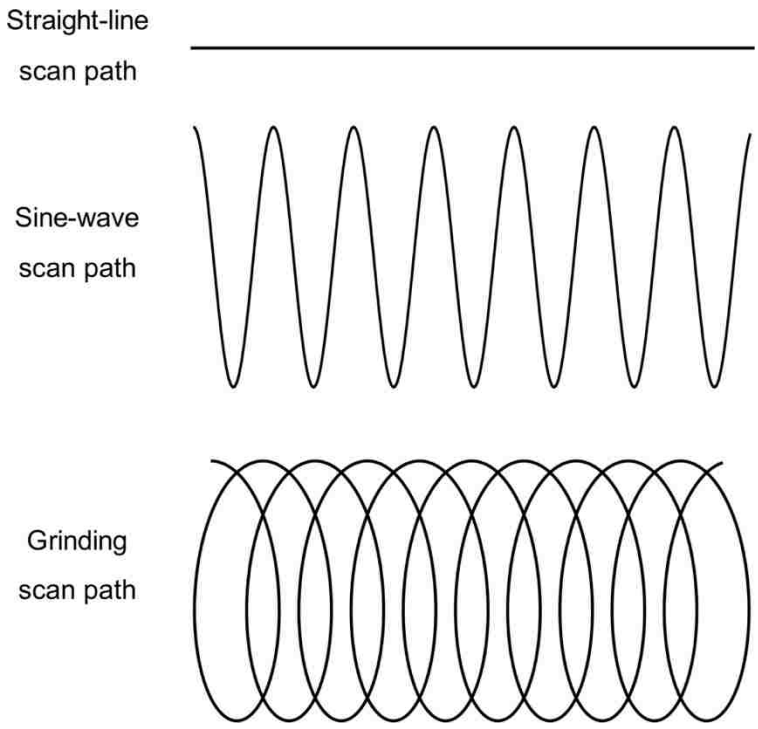

Figure 2.2. The three different scan paths for the single polishing track

The mathematical expression for the sine-wave scan path can be written in the parametric equations,

$$X(t) = s \cdot t, \tag{1}$$

$$Y(t) = \frac{A}{2}\sin(2\pi f t), \tag{2}$$

where X and Y are the coordinates of scan path, s the processing speed along the track, t the time, A the scan trace width, f the vibration frequency of the scan path, which could be used to adjust the trace spatial density. The motion in the X direction is a linear motion and the motion in Y direction is a harmonic vibration. The parametric equations for the grinding scan path are

$$X(t) = s \cdot t + \frac{A}{2}\cos(2\pi f t), \tag{3}$$

$$Y(t) = \frac{A}{2}\sin(2\pi f t). \tag{4}$$

This kind of rotating scan path is called the grinding scan path because it looks like the mechanical grinding process in some way. The motion of the X axis is a linear motion plus a harmonic vibration, while the motion of Y axis is only a harmonic vibration. The motivation of coming up the sine-wave and grinding scan paths is to emulate a laser beam with a large spot size and a flat-top intensity distribution. When the laser scan speed is set very high, 2000 mm/s in the study, and the beam spot size is suitable, 225 μm compared with the scan path width 1000 μm in this study, the sine-wave scan path could emulate a rectangular beam shape in some degree, and the grinding scan path could emulate a disk or oval beam shape.

In the previous studies of laser polishing process [23-28], a combined processing parameter, the energy density E_s, was used as a major performance indicator of a laser polishing process, which is defined as

$$E_s = \frac{P}{D_0 \cdot V_s}, \tag{5}$$

where P is the delivered laser power, D_0 the laser spot diameter on the workpiece surface, and V_s the beam scan speed. In this study, the energy density is also defined with the above equation, but the physical meaning of the symbols in the equation was adjusted. D_0 represents the scan track width instead, and V_s represents the processing speed, i.e. s in Eq. (1) and Eq. (2), instead of the laser scan speed. In this way, the polishing performances of different scan strategies with a same energy density could be compared.

3. RESULTS AND DISCUSSION

3.1. INITIAL SURFACE CONDITION

Figures 3.1a and 3.1b show two typical parts fabricated by the LFP process, with the vertical side surface and the 45º inclined surface respectively, for the surface post-processing study. The thickness of AISI 1010 steel foil for building the parts is 200 μm. From the photos, the stair steps on the 45º inclined surface look significant, but the vertical side surface looks smoother. The surface morphologies of the two typical side surfaces are measured and shown in Figure 3.1b and Figure 3.1d, respectively. The morphology of the vertical side surface is composed of the striations of the laser cutting edge, mainly along the Y direction, and the tapers of cutting edge, uniform in the X direction and periodic in the Y direction with a period of the layer thickness 200 μm. And the surface roughness is measured as 4.39 μm in *R*a. Figure 3.1d presents the topography of the 45º inclined side surface, where the major surface roughness is the stair steps. The asperities of the striations and tapers of cutting edges still contribute to the roughness of the inclined surface, but the magnitudes of them are much smaller than that of stair steps. The surface roughness is measured as 24.22 μm in *R*a. Based on the purely geometrical consideration of stair step profile, the surface roughness of the 45º inclined side surface can be calculated as 25 μm, very close to the above measurement. This study focuses on the laser polishing process of these two typical side surfaces of LFP fabricated parts.

It should be noted that the stair step in additive manufacturing fabricated parts is inevitable because the manufacturing process is layer wised. It is possible to reduce the stair-step effect by using very thin layer thickness, but that would increase the manufacturing time significantly.

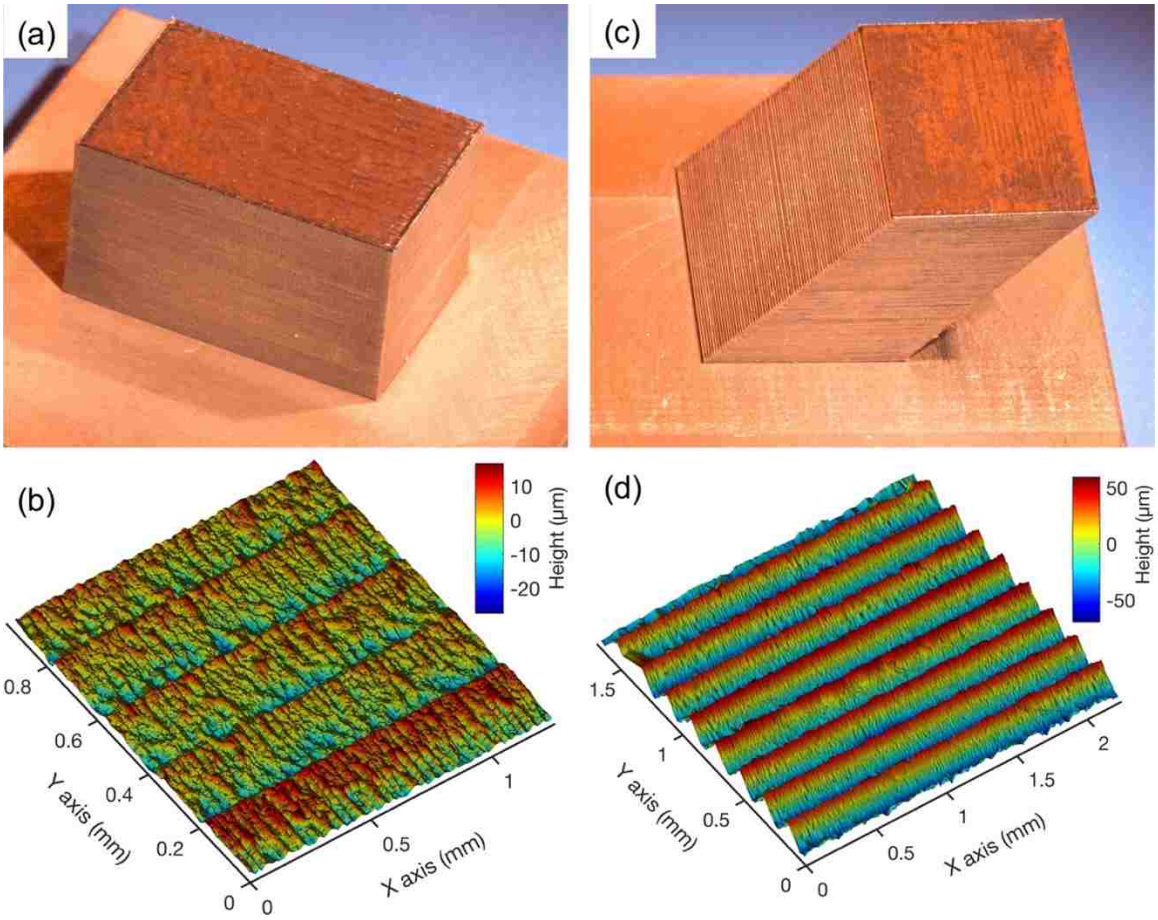

Figure 3.1. Two LFP fabricated parts with (a) the vertical side surface and (c) the 45º inclined surface, (b) the surface morphology of the vertical side surface, and (d) the surface morphology of the 45º inclined side surface

Shown in Figure 3.2 are the microscopic images of the cross-sections of the fabricated parts. As indicated by the dash line in Figure 3.2a, the sectioning direction is perpendicular to the laser weld tracks. The etched cross-section of the inner region of the fabricated part is shown in Figure 3.2b. The laser weld tracks are neat and orderly. Note the laser welding process in the part manufacturing process is not conducted track by track successively. Instead, the order of welding process is in a way to recursively let the next weld track split the un-welded area evenly until the entire surface is covered by the weld tracks. Such the welding order could avoid the heat distortion accumulating in one direction

and make the thermal stress evenly distributed. As shown in Figure 3.2b, the displacement between two adjacent weld tracks is 250 μm, the depth of weld tracks is very stable, and there are no pores, micro-cracks or un-welded interlayer gaps observed from the cross-section. Figures 3.2c and 3.2d present the cross-section close to the side surface, for the vertical and 45º-inclined surfaces, respectively. The foils near the side surface are not bonded by the weld tracks, and the thickness of the non-fused layer at the side surfaces is about 100 μm. Note, in the manufacturing process of LFP, the foil in each layer is bonded onto the substrate or the top surface of un-finished parts by the laser welding process, and then the foil of un-welded region is removed away by the laser cutting process. In order to ensure the foil cutting efficiency, the cutting path is kept a certain distance from the boundary of welded region. Therefore, the foils near the cutting edges are not bonded together, which could lead to the poor mechanical properties for the side surface of fabricated parts, and a post-process of surface polishing is required to improve the bonding quality on the side surfaces.

3.2. SURFACE POLISHING WITH THE STRAIGHT-LINE SCAN PATH

Generally, in most laser polishing studies, the polished surface is composed of successive polished tracks with some overlap, and the polished tracks are produced by a linearly moving laser irradiation. Therefore, the linearly-scan polished tracks with different successive displacements were firstly tested on the vertical side surface of LFP part. After some preliminary tests on the substrate plate, the processing parameters for the single-track polishing was selected as the laser power of 335 W, the scan speed of 200 mm/s and the beam spot size of 225 μm, which can achieve the melted depth of about 270 μm and the polished width of about 210 μm. Note, the material thermal properties are not spatially

continuous and uniform on the surface to be polished, because of the insufficient bonding of foils near the side surface. Hence, the actual polished track width and depth on the side surface would vary with position. In order to repair the foil-bonding defects on the side surface, the depth of polished tracks should reach or surpass 150 μm. Besides, compared with the initial surfaces of Selective-Laser-Melting parts or the mechanically machined surfaces, the typical wavelength of initial surface roughness in this study is very large, 200 μm for the vertical side surface and 283 μm for the 45º inclined side surface.

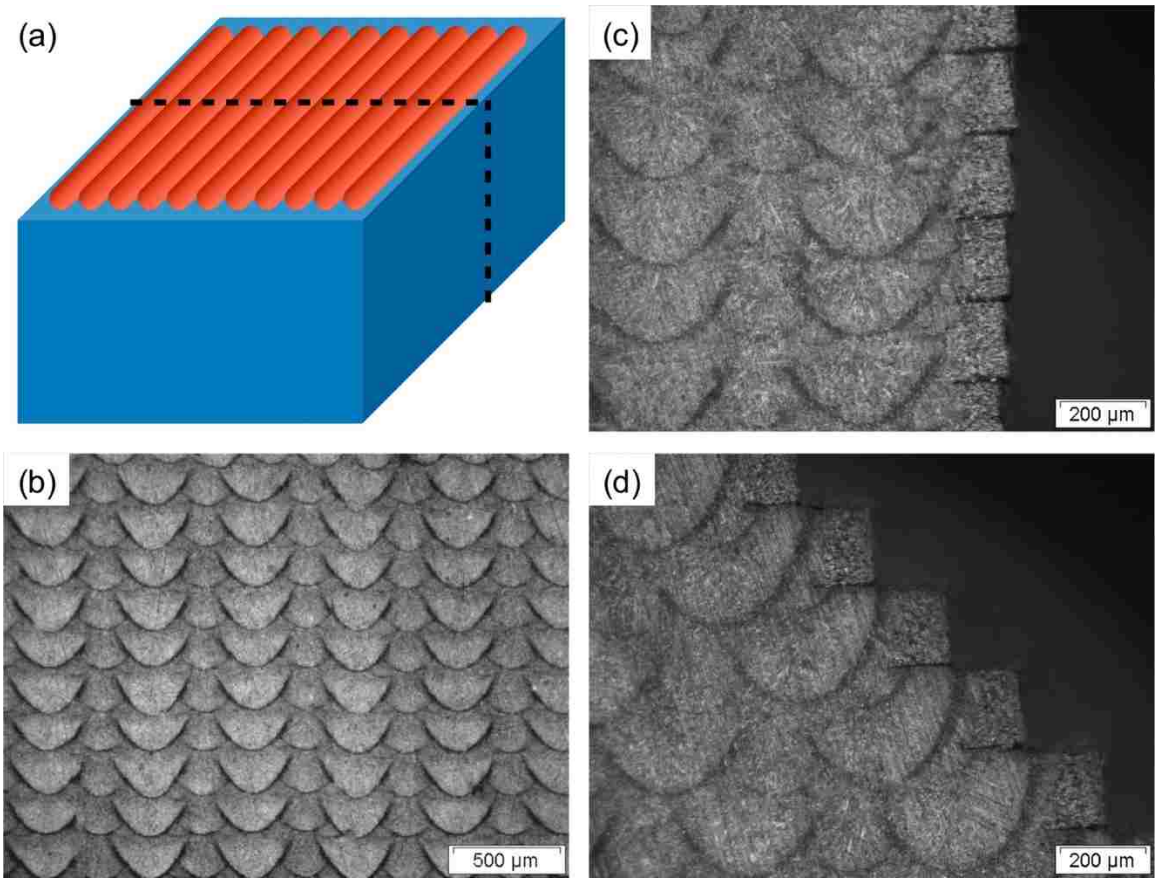

Figure 3.2. (a) Illustration of the sectioning direction of fabricated part, (b) the cross-section of the inner region of fabricated part, (c) the cross-section of the vertical side surface, and (d) the cross-section of the 45º inclined side surface

Then, the selected processing parameters were applied to polishing the vertical side surfaces, the polished tracks are parallel with the initial surface roughness ridges, and the successive-track displacements of 120 μm, 60 μm and 30 μm were tested. For the polished track displacement of 120 μm, the polished surface shown in Figure 3.3a is still covered by the ridges, and the resulted roughness is 12.2 μm in *S*a. For the track displacement of 60 μm, the polished surface morphology, shown in Figure 3.3b, has a surface roughness of 6.6 μm in *S*a. For the track displacement of 30 μm, the resulted surface morphology is shown in Figure 3.3c, and has a surface roughness of 5.44 μm in *S*a. The surface roughness of initial vertical side surface is 4.39 μm. Through this laser surface polishing test with linearly-scan polished tracks, the surface roughness was not improved at all. The major reason could be the discontinuous thermal properties at the side surface and the large wavelength of initial surface roughness, and the resulted polishing tracks could be much different track from track. In order to obtain successively stable polished tracks, the polished width should be much larger than the typical wavelength of initial surface roughness (200 μm for the vertical side surface), such that the negative influence of the discontinuous thermal properties and the long-wavelength surface roughness could be kept minimum.

As reported in some literature about the laser polishing process on selective laser sintering fabricated parts, the polished track by the larger laser beam size owns better polished finish quality than those polished by the small-spot-size laser beam. It was concluded that the larger laser beam could lead to a large melting pool, and the smoothing effect by the thermos-capillary force is generally more significant on the large melting pool surfaces.

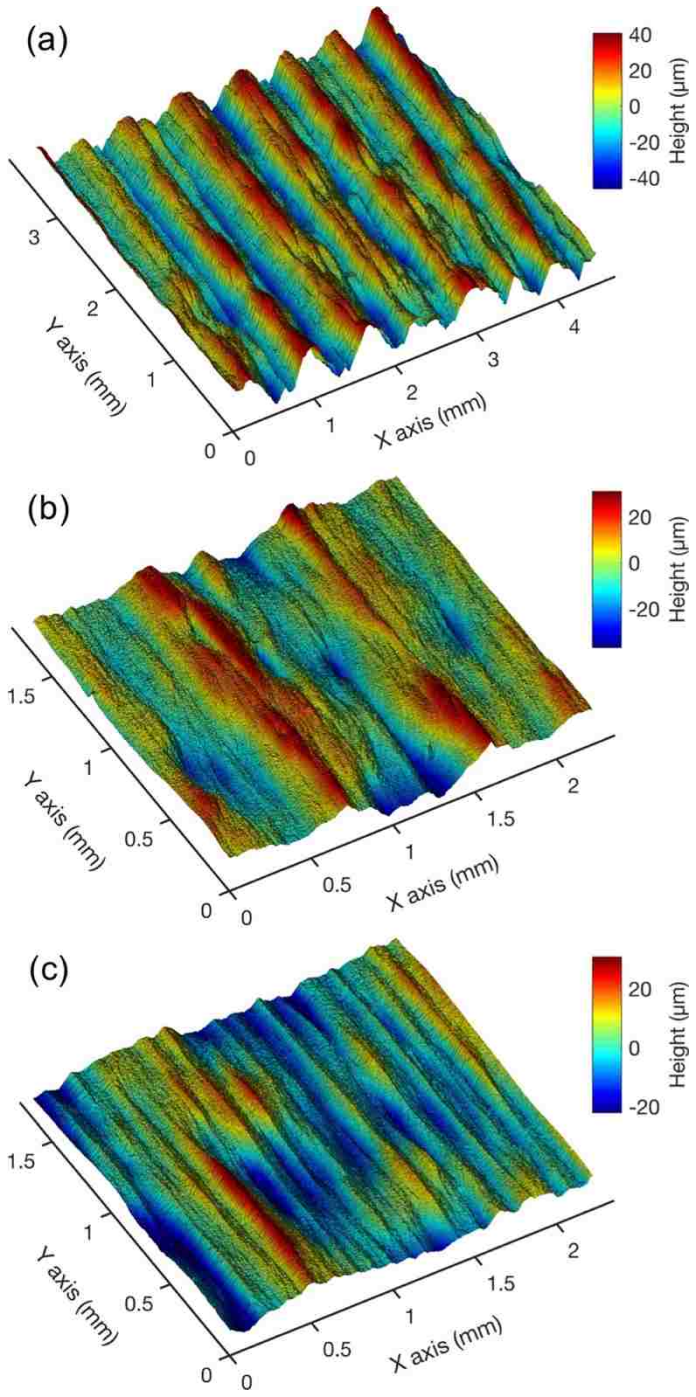

Figure 3.3. The post-processed vertical side surfaces by the straight-line melting tracks with the successive track displacements of (a) 120 μm, (b) 60 μm and (c) 30 μm

3.3. SURFACE POLISHING WITH THE GRINDING AND SINE-WAVE SCAN PATHS

To obtain a wide polished track, an obvious way is to further defocus the laser beam. However, because the laser intensity is Gaussian distributed, when the laser beam spot is enlarged, the negative effect of the uneven intensity distribution would become significant. Usually, when the intensity at the edge of beam spot is decent for polishing, the intensity at the center would be too intense and cause significant evaporation. In this study, we came up with two new scan paths for single polished track, the grinding scan path and the sine-wave scan path (Figure 2.2). The motivation of the grinding scan path is to emulate a laser beam with a disk-shape and flat-top intensity distribution, since the scan speed in this experiment can be very high (e.g. 3000 mm/s). And the sine-wave scan path is to emulate a laser beam with a rectangular-shape and flat-top intensity distribution. In the study of the influence of laser intensity distribution on the laser micro polishing process [29], it was found that the flat-top intensity distribution leads to a lower surface roughness than the near-Gaussian distribution, and the uniform, disk intensity distribution leads to a lower surface roughness than the uniform, square distribution.

Figure 3.4 shows the single-track polishing tests with the grinding scan path and the sine-wave scan path on the vertical side surface and the 45º inclined side surface. The width of two scan paths is set as 1 mm, the laser beam size is 225 μm, and the resulted polished track width is about 1.2 mm for all four cases. The laser power applied is 270 W, and the scan speed is 2000 mm/s. From the microscopic image in Figure 3.4, the surface of polished tracks looks quite smooth with minor ripples. Sometimes, the edge of polished track is not very stable (e.g. Figure 3.4a and 3.4b), due to the discontinuous thermal property.

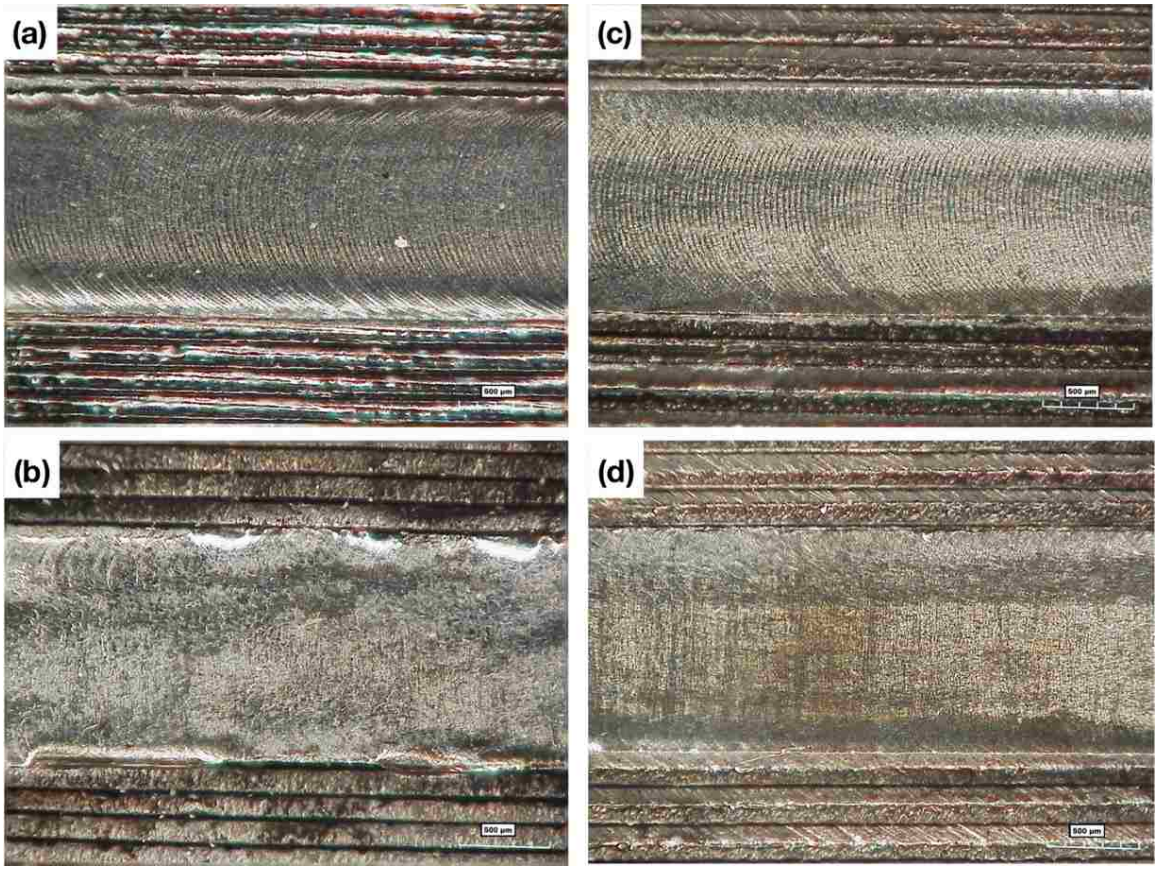

Figure 3.4. The microscopic images of (a) the grinding polished track on the vertical side surface, (b) the sine-wave polished track on the vertical side surface, (c) the grinding polished track on the 45º inclined side surface, and (d) the sine-wave polished track on the 45º inclined side surface

Figure 3.5 shows the corresponding surface morphologies of the polished tracks produced by the grinding and sine-wave scan paths on the vertical and inclined side surfaces. The surface quality for all four cases was significantly improved. For the grinding scan path, the linear surface roughness in the track direction is about 0.4 μm in *R*a, and, for the sine-wave scan path, the linear surface roughness in the track direction is about 0.35 μm in *R*a. In addition, it is found that the initial surface condition (vertical or inclined side surfaces) does not have significant influence on the resulted polished track, because the surface material is completely melted down.

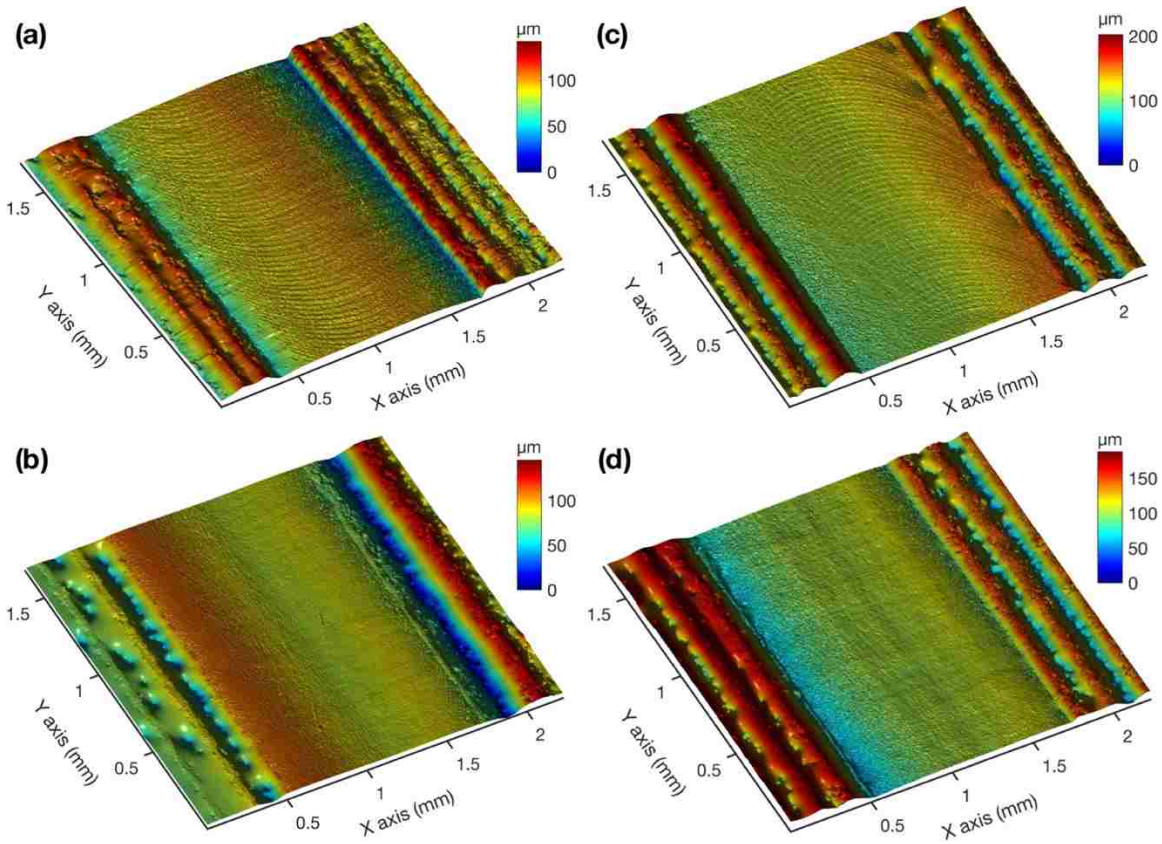

Figure 3.5. The surface morphologies of (a) the grinding polished track on the vertical side surface, (b) the sine-wave polished track on the vertical side surface, (c) the grinding polished track on the 45º inclined side surface, and (d) the sine-wave polished track on the 45º inclined side surface

With the determined polishing parameters in the single-track polishing tests, the large-area multi-track laser polishing process was conducted. Figure 3.6 shows the multi-track polished surfaces produced by the grinding scan path (Figure 3.6a and 3.6b) and the sine-wave scan path (Figure 3.6c and 3.6d). The successive track displacements in Figure 3.6a and 3.6c are 1 mm, i.e. the width of scan path. And the successive track displacements in Figure 3.6b and 3.6d are 0.5 mm. It can be observed that the polished surfaces are rather smooth except for the overlapped region of tracks. Note, the polished surfaces on the

vertical and inclined side surfaces are almost same, since the initial surface condition has no significant influence on the polishing process of both the grinding scan path and the sine-wave path.

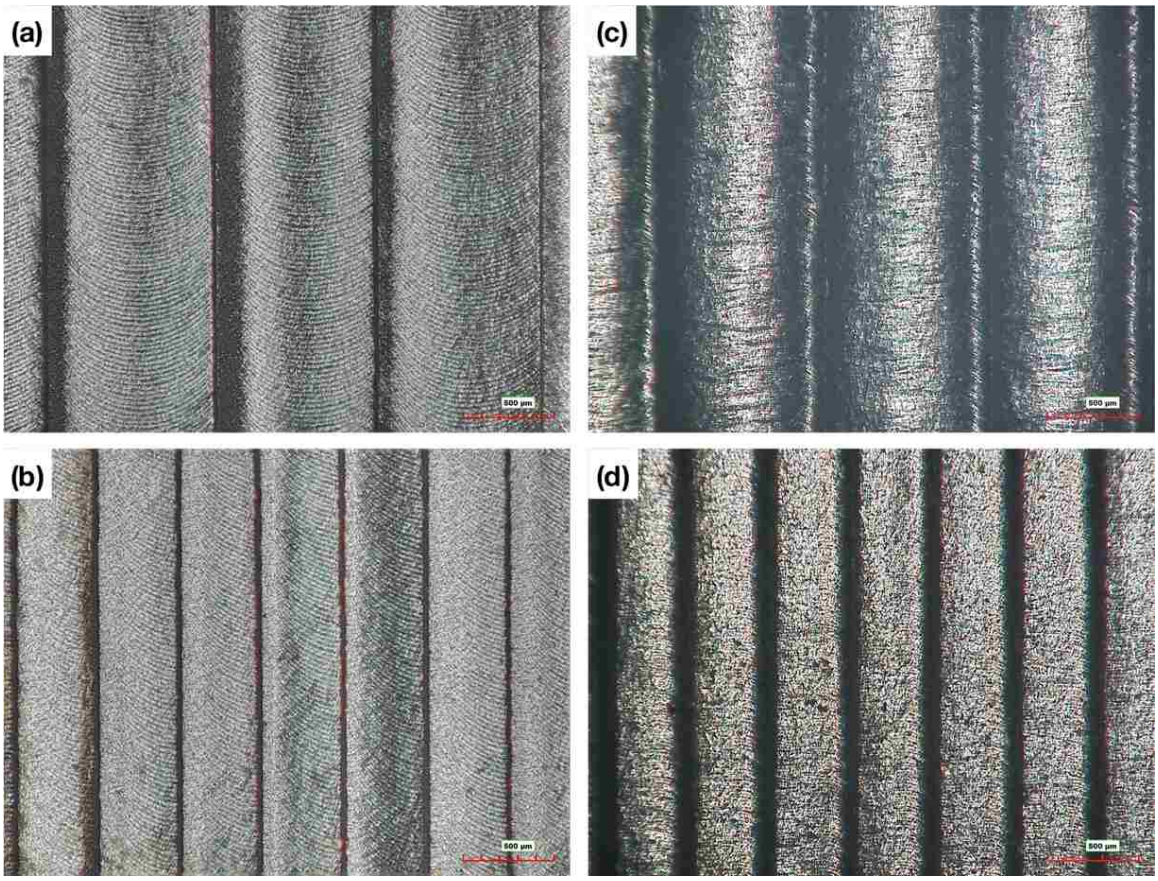

Figure 3.6. The microscopic images of the grinding-scan polished surfaces with the successive track displacements of (a) 1 mm and (b) 0.5 mm, and the microscopic images of the sine-wave-scan polished surfaces with the successive track displacements of (c) 1mm and (d) 0.5 mm

Figure 3.7 shows the corresponding morphologies of the multi-track polished surfaces by the grinding scan path and the sine-wave scan path with the successive track displacements of 1 mm and 0.5 mm, respectively. The surface roughnesses in Figure 3.7a, 3.7b, 3.7c, and 3.7d are 1.41 μm, 1.20 μm, 1.58 μm and 1.25 μm, respectively. It can be

found that the surface quality produced by the grinding scan path is relatively better than that polished by the sine-wave scan path, for the track displacements of both 1 mm and 0.5 mm. The amplitudes of overlapped ridges produced by the grinding scan path is smaller than those by the sine-wave scan path. Generally, the effect of the overlapping process of polished tracks is not very remarkable. A better way to further reduce the surface roughness could be to use the straight-line scan path to further polish the surface with a much smaller polished track displacement.

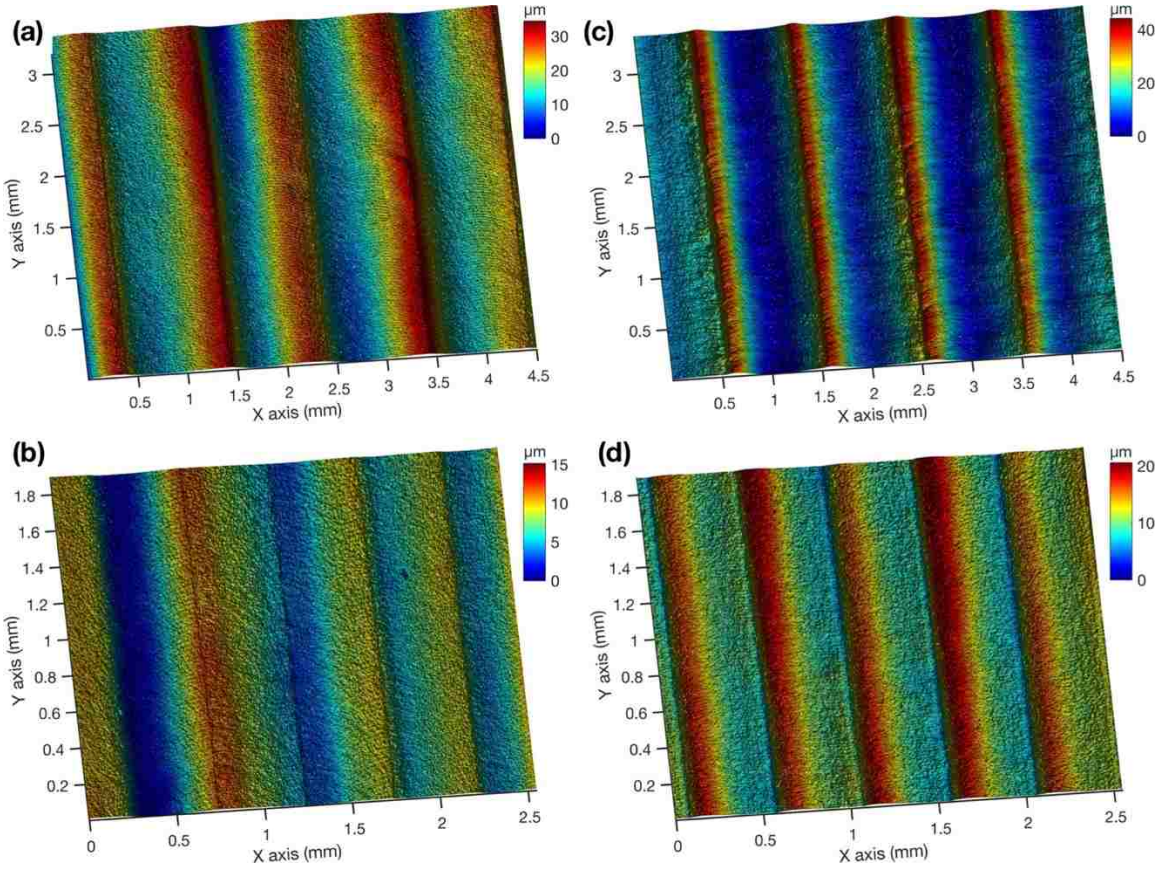

Figure 3.7. The surface morphologies of the grinding-scan polished surfaces with the successive track displacements of (a) 1 mm and (b) 0.5 mm, and the surface morphologies of the sine-wave-scan polished surfaces with the successive track displacements of (c) 1mm and (d) 0.5 mm

Figure 3.8a and 3.8b show the final polished side surfaces of the sloped block and vertical block, respectively, with the side surfaces half-polished and half-unpolished. In the final polishing procedure, the side surfaces were first polished by the grinding-scan tracks and a successive-track displacement of 500 μm, and then polished by the linear-scan tracks with a successive-track displacement of 50 μm. The laser power is 270 W, the scan speed is 200 mm/s and the beam diameter is 350 μm for the linear-scan polishing tracks. From the photos, the polished area looks much brighter than the unpolished area. Figure 3.8c presents the microscopic image of the final polished surfaces, where the overlapping pattern of polished tracks is still clear. Figure 3.8d is the corresponding morphology of the final polished surface. The major asperities of the polished surface are the phase-transition induced martensitic needles and the overlap ridges, and the surface roughness is measured as 0.72 μm in *S*a. In summary, it can be concluded that the effect of the laser polishing process on the side surfaces of LFP parts is very significant, and the surface finish quality is effectively improved.

Figure 3.9a and 3.9b show the cross-sections of the inclined and vertical side surfaces of processed parts, respectively. Through the laser polishing process, the initial foil bonding defects at the side surfaces were completely repaired.

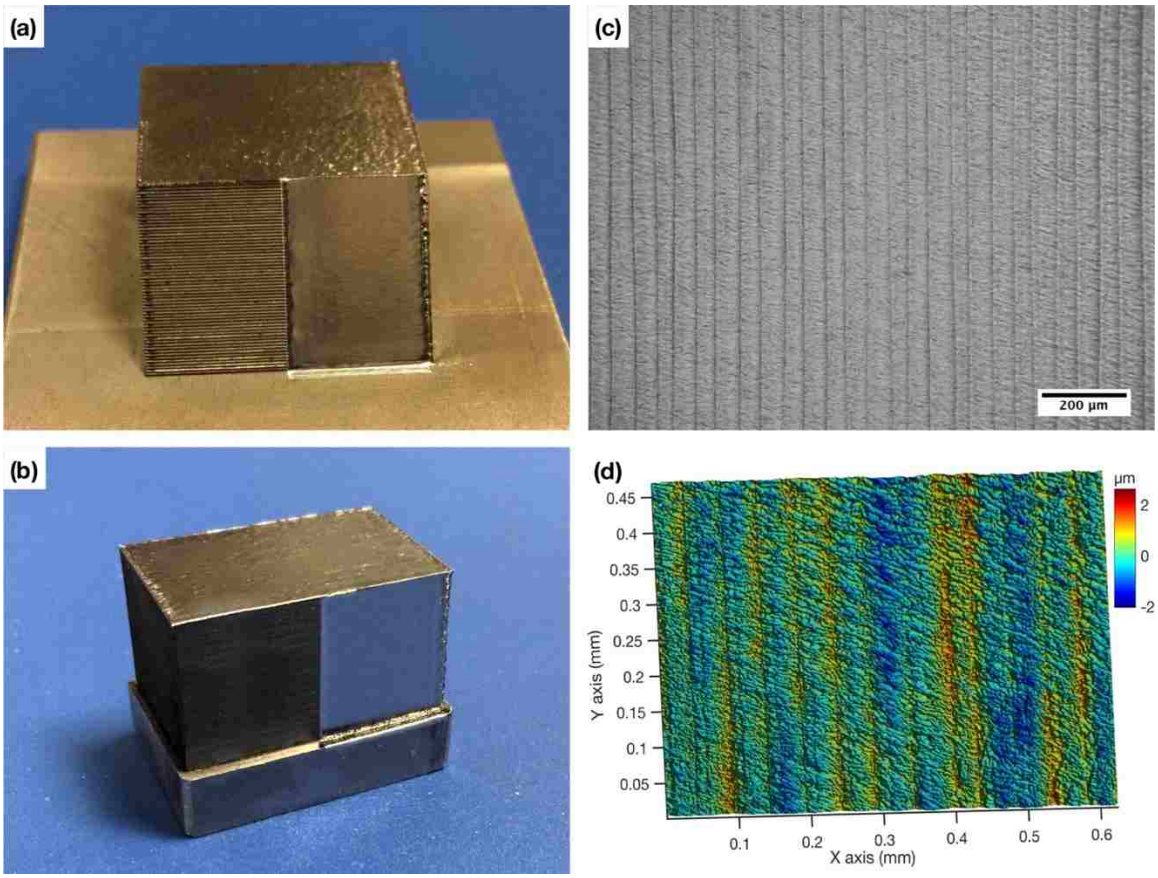

Figure 3.8. The half-polished (a) 45º inclined side surface and (b) vertical side surface of LFP parts, (c) the microscopic image of the polished surface and (d) the corresponding surface morphology

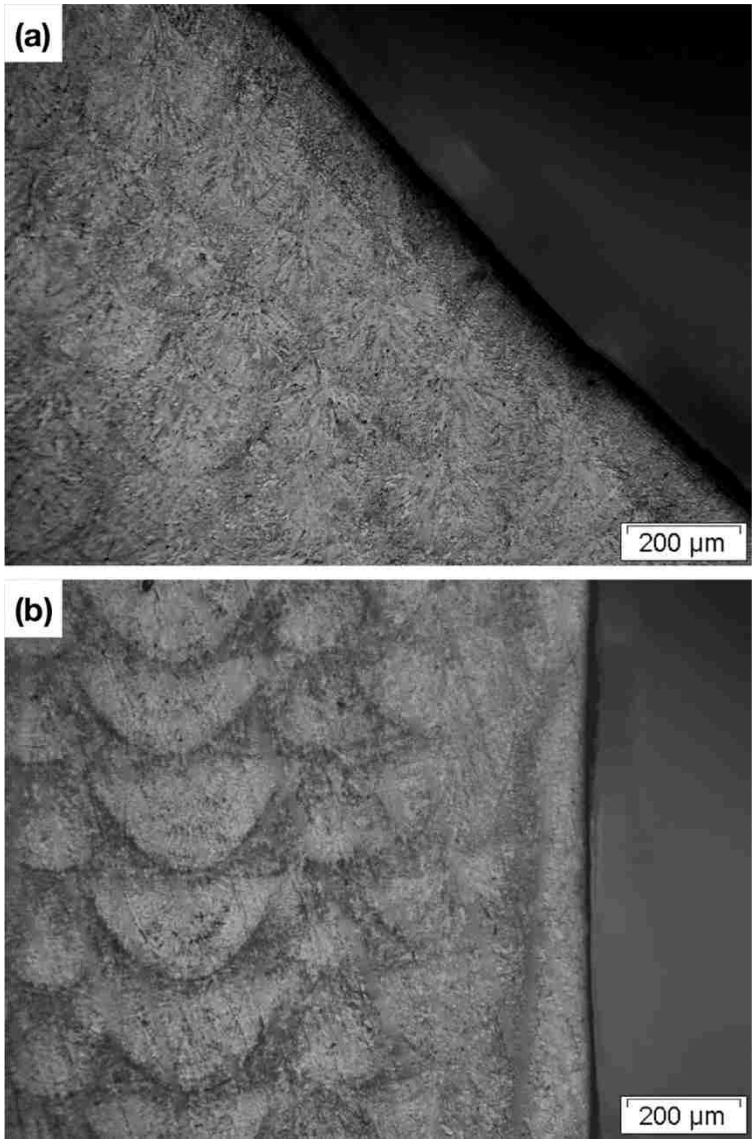

Figure 3.9. The cross-sections of (a) the polished 45º inclined side surface and (b) the polished vertical side surface

4. CONCLUSION

The laser surface polishing process was studied in this paper to enhance the side surface of Laser-Foil-Printing parts. The parts were fabricated with AISI 1010 steel foils of the thickness 200 μm. Two typical side surfaces, the vertical and 45º inclined side surfaces, were studied in this paper. The initial surface roughnesses of the vertical and 45º inclined side surfaces are 4.39 and 24.22 μm, respectively. And the foils near the side surface are not sufficiently bonded during the manufacturing process. Hence, the objectives of this study are to improve the surface finish quality and the foil bonding quality on the side surface of LFP fabricated parts.

Three kinds of scan paths were generated for the single-track polishing process, which are the straight-line scan path, the sine-wave scan path and the sine-wave scan path. Generally, the polishing study consists two steps, selecting suitable laser processing parameters for single-track polishing process and selecting a decent successive track displacement for the areal multi-track polishing process. At first, the straight-line scan path was applied to polish the vertical side surface with the successive track displacements of 120 μm, 60 μm and 30 μm. The surface roughness does not get any improvement with the linear-scan polished tracks, because the thermal properties of the surface material is discontinuous and the wavelength of the initial roughness is very large, and the laser polishing process could be not stable track by track.

In order to obtain a wide polished track, the grinding and sine-wave scan paths were employed, which could emulate the large-spot-size laser beams with the disk shape and uniform intensity distribution or with the rectangle shape and uniform intensity distribution, respectively. The resulted single polished tracks for both scan paths are quite

smooth and stable, and the surface roughness along the track direction is less than 0.5 μm. And the polished track width is about 1.2 mm for both cases, which is much larger than the initial roughness wavelength. In the multi-track polishing tests, the track displacements of 1mm and 0.5 mm were studied. The resulted areal surface roughness could be reduced to around 1.3 μm, and it is found that the decrease of track displacement does not have remarkable effect on the surface roughness improvement.

Finally, the surface polishing procedure is determined as the grinding-scan polishing process with the track displacement of 500 μm and then the linear-scan polishing process with the track displacement of 50 μm. The final surface roughness of 0.72 μm in *S*a can be achieved, and the foil bonding defects on the side surface is completely repaired.

ACKNOWLEDGMENTS

The authors gratefully acknowledge the financial support from the Department of Energy (Grant No. DE-FE0012272).

BIBLIOGRAPHY

[1] Wohlers, T. T., and Gornet, T., 2014, "History of Additive Manufacturing," Wohlers Associates, Fort Collins, CO.

[2] Gu, D., 2015, *Laser Additive Manufacturing of High-Performance Materials,* Springer.

[3] Gibson, I., Rosen, D.W., and Stucker, B., 2010, *Additive Manufacturing Technologies,* Vol. 238, Springer.

[4] Wong, K. V., and Hernandez, A., 2012, "A Review of Additive Manufacturing," ISRN Mech. Eng., 2012, p. 208760.

[5] Frazier, W. E., 2014, "Metal Additive Manufacturing: A Review," J. Mater. Eng. Perform., 23(6), pp. 1917–1928.

[6] Król, M., Dobrzański, L., and Reimann, I.C., 2013, "Surface quality in selective laser melting of metal powders," Arch. Mater. Sci., 88, pp. 88.

[7] Townsend, A., Senin, N., Blunt, L., Leach, R. K., and Taylor, J. S., 2016, "Surface Texture Metrology for Metal Additive Manufacturing: A Review," Precision Engineering, 46, pp. 34-47.

[8] Strano, G., Hao, L., Everson, R. M., and Evans, K. E., 2013, "Surface Roughness Analysis, Modelling and Prediction in Selective Laser Melting," J. Mater. Process. Tech., 213(4), pp. 589-597.

[9] Abele, E., and Kniepkamp, M., 2015, "Analysis and Optimisation of Vertical Surface Roughness in Micro Selective Laser Melting," Surf. Topogr.: Metrol. Prop., 3(3), pp. 34007.

[10] Lamikiz, A., Sanchez, J. A., Lopez de Lacalle, L. N., and Arana, J. L., 2007, "Laser Polishing of Parts Built Up by Selective Laser Sintering," Int. J. Mach. Tool. Manu., 47(12-13), pp. 2040-2050.

[11] Pyka, G., Kerckhofs, G., Papantoniou, I., Speirs, M., Schrooten, J., and Wevers, M., 2013, "Surface Roughness and Morphology Customization of Additive Manufactured Open Porous Ti6Al4V Structures," Materials, 6(10), pp. 4737-4757.

[12] Kamran, M., and Neil, H., 2009, "Top Surface and Side Roughness of Inconel 625 Parts Processed Using Selective Laser Melting," Rapid Prototyping J., 15(2), pp. 96-103.

[13] Yasa, E., Deckers, J., and Kruth, J. P., 2011, "The Investigation of the Influence of Laser Re-melting on Density, Surface Quality and Microstructure of Selective Laser Melting Parts," Rapid Prototyping J., 17(5), pp. 312-327.

[14] Calignano, F., Manfredi, D., Ambrosio, E. P., Iuliano, L., and Fino, P., 2013, "Influence of Process Parameters on Surface Roughness of Aluminum Parts Produced by DMLS," Int. J. Adv. Manuf. Tech., 67(9-12), pp. 2743-2751.

[15] Alrbaey, K., Wimpenny, D., Tosi, R., Manning, W., and Moroz, A., 2014, "On Optimization of Surface Roughness of Selective Laser Melted Stainless Steel Parts: A Statistical Study," J. Mater. Eng. Perform., 23(6), pp. 2139-2148.

[16] Ramos, J. A., Bourell, D. L., and Beaman, J. J., 2003, "Surface Over-Melt During Laser Polishing of Indirect-SLS Metal Parts," Mater. Res. Soc. Symp. P., 758, pp. 53-61.

[17] Ramos-Grez, J. A. and Bourell, D. L., 2004, "Reducing Surface Roughness of Metallic Freeform-Fabricated Parts Using Non-tactile Finishing Methods," Int. J. Mater. Prod. Tec., 21(4), pp. 297-316.

[18] Lamikiz, A., Sánchez, J. A., López de Lacalle, L. N., del Pozo, D., and Etayo, J. M., 2006, "Surface Roughness Improvement Using Laser-Polishing Techniques," Mater. Sci. Forum, 526, pp. 217-222.

[19] Dadbakhsh, S., Hao, L., and Kong, C. Y., 2010, "Surface Finish Improvement of LMD Samples Using Laser Polishing," Virtual Phys. Prototyp., 5(4), pp. 215-221.

[20] Rosa, B., Mognol, P., and Hascoet, J. Y., 2015, "Laser Polishing of Additive Laser Manufacturing Surfaces," J. Laser Appl., 27. p. S29102.

[21] Rosa, B., Mognol, P., and Hascoet, J. Y., 2016, "Modelling and Optimization of Laser Polishing of Additive Laser Manufacturing Surfaces," Rapid Prototyping J., 22(6), pp. 956-964.

[22] Chen, C., Shen, Y. Y., and Tsai, H. L., 2017, "A Foil-Based Additive Manufacturing Technology for Metal Parts," J. Manuf. Sci. E-T ASME, 139(2), p. 024501-6.

[23] Heng, Q., Tao, C., and Zuo, T. C., 2006, "Surface Roughness Analysis and Improvement of Micro-Fluidic Channel with Excimer Laser," Microfluid. Nanofluid., 2(4), pp. 357-360.

[24] Ukar, E., Lamikiz, A., López de Lacalle, L. N., del Pozo, D., and Arana, J. L., 2010, "Laser Polishing of Tool Steel with CO2 Laser and High-Power Diode Laser," Int. J. Mach. Tool. Manu., 50(1), pp. 115-125.

[25] Hafiz, A. M. K., Bordatchev, E. V., and Tutunea-Fatan, R. O., 2012, "Influence of Overlap Between the Laser Beam Tracks on Surface Quality in Laser Polishing of AISI H13 Tool Steel," J. Manuf. Process., 14(4), pp. 425-434.

[26] Ukar, E., Tabernero, I., Liebana, F., Saitua, I., Villaseca, R., and Sobrado, J., 2012, "Parameter Study on Laser Surface Finishing with 2D Scan Head," Advances in Non-Conventional Materials Processing Technologies, 713, pp. 109-114.

[27] Rosa, B., Hascoet, J. Y., and Mognol, P., 2014, "Topography Modeling of Laser Polishing on AISI 316L Milled Surfaces," Mech. Ind., 15(1), pp. 51-61.

[28] Ma, C. P., Guan, Y. C., and Zhou, W., 2017, "Laser Polishing of Additive Manufactured Ti Alloys," Opt. Laser Eng., 2017. 93, p. 171-177.

[29] Nusser, C., Wehrmann, I., and Willenborg, E., 2011, "Influence of Intensity Distribution and Pulse Duration on Laser Micro Polishing," Physcs. Proc., 12, pp. 462-471.

IV. FUNDAMENTAL STUDY OF THE BULGE STRUCTURE GENERATED IN LASER POLISHING PROCESS

Chen Chen Yiyu Shen Hai-Lung Tsai

Department of Mechanical and Aerospace Engineering

Missouri University of Science and Technology, Rolla, MO, 65409, U.S.A.

ABSTRACT

Laser polishing is an innovative part-finishing process to reduce the surface roughness by melting a thin layer of material on the part surface. The polished surface quality is influenced by many factors including initial surface condition, properties of material, laser power, scan speed, focal offset, beam shape, percentage of overlap, etc. In addition to removing the original asperities, the laser polishing process may also introduce new asperities including bulges, ripples, undercuts, etc. In this paper, a fundamental study is carried out on Ti-6Al-4V alloy slabs to investigate the formation of bulge structure and the influence of processing parameters (the laser power, scan speed, focal offset and successive track displacement) on the bulge structure through parametric analyses. The formation of bulge structure is mainly caused by the phase transition in the heat-affected zone and the mass transport of the fluid flow in melting pool. The parameters of the laser power, scan speed and focal offset have significant influences on the width and depth of polished tracks, the amplitude of bulge structures and the relative volume expansion by the bulge structures. Two different melting modes and a maximum

track width can be found in the parametric study of focal offset. The scan speed has a significant influence on the relative volume expansion at low speeds. By reducing the successive track displacement, the overlapped bulge amplitude can be reduced rapidly, but the finer solidification-induced surface structure would get intensified.

1. INTRODUCTION

Recent years, additive manufacturing (AM) has become an important and promising technology especially for the fabrication of aero industrial parts [1-3], because AM processes can achieve highly complex 3D geometries and the very low material wastage, compared with the traditional subtractive manufacturing processes. However, AM fabricated parts usually have a poor surface quality, which could lead to unacceptable tolerance and increased friction, and potentially become a source of fatigue crack initiation [4-6]. So, the post-processing of AM fabricated parts, especially surface polishing, is essentially required in the actual applications. Recently, laser polishing is a promising and competent polishing process [7]. And it has the following obvious advantages over some traditional polishing processes (e.g. abrasive polishing and electro-chemical polishing): non-contact, no material removal, no pollution, high automation, selective processing and less polishing times [8]. Laser polishing, as a physical process, involves creating a thin molten layer on the substrate with laser radiation, and the surface asperities would be reduced or eliminated by the capillary or thermo-capillary effect of molten material.

Many studies on laser polishing processes have been reported [4, 9-26], and have shown promising results. However, a majority of the available research is based on the statistical Design of Experiment methods, and few research was concerned with the fundamental study of the laser polishing processes. Ramos et al. [4], studied the laser macro polishing process [8] on the selective laser sintering (SLS) fabricated parts, and identified two different laser polishing regimes: surface shallow melting (SSM) and surface over melting (SOM). In the regime of SSM, the thickness of the melted layer is

less than the peak-to-valley height of the typical surface asperities, and the molten material flows from the peaks to the local valleys under the capillary pressure. In the regime of SOM, the thickness of the melted layer is greater than the peak-to-valley height of asperities, then the original surface topography may completely disappear and a continuously moving melting pool is created. In the research of laser micro polishing [8] with the pulsed laser radiation, two polishing regimes, similar to SSM and SOM, were recognized as the capillary regime and the thermo-capillary regime [27, 28]. The capillary regime is performed with short laser pulses (e.g. hundreds of nanosecond) and the thermo-capillary regime with relatively longer laser pulses (e.g. several microsecond).

In the experimental studies of laser polishing processes [14, 16, 29], the SOM regime and thermocapillary regime, which have a relatively higher energy input, exhibit a better polishing capability than the SSM regime and the capillary regime. However, the SOM and thermocapillary regimes can also bring some drawbacks. The polishing process in the SOM and thermocapillary regimes may eliminate or distort some desired surface microstructures or micro-feature geometries. And the material bulging phenomenon is usually resulted in along the polishing tracks [14, 29]. In the study by Nusser et al. [30], the polishing-induced bulge was identified as one of five possible material-/process-induced surface structures in laser macro polishing processes, which are ripples, undercuts, bulges, step structures and martensite needles. And they may have some impacts on the final polished surface finish. However, it has not been reported of any specific studies on the bulge structures produced by laser polished tracks so far. Therefore, we hope in this work to conduct an experimental study on the bulging phenomenon in the laser macro polishing processes under the SOM regime.

In the research of this paper, the experimental study of the bulge structures in the laser macro polishing processes was conducted on the Ti-6Al-4V alloy substrates which is an important material in the aviation manufacturing. First the bulge structure on a single polishing track is examined, and parametric studies were then carried out to study the influence of laser processing parameters on the bulges structures. The possible reasons of the formation of bulge were analyzed. Furthermore, the reduction and elimination of bulge structure by LP tracks overlapping was studied.

2. EXPERIMENTAL PROCEDURE

2.1. MATERIAL AND EXPERIMENTAL SETUP

The Ti-6Al-4V alloy substrates of the thickness 5 mm were provided in this study.

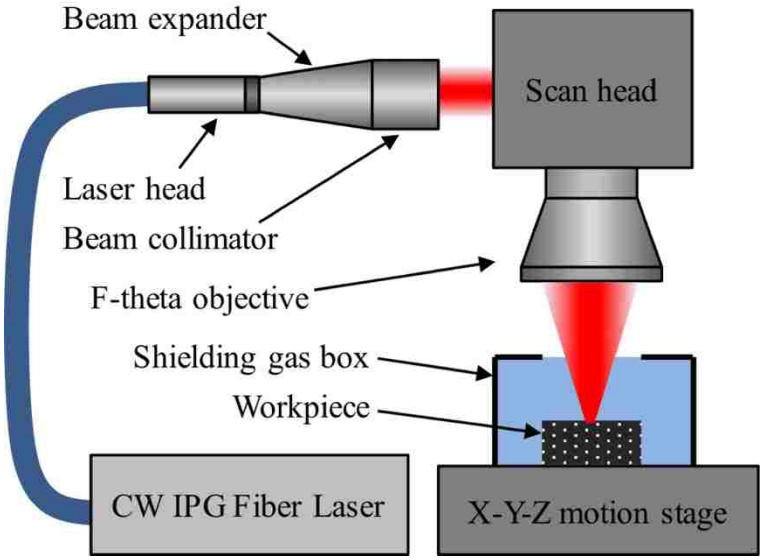

Figure 2.1. The experimental setup for the laser macro polishing study

The basic experimental setup is illustrated in Figure 2.1. The laser applied is a 1070-nm 1000-W continuous wave (CW) fiber laser (IPG Lasers, Model: YLR-1000-MM-WC-T11). The CW laser beam is directed into a scan head (ScanLab, HurryScan 30 mm) allowing for high-speed two-dimensional scanning, and focused by an F-theta lens with a focal length of 300 mm. The workpiece is put in a shielding gas chamber filled with argon gas flow, which has a top opening for the incoming laser beam and is fixed on an X-Y-Z motion stage (Aerotech, Model: ATS 10060-H-M-80P-NC), which provides a motion resolution of 1 μm in the X and Y directions and a 0.1 μm resolution in the Z direction.

The sample surface topographies before and after the polishing process were measured with a Wyko NT9100 white light interferometer having a 1 nm height measurement resolution in the VSI mode.

2.2. RESEARCH METHODOLOGY AND PROCEDURE

Prior to the laser polishing experiments, the prepared Ti-6Al-4V substrates were mechanically polished by a sand paper, with a resulted surface roughness of 0.1 μm in *R*a. As stated in Ref [30], the final surface roughness after laser polishing does not only contain the remains of the initial surface roughness, but also contains new roughness induced by the laser polishing process. Since the subject of this research is the bulge structures formed during the laser macro polishing processes, the influence of the initial surface condition on the final surface finish should be reduced to a minimum level.

The experimental study of the bulge phenomenon in laser polishing processes comprises two major steps: single-line polishing tests and the overlapped multi-line polishing tests. The objective of single-line polishing tests is to analyze the influences of laser polishing parameters on the bulge structures, and the parametric-studied polishing parameters includes the laser power, the laser scan speed and the focal offset distance. Here the adjustment of the focal offset distance corresponds to the change of the laser beam diameter, which is shown in Figure 2.2 as a function of the focal offset distance, where the focal offset of zeros means the location of focal plane, the focal offset of negative values means the location inside the focal length and the positive values correspond to the location outside the focal length.

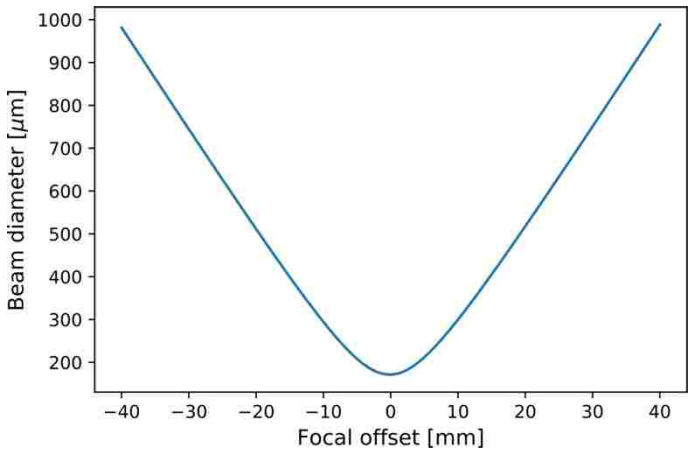

Figure 2.2. The relation between the laser beam diameter and the focal offset

These three parameters work together to influence the induced bulge structure. However, the parametric study in this step is carried out based on the way of the change of one-factor-at-a-time. In the experiment, a baseline of laser polishing parameter was set as the laser power of 400 W, the scan speed of 200 mm/s, and the focal offset distance of 20 mm. When one parameter is studied the other two parameters keep as the base values. In detail, the studied values of the three parameters are listed in Table 2.1. And the laser beam diameters corresponding to the listed focal offsets are 195, 256, 335, 421, 511, 604, 697 and 791 μm, respectively.

Table 2.1. The parameter values of the laser power, scan speed and focal offset in the single-line polishing tests

Studied parameters	**Parameter values**
Laser power (W)	150, 200, 250, 300, 350, 400, 450, 500
Scan speed (mm/s)	100, 200, 300, 400, 500, 600, 700, 800
Focal offset (mm)	4, 8, 12, 16, 20, 24, 28, 32

After the single-line polishing tests, the samples were examined and measured with an optical microscope and optical profiler. Then the samples were sectioned, polished, and etched, and the etched cross-section of samples were examined under the optical microscope.

In the second step of overlapped multi-line polishing tests, the polishing process was carried out line by line successively and the polishing tracks have certain extent of overlap. The studied parameter in this step is the successive displacement of polished tracks, and the displacement in this study are 180, 120, 60 and 30 μm, respectively. The influence of the polished track displacement on the bulge structures and the final surface roughness was analyzed in both the real and spectral spaces.

3. RESULTS AND DISCUSSION

3.1. BULGE STRUCTURE ALONG SINGLE-LINE LP TRACK

Figure 3.1 shows the experiment results for one test of the parametric study, where the laser polishing parameters are the laser power of 400 W, the scan speed of 200 mm/s and the focal offset distance of 20 mm. Figure 3.1a shows the top surface of the polished track, where the width of polished track was measured as 466 μm, smaller than the beam diameter 511 μm there. The 3D surface topography of the polished track is presented as Figure 3.1b, where a uniform bulge ridge was formed along the center of the polished track, and two grooves formed near the fringe of the track. An obvious conclusion could be drawn here that the mass transport from the edge to the center of track during the polishing process contributes to the formation of the bulge phenomenon in the laser macro polishing process on Ti-6Al-4V alloy. Since the topography is generally uniform along the polished track, an averaged transverse surface profile of the polished track is calculated from the 3D topography, and shown in Figure 3.1d. In this way, the potential plastic deformation due to thermal stress [30] along the outside of the polished track can be captured conveniently. From the profile near the location of x = 0.2 and 0.75 mm in Figure 3.1d, the plastic deformation due to thermal stress is not significant here, and its influence on the process-induced surface roughness is much less than that of bulge structure. Besides, the peak-to-valley height of the bulge structure can be measured as 13.6 μm from Figure 3.1d. The transverse cross-section of the polished track is presented in Figure 3.1c, from which the melted layer depth can be measured as 71 μm in this test.

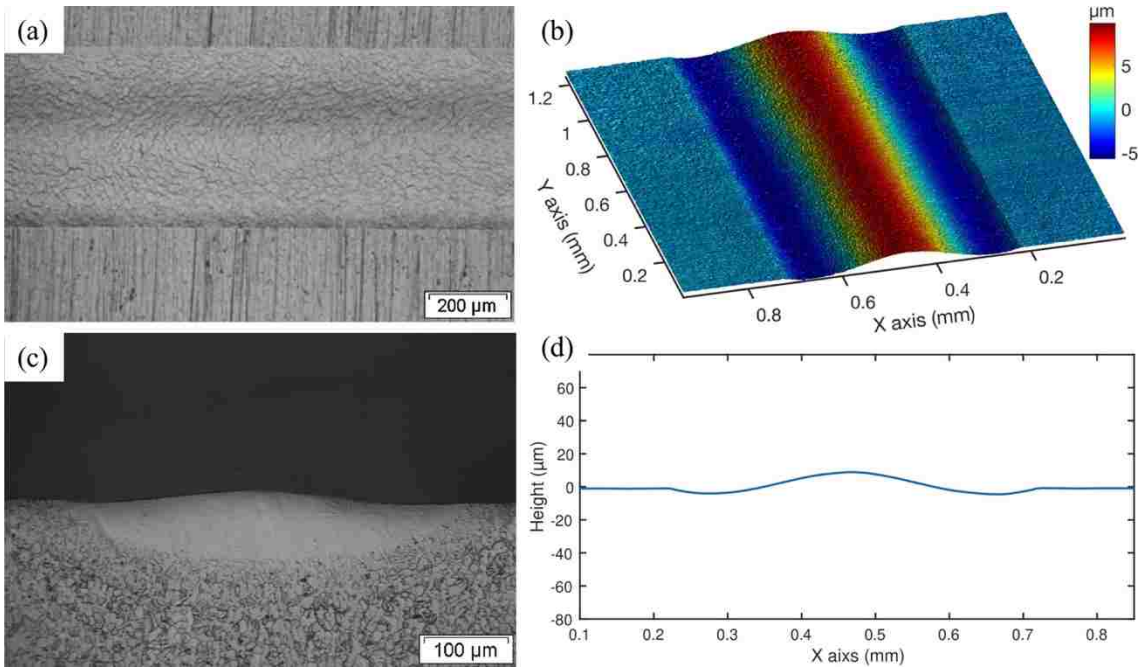

Figure 3.1. (a) The microscopic image of top surface, (b) surface topography, (c) microscopic image of cross-section, and (d) the averaged surface profile in the transverse direction of the polishing track, produced with the processing parameters of the laser power of 400 W, the scan speed of 200 mm/s and the focal offset of 20 mm

In addition to the bulge structure, there also presents finer micro structures over the polished track, and shown in Figure 3.2 is an enlarged view of the morphology at the center of polished track of Figure 3.1b. The formation of the fine micro structures could be caused by the phase transformation and crystallization during the solidifying process of the melted material. And the surface roughness of the micro structure was measure as 0.34 µm in R_a for this test.

For the parametric study of single-line laser polishing tests, the studied parameters are the laser power, the scan speed and the focal offset, respectively. The analyzed features of the polished tracks are the polished track width, the melted layer depth, the amplitude of bulge structure and the relative volume expansion of the polished tracks,

respectively. The polished track width and melted layer depth can be measured from the microscopic images of the top surface and cross-section of polished tracks (e.g. Figure 3.1a and 3.1b). The amplitude of bulge structure, defined as the peak-to-valley height of bulge, can be calculated from the averaged transverse surface profile (e.g. Figure 3.1d). The relative volume expansion is defined as the absolute volume expansion divided by the volume of melted zone. Since the surface topographies are uniform along the polished tracks, the absolute volume expansion can be calculated as the area increment from the averaged transverse profile (e.g. Figure 3.1d) compared with the originally flat profile, and the volume of melted zone thus can be calculated as the area of the cross-section of the melted zone (e.g. Figure 3.1c).

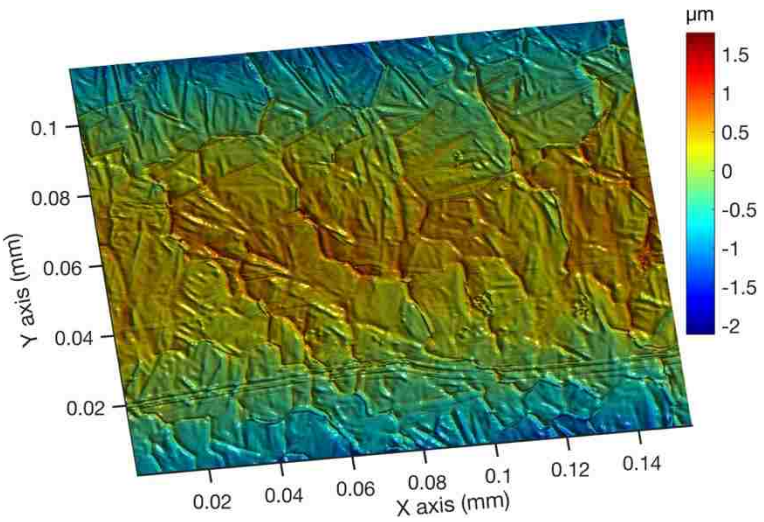

Figure 3.2. The surface microstructure covering the polishing track produced by the crystallization of re-solidified material

Figure 3.3 presents the parametric study results about the polished track width. The three x axes represent the three laser processing parameters and relate to the three curves respectively. It is obvious that the polished track width increases with the laser

power and decreases with the scan speed. The melting threshold of material basically relates to the energy density absorbed which is defined as the laser power divided by the scan speed and the beam diameter [29]. For the parametric study of the beam focal offset, the polished track width increases to a maximum at the focal offset of 20 mm, but decreases as the focal offset increase further. Here the absolute value of focal offset is proportional to the beam diameter, as shown in Figure 2.2. The laser intensity conforms to a Gaussian distribution. When the beam size expands to a certain extent, the energy density near the edge of the track would not be sufficient to melt the material. In this parametric study of focal offset, the maximum polished width of 466 μm was achieved by the beam focal offset of 20 mm.

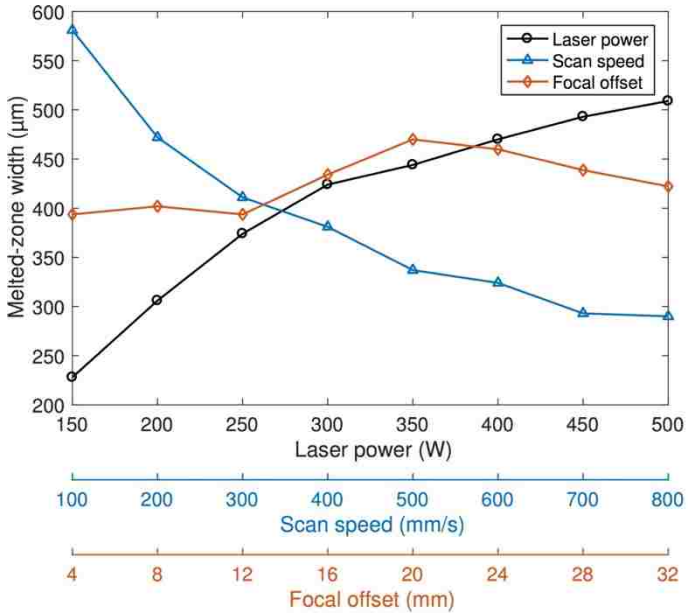

Figure 3.3. The parametric study results of the polished-track widths by different laser powers, scan speeds and foal offsets

Figure 3.4 shows the parametric study results about the melted zone depths of the polished tracks. It is remarkable that the melted zone depths for the focal offsets of 4 mm

and 8 mm are significantly greater than other parameters. For these two tests, the sample surface is close to the focal plane of laser beam, and the laser melting process works in the keyhole penetration mode [31]. However, for other tests, the laser melting process works in the conduction mode [31]. When a laser melting process works in the keyhole penetration mode, the laser energy absorptivity is significantly higher than those in the conduction mode, so the melted depth and volume can be much greater than those in the conduction mode. The conduction melting mode is desired in the laser macro polishing process, because the vapor recoil pressure in the keyhole mode has some negative effects on the roughness smoothing process, and such deep melted layer is not necessary in the polishing process. For the trends of melted depth, it decreases with the scan speed and focal offset but increases with the laser power, which indicates that the melted depth is basically proportional to the absorbed laser energy density.

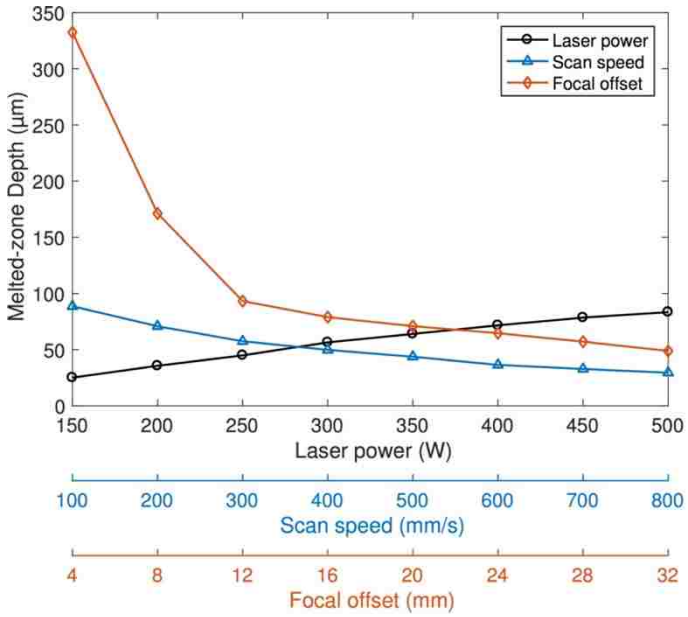

Figure 3.4. The parametric study results of the polished-track depths by different laser powers, scan speeds and focal offsets

Figure 3.5 presents the parametric study results about the bulge amplitude of the polished tracks. The bulge amplitude is almost linearly proportional to the laser power, which is as expected because the laser energy absorbed linearly increases with the laser power. For the parametric study of scan speed, the laser energy absorbed is proportional to the reciprocal of the scan speed, but the amplitude changing with scan speed values is not as steep as expected. For example, the energy input of the scan speed 100 mm/s is two times of that of the scan speed 200 mm/s, but the amplitude of 100 mm/s is only slightly higher than that of 200 mm/s. This should relate to the solidification time of melting pool. As analyzed earlier, the fluid flow in the melting pool has an important influence on the bulge formation. So, a long solidification time (i.e. a slow scan speed) facilitates the fluid flow to reduce the bulge amplitude. However, it should also note that the slow scan speed is not good for the melting efficiency of laser energy [32]. For the parametric study of beam focal offset, the tests of the 4-mm and 8-mm focal offsets, the laser melting process works in the keyhole penetration mode, and the resulted bulge amplitudes are significantly higher than other values. For the focal offset changing from 12 mm to 32 mm, the bulge amplitude gradually decreases.

From the transverse surface profile of the polished track in Figure 3.1d, there seems a volume increment of material after the laser polishing process. Hence, the parametric study results about the relative volume expansion of polishing tracks is presented in Fig 3.6, where the relative volume expansion is calculated with the absolute volume increment divided by the total melted zone size. It is counterintuitive that the relative volume expansion decreases as the laser power increases. For the focal offset varying from 12 mm to 32 mm, where the melting process operates in the conduction

mode, the relative volume expansion increases with the focal offset distance counterintuitively. As for the parametric study of scan speed, the relative volume expansion increases as the scan speed changes from 100 mm/s to 400 mm/s, and it then keeps basically stable but have a slight decrease as the scan speed increases further.

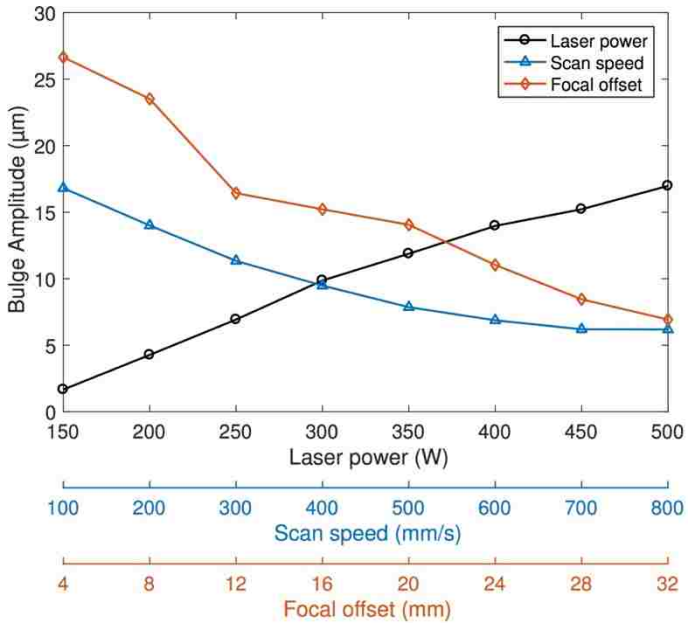

Figure 3.5. The parametric study results of the bulge-structure amplitudes by different laser powers, scan speeds, and focal offsets

The volume expansion phenomenon mainly relates to the phase transition during the re-solidification process, which could occur in both the melted zone and heat-affected zone (HAZ). For a transforming steel, the formation of martensitic microstructure due to the high cooling rate can result in the volume expansion of the laser heated region [31], because the different microstructures have different densities, and, for instance, the maximum density difference between pearlite and martensite is about 4 percent [30]. For the Ti-6Al-4V alloy, laser surface melting leads to an increased volume fraction of acicular martensite (α phase) and a decreased volume fraction of the β phase in the

microstructure [33]. And the phase transformation of the β phase to α+β phase starts at 950 °C and finishes at 870 °C [38], and the density of the β phase is higher than that of the α+β phase [39]. So, the volume expansion in our experimental study should be caused by the phase transition in Ti-6Al-4V alloy. The possible reason for the decreased relative volume expansion by the increasing energy input, could be that the volume expansion is mainly contributed by the phase transition in HAZ, and the HAZ size increases slower than the melted zone size as the input laser energy input increases. The abnormal value of the relative volume expansion at the focal offset 4 mm could be due to the different melting mode, where the melted zone is narrow and deep in contrast to the shallow and wide melted zone in the conduction mode. For the slightly decreasing of the relative volume expansion as the scan speed changes from 400 to 800 mm/s, the possible reason could be that the melting efficiency [32] increases with the scan speed, that is the melted zone size decreases slower than the heat-affected zone.

Generally, there are three possible reasons for the bulge formation: the mass transport during laser polishing process, the phase transition during material re-solidification, and the plastic deformation by the thermal strain. Through the above analysis, the main reasons for the bulge formation in the laser polishing Ti-6Al-4V alloy process should be the mass transport and phase transition.

3.2. BULGE STRUCTURE REDUCTION AND ELIMINATION BY LP TRACK OVERLAPPING

In the most experimental studies [34-37] of laser polishing processes, the overlapping of melted tracks is necessary. Hafiz et al. [16] studied the influence of the overlap between melted tracks on the final polished surface quality, using four different

overlap percentages of 80%, 90%, 95% and 97.5%. It was found that the parameter of overlap has a significant effect over the final surface quality, and the optimal value of overlap percentage was 95% with the combination of other processing parameters in their cases. Nusser et al. [30] demonstrated that the overlapping operation can effectively reduce or eliminate the polishing process induced surface structures of ripples, undercuts and bulges. Therefore, in this part, a parametric study is carried out to analyze the influence of track overlap on bulge structures and the final surface quality.

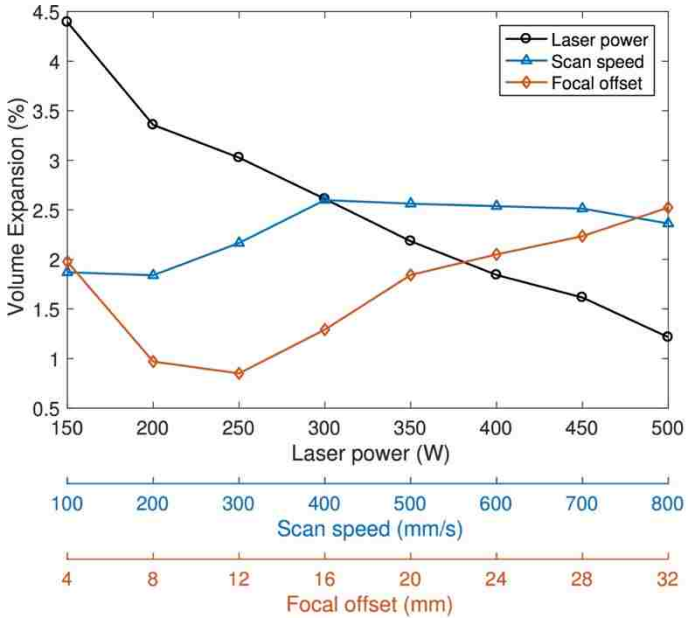

Figure 3.6. The parametric study results of the relative volume-expansions of polishing tracks by different laser powers, scan speeds, and focal offsets

Shown in Figure 3.7 are the microscopic photos of the surfaces of overlapped polished tracks with four different displacements between successive polished tracks, which are 180 µm, 120 µm, 60 µm and 30 µm, corresponding to Figure 3.7a, 3.7b, 3.7c and 3.7d, respectively. Note the displacement of polished tracks is used here instead of

the overlap percentage, but they have a simple relation that the overlap percentage equals the width of polished track subtracting the displacement and then divided by the width of track. Other processing parameters are the laser power of 400 W, the scan speed of 200 mm/s and the focal offset of 20 mm, same for all tests of different track displacements. The resulted single-line polished track width is 466 μm, and the bulge amplitude is 13.6 μm for the single-line track. From the four microscopic images, the periodic ridges of overlapped bulges rapidly get less and less significant as the polished track displacement decreases, and for the test of the 30-μm displacement, the ridge structures almost disappear from the surface. However, the finer surface structure covering the tracks looks clearer and clearer as the track displacement decreases, which could relate to the increased remelting times.

Figure 3.8 presents the measured surface topographies for the track displacements of 180 μm, 120 μm, 60 μm and 30 μm, respectively. And the surface roughnesses of the overlapped polished tracks were measured as 2.11 μm, 1.17 μm, 0.585 μm and 0.650 μm in *R*a, respectively, for the four different displacements. It is obvious that the ridge amplitude by the overlapped bulges is effectively suppressed as the polished track displacement gets smaller, and the ridge structures nearly disappear for the track displacement of 30 μm in Figure 3.8d. From the microscopic images and measured topographies in Figure 3.7 and Figure 3.8, there mainly exists two kinds of asperities on the surface of overlapped polished tracks, one is the periodic ridge structure in the transverse direction of the polished tracks, and the other is the solidification-induced fine surface structure which is isotropic and uniform. Besides, the bulge amplitude of the final overlapped track increases as the polished track displacement decreases, which could be

due to the increased energy input, i.e. the increased remelting times. In the practical applications, the final overlapped bulge structure may be removed at the boundary of polished surface.

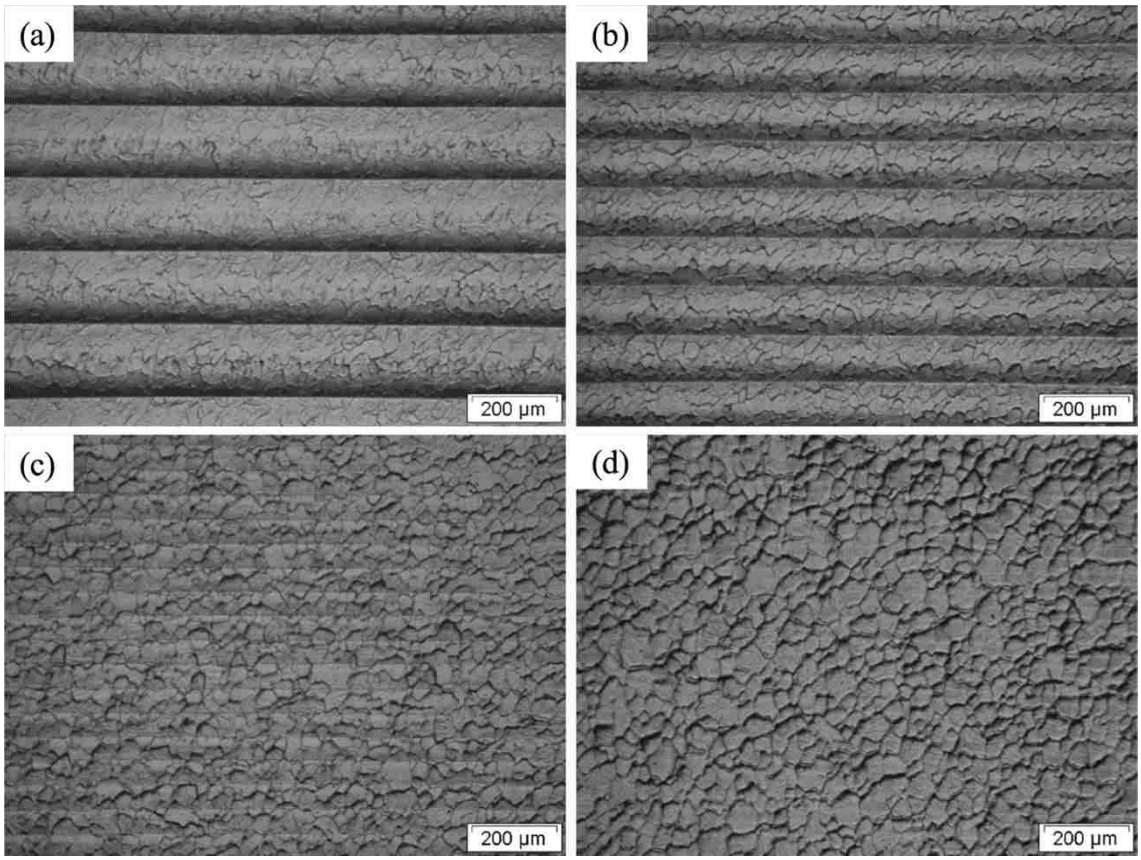

Figure 3.7. The top surfaces of overlapped polishing tracks with the successive track displacements of (a) 180 μm, (b) 120 μm, (c) 60 μm and (d) 30 μm

Additionally, the indentation of polished surface of the first few tracks, for the small displacement cases, can be observed. For instance, Figure 3.9 presents the Y-direction-averaged linear surface profile for the case of track displacement of 60 μm. The first few tracks have an indentation of around 1.7 μm, but the indentation gradually disappear subsequently. This kind of indentation should be caused by the mass transport

of polished track, i.e. the formation of grooves at the edge of polished track, which cause the surface material moves a little bit in the X-axis direction.

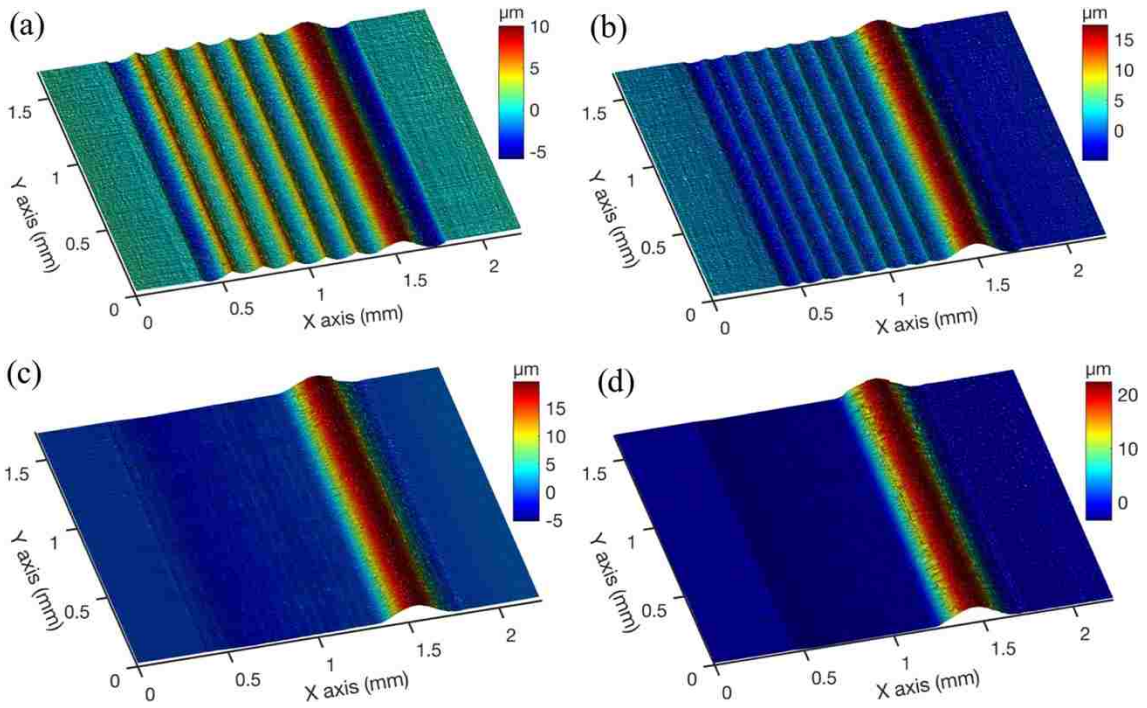

Figure 3.8. The topographies of overlapped polishing tracks with the successive track displacements of 180 μm, 120 μm, 60 μm and 30 μm

Based on the above analysis, the linear roughness in the transverse direction of overlapped polished tracks should be dominated by the asperities of the periodic ridges of overlapped bulges and the fine solidification-induced surface structures, while the linear roughness along the parallel direction of polished tracks should be determined mainly by the fine solidification-induced structures.

In order to further analyze the effects of two kinds of asperities on the final surface, the spatial frequency spectra of the linear surface profiles in the two directions were calculated from the surface topography measurements and presented in Figure 3.10. With the spatial frequency spectrum, the contributions to the final surface roughness from the

periodic ridges and the irregular solidification-induced structures can be conveniently differentiated, since the spatial frequency features of them are very different. The spectrum for the periodic ridges should be featured as the harmonic peaks with the frequencies equal to the multiples of the reciprocal of the ridge period, while the spectrum of the solidification-induced structures should be featured smoother than that of periodic ridges because its spatial profile looks like noise. Note the spatial spectra presented is actually the average of the spectra of all parallel liner profile in one direction. Figure 3.10a shows the spatial spectrum in the transverse direction for the four track-displacements of 180, 120, 60 and 30 μm. For the track displacement of 180 μm, the first harmonic peak occurs at f = 5.55 [1/mm] and the amplitudes of the second, third and fourth harmonic peaks decreases very rapidly. Note these harmonic peaks represents the periodic ridges. For the displacement of 120 μm, the first harmonic peak occurs at f = 8.33 [1/mm]; for the displacement of 60 μm the first harmonic peak is at f = 16.7 [1/mm]; for the displacement of 30 μm the first harmonic peak is at f = 33.3 [1/mm], the amplitude of which is very small. As the displacement decreases the first harmonic peak amplitude decreases very rapidly, which indicates that the overlapping process can effectively suppress the bulge structure. However, there exist the similar base components of spatial spectra for all four displacements, contributed by the asperities of solidification-induced surface structures, the amplitudes of which do not decrease as the displacement decreases. Figure 3.10b shows the spatial spectra in the parallel direction for the four different track displacements. The amplitudes in this direction is generally much smaller than that in the perpendicular direction, where the Y-axis range is one tenth of that of Figure 3.10a. There are no harmonic peaks presented, and the overall shapes of four spectra are similar, which

confirms the dominant asperity of solidification-induced fine surface structures. And the overall amplitudes of spatial spectra increase as the track displacement decreases, which confirms that the solidification-induced surface structures are more and more significant with the decreased displacement, or the increased remelting times.

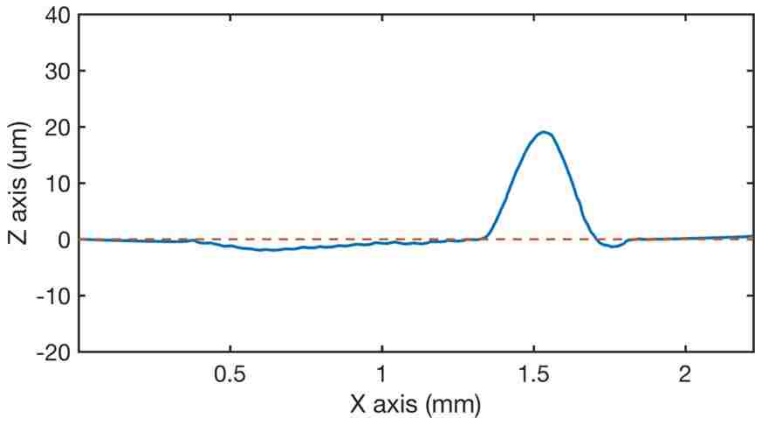

Figure 3.9. The linear surface profile of polished surface for the case of track displacement of 60 μm, averaged in the Y direction

Furthermore, for the polished track displacement of 30 μm, the linear spatial spectra in the transverse and parallel directions are compared in Figure 3.11. It is obvious that the base spectral component distribution of the two directions, caused by the fine solidification-induced surface structures, are almost the same, which confirms that the asperities of solidification-induced surface structures are isotropic. For the linear spectrum of the transverse direction, the harmonic peak component occurring at f = 33 [1/mm], caused by the ridges of overlapped bulges, is much less significant than the base component, that is, the periodic ridge asperities turn into the minor component of surface roughness when the displacement of polished tracks reduces to a certain value. And, combined with the conclusion drawn from Figure 3.10b, this explains why the overall

surface roughness of polished surfaces increased from 0.585 µm to 0.650 µm in *R*a when the polished-track displacement decreased from 60 µm to 30 µm.

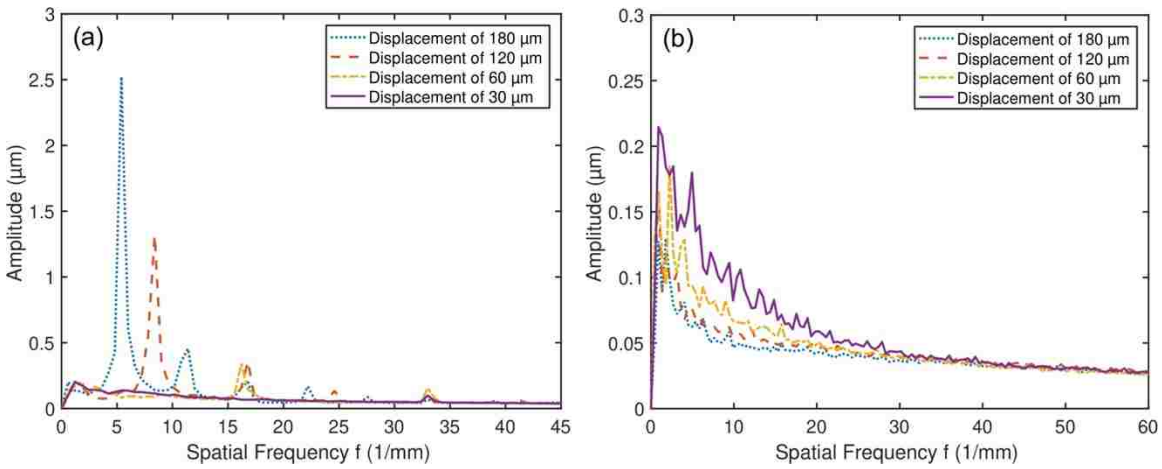

Figure 3.10. The spatial frequency spectra of overlapped polishing tracks with the displacements of 180, 120, 60 and 30 µm, in the (a) parallel and (b) perpendicular directions to the polished tracks

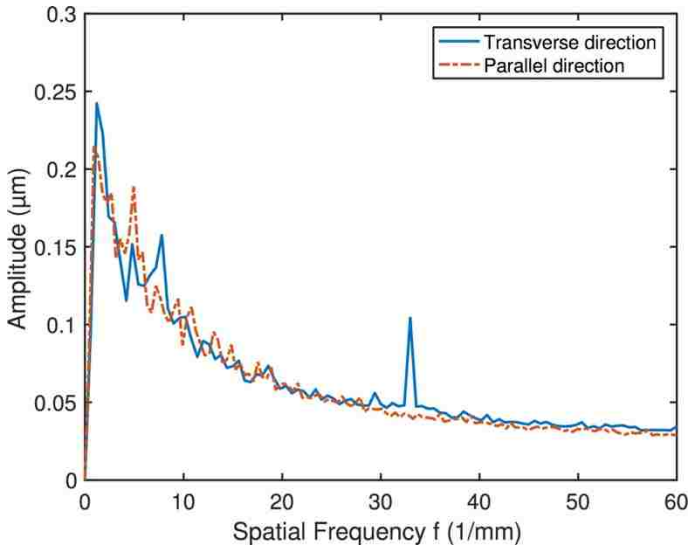

Figure 3.11. The spatial frequency spectra in the parallel and perpendicular directions of the overlapped polishing tracks with the successive track displacement of 30 µm

4. CONCLUSION

A fundamental experimental study about the bulge structure generated by laser polished tracks on Ti-6Al-4V alloy slabs was carried out in this paper. And the main focus is on the influences of different laser polishing parameters on the bulge structure, including the laser power, beam scan speed, beam focal offset and the polished track displacement during the track overlapping process. The experimental study contains two parts: the single-line laser polishing tests and the overlapped multi-lines laser polishing tests.

Through the experiments of the laser polishing processes of single-line track and multi-lines overlapped tracks, it is found that the effect of the single polishing track is mainly redistributing material in the direction along the track, and the effect of the overlapping of tracks is mainly redistributing material in the transverse direction of polished tracks, where the moving final polished track acts like a buffer zone for asperities. The single-line polished track could create the asperities of bulge structure in the transverse direction of the track, but the track overlapping process could effectively reduce the created bulge structures.

Through the parametric study of single-line laser polishing track, the formation of bulge structure should be mainly due to the phase transition of material in the heat affected zone and the mass transportation caused by the fluid convection in the melting pool. The increasing of laser power causes the increasing of the width and depth of polished tracks and the amplitude of bulges, but causes the decreasing of relative volume expansion, which should be due to that the volume expansion mainly occurring in the heat affected zone, and the heat affected zone increases slower than the melted zone. The

increasing of scan speed causes the decreasing of the width and depth of polished tracks and the amplitude of bulges, and it causes the increasing of relative volume expansion for the speed changing from 100 to 400 mm/s, but a slightly decreasing for the speed from 400 to 800 mm/s, because of the increased melting efficiency with the increasing scan speed. For the focal offset of 4 and 8 mm, the laser melting process works in the keyhole penetration mode, and for the focal offset from 12 to 32 mm, the polishing process works in the conduction mode. The polished track width achieves a maximum value at the focal offset of 20 mm in the experiment condition. For the focal offsets in conduction mode, the melted layer depth and bulge amplitude decreases as the focal offset increases, and the relative volume expansion increases with the increasing offset values.

Through the parametric study of multi-line overlapped polishing tracks, accompanied with the spectral analysis of linear profiles, the successive track displacement has a significant effect on the amplitude of the periodic ridges by the overlapped bulges. The ridge amplitude decreases rapidly with the decreasing track displacement. However, the overlapping process, which increases the melting times of material, increases the asperities amplitude of the fine solidification-induced surface structure. Therefore, there exists a lower limit of surface roughness for the overlapping process to reduce the bulge structure produced by the single polished track. The knowledge generated in this study would lay an experimental basis to develop advanced laser polishing technology for a variety of practical industrial applications. And the influence of the initial roughness on the bulge structure, in the practical applications, could need some further studies.

ACKNOWLEDGMENTS

The authors gratefully acknowledge the financial support from the Department of Energy (Grant No. DE-FE0012272).

BIBLIOGRAPHY

[1] Gibson I, Rosen DW, Stucker B. Additive manufacturing technologies. Springer; 2010.

[2] Chen C, Shen YY, Tsai HL. A foil-based additive manufacturing technology for metal parts. J Manuf Sci E-T ASME 2017;139:024501-6.

[3] Wong KV, Hernandez A. A review of additive manufacturing. ISRN Mech Eng 2012;2012:1-10.

[4] Ramos-Grez JA, Bourell DL. Reducing surface roughness of metallic freeform-fabricated parts using non-tactile finishing methods. Int J Mater Prod Tec 2004;21:297-316.

[5] Abele E, Kniepkamp M. Analysis and optimisation of vertical surface roughness in micro selective laser melting. Surf Topogr Metrol Prop 2015;3:034007-1-8.

[6] Calignano F, Manfredi D, Ambrosio EP, Iuliano L, Fino P. Influence of process parameters on surface roughness of aluminum parts produced by DMLS. Int J Adv Manuf Tech 2013;67:2743-51.

[7] Temmler A, Willenborg E, Wissenbach K. Laser polishing. Proc SPIE 2012;8243:82430W-W-13.

[8] Poprawe R. Tailored light. Springer; 2012.

[9] Lamikiz A, Sanchez JA, Lopez de Lacalle LN, Arana JL. Laser polishing of parts built up by selective laser sintering. Int J Mach Tool Manu 2007;47:2040-50.

[10] Perry TL, Werschmoeller D, Li X, Pfefferkorn FE, Duffie NA. Pulsed laser polishing of micro-milled Ti6Al4V samples. J Manuf Process 2009;11:74-81.

[11] Dadbakhsh S, Hao L, Kong CY. Surface finish improvement of LMD samples using laser polishing. Virtual Phys Prototyp 2010;5:215-21.

[12] Chow, M.T.C., et al. Experimental statistical analysis of laser micropolishing process. Proceedings of the ISOT 2010 International Symposium on Optomechatronic Technologies, Toronto, Ontario, Canada, Paper No. LPTI-1, 6p.

[13] Saleh AF, Abboud JH, Benyounis KY. Surface carburizing of Ti–6Al–4V alloy by laser melting. Opt Laser Eng 2010;48:257-67.

[14] Ukar E, Lamikiz A, López de Lacalle LN, del Pozo D, Arana JL. Laser polishing of tool steel with CO2 laser and high-power diode laser. Int J Mach Tool Manu 2010;50:115-25.

[15] Gisario A, Boschetto A, Veniali F. Surface transformation of AISI 304 stainless steel by high power diode laser. Opt Laser Eng 2011;49:41-51.

[16] Hafiz AMK, Bordatchev EV, Tutunea-Fatan RO. Influence of overlap between the laser beam tracks on surface quality in laser polishing of AISI H13 tool steel. J Manuf Process 2012;14:425-34.

[17] Bordatchev EV, Hafiz AMK, Tutunea-Fatan OR. Performance of laser polishing in finishing of metallic surfaces. Int J Adv Manuf Tech 2014;73:35-52.

[18] Hafiz AMK, Bordatchev EV, Tutunea-Fatan RO. Experimental analysis of applicability of a picosecond laser for micro-polishing of micromilled Inconel 718 superalloy. Int J Adv Manuf Tech 2014;70:1963-78.

[19] Heidrich S, Richmann A, Schmitz P, Willenborg E, Wissenbach K, Loosen P, Poprawe R. Optics manufacturing by laser radiation. Opt Laser Eng 2014;59:34-40.

[20] Ma C, Vadali M, Li X, Duffie NA, Pfefferkorn FE. Analytical and experimental investigation of thermocapillary flow in pulsed laser micropolishing. J Micro Nano-Manuf 2014;2:021010-1-8.

[21] Rosa B, Hascoet JY, Mognol P. Topography modeling of laser polishing on AISI 316L milled surfaces. Mech Ind 2014;15:51-61.

[22] Ukar E, Lamikiz A, Martinez S, Tabernero I. Polishing of ductile cast iron with scan-head guided fiber laser. Mater Sci Forum 2014;797:151-6.

[23] Rosa B, Mognol P, Hascoet JY. Laser polishing of additive laser manufacturing surfaces. J Laser Appl 2015;27:S29102-1-7.

[24] Ukar E, Lamikiz A, Liébana F, Martínez S, Tabernero I. An industrial approach of laser polishing with different laser sources. Materialwiss Werkst 2015;46:661-7.

[25] Rosa B, Mognol P, Hascoet JY. Modelling and optimization of laser polishing of additive laser manufacturing surfaces. Rapid Prototyping J 2016;22:956-64.

[26] Ma CP, Guan YC, Zhou W. Laser polishing of additive manufactured Ti alloys. Opt Laser Eng 2017;93:171-7.

[27] Vadali M, Ma C, Duffie NA, Li X, Pfefferkorn FE. Pulsed laser micro polishing: Surface prediction model. J Manuf Process 2012;14:307-15.

[28] Pfefferkorn FE, Duffie NA, Li X, Vadali M, Ma C. Improving surface finish in pulsed laser micro polishing using thermocapillary flow. Cirp Ann-Manuf Techn 2013;62:203-6.

[29] Chow MTC, Bordatchev EV, Knopf GK. Experimental study on the effect of varying focal offset distance on laser micropolished surfaces. Int J Adv Manuf Tech 2013;67:2607-2617.

[30] Nusser C, Kumstel J, Kiedrowski T, Diatlov A, Willenborg E. Process- and material-induced surface structures during laser polishing. Adv Eng Mater 2015;17:268-277.

[31] Steen WM, Mazumder J. Laser surface treatment. In: Laser material processing, London: Springer; 2010, p. 295-348.

[32] Steen WM, Mazumder J. Laser cutting, drilling and piercing. In: Laser material processing, London: Springer; 2010, p. 131-198.

[33] Biswas A, Li L, Maity TK, Chatterjee UK, Mordike BL, Manna I, Dutta MJ. Laser surface treatment of Ti-6Al-4V for bio-implant application. Laser Eng 2007;17:59-73.

[34] Perry TL, Werschmoeller D, Duffie NA, Li X, Pfefferkorn FE. Examination of selective pulsed laser micropolishing on microfabricated nickel samples using spatial frequency analysis. J Manuf Sci E-T Asme 2009;131:021002-1-9.

[35] Alrbaey K, Wimpenny D, Tosi R, Manning W, Moroz A. On optimization of surface roughness of selective laser melted stainless steel parts: a statistical study. J Mater Eng Perform 2014;23:2139-48.

[36] Pfefferkorn FE, Duffie NA, Morrow JD, Wang Q. Effect of beam diameter on pulsed laser polishing of S7 tool steel. Cirp Ann-Manuf Techn, 2014;63:237-240.

[37] Temmler A, Walochnik MA, Willenborg E, Wissenbach K. Surface structuring by remelting of titanium alloy Ti6Al4V. J Laser Appl 2015;27:S29103-1-8.

[38] Sieniawski J, Ziaja W, Kubiak K, Motyka M. Microstructure and mechanical properties of high strength two-phase titanium alloys. Titanium Alloys-Advances in Properties Control. 2013, InTech.

[39] Pederson R. Microstructure and phase transformation of Ti-6Al-4V. 2002, Luleå tekniska universitet.

SECTION

2. CONCLUSIONS

A foil-based additive manufacturing technology for fabricating metal parts, called Laser Foil Printing (LFP), was proposed and developed in this dissertation. The manufacturing sub-processes comprising the LFP technology were comprehensively studied, which include the laser spot welding of foil, laser raster-scan welding of foil, laser cutting of foil, and laser polishing processes. The fabricated free-form parts were demonstrated and own very good mechanical properties (micro hardness and tensile strength). The post-processing of laser polishing on the side surface of LFP parts was studied. The final side surface roughness could be reduced to 0.72 μm in Sa, for both the vertical side surface (with the initial surface roughness of 4.39 μm) and the 45º-inclined side surface (with the initial roughness of 24.22 μm). And the foil bonding defects on the side surface can be completely repaired in the post-processing of laser polishing. Finally, the bulge structure along polished tracks was noticed in the experiments and studied on Ti-6Al-4V slabs. The spatial spectra analysis shows that the overlapping process of polished tracks can effectively reduce the induced bulge structures.

In the study of the laser spot welding and raster-scan welding processes of foil, the welding process works in the keyhole penetration mode. The role of laser spot welding process is to anchor the fresh foil upon the substrate or un-finished part, and the role of laser rater-scan welding process is to form a full and strong bond between the foils. The cross-section of fabricated parts shows a good bonding quality, with no micro-cracks or pores observed. In the study of the laser cutting process of foil, the role of laser cutting is

to remove the redundant foil in the un-welded regions. The resulted cutting edge is quite clean and accurate, with no burr or thermal distortion. The resulted mechanical properties of the fabricated parts are better than the raw material because of the rapid-cooling process of laser welding.

In the study of the laser polishing process on raster-scan laser weld surface, it is found that the polishing capability is closely related to the polished track width and melted depth. In detail, the polished track width relates to the range of spatial frequency of surface asperities that can be effectively removed, and the melted depth relates to the range of the vertical magnitude of asperities that can be effectively removed. A parametric study shows that the laser power and scan speed have significant effects on the polished track width and depth. In the numerical simulation of laser polishing process, the temperature field and the convection flow in the melting pool were analyzed, and the convection vortices have a significant influence on deepening the depth of polished track.

In the study of post-processing of the side surface of LFP parts, the vertical side surface and the 45º-inclined side surface are processed by laser polishing. The grinding and sine-wave scan paths, which could emulate the large-spot-size and intensity-uniformed laser beams with the disk shape and rectangle shape, show a better polishing performance than the straight-line scan path, with the resulted linear roughness less than 0.5 μm along the track direction. The finally determined polishing procedure, combining the grind-scan polishing process and linear-scan polishing process, results in an areal surface roughness of 0.72 μm for both the vertical and inclined side surfaces. And the foil bonding defects on the side surface can be completely repaired.

In the study of the bulge structure produced by laser macro polished tracks, through the parametric study about the bulge width, melted depth, bulge amplitude and relative volume expansion, the formation of bulge structure should be mainly caused by the mass transport and the phase transition during the polishing process. With the spatial spectra analysis, the overlapping process of polished tracks can effectively reduce the amplitude of bulge structure. When the track displacement decreases to a certain value (e.g. 30 μm), the overlapped bulge structure would become the minor surface asperities than the solidification-induced surface structure.

Currently, the automation work of LFP manufacturing process has not been completed, especially for the removal of redundant foil and the change and fixture of fresh foil. With the future work of procedure automation being done, the actual manufacturing time would be reduced substantially, the foil bonding process in each layer would be more stable and the mechanical properties of fabricated parts would be better.

The laser polishing is a complicated physical process involving heat transfer, thermal fluid, and thermal stress, and the resulted surface finish quality involves a lot of factors, including the initial surface topography, thermal and optical properties of material, laser power, scan speed, beam size, beam shape, scan path trajectory, number of passes, overlap percentage of tracks, etc. The underlying physical processes still have not been studied thoroughly, and a comprehensive numerical model is required, which includes all potential physical processes and could simulate the evolving of surface topography during the polishing process. Furthermore, a good numerical model should be able to approximate the actual polishing process, rather than simulating on a flat surface.

BIBLIOGRAPHY

[1] Wong, K.V. and Hernandez, A., 2012, "A review of additive manufacturing," ISRN Mechanical Engineering, 2012.

[2] Wohlers, T. and Gornet, T., 2014, "History of additive manufacturing," Wohlers Report, 24, pp. 2014.

[3] Huang, S.H., Liu, P., Mokasdar, A., and Hou, L., 2013, "Additive manufacturing and its societal impact: a literature review," The International Journal of Advanced Manufacturing Technology, pp. 1-13.

[4] Frazier, W.E., 2014, "Metal additive manufacturing: a review," Journal of Materials Engineering and Performance, 23(6), pp. 1917-1928.

[5] Gu, D., Laser additive manufacturing of high-performance materials. 2015: Springer.

[6] Palcic, I., Balazic, M., Milfelner, M., and Buchmeister, B., 2009, "Potential of laser engineered net shaping (LENS) technology," Materials and Manufacturing Processes, 24(7-8), pp. 750-753.

[7] Feygin, M., Shkolnik, A., Diamond, M.N., and Dvorskiy, E., Laminated object manufacturing system. 1998, Google Patents.

[8] Yoshino, M., 1998, "Rapid manufacturing system by sheet steel lamination," Proc. CAPE, pp. 265-270.

[9] Himmer, T., Nakagawa, T., and Anzai, M., 1999, "Lamination of metal sheets," Computers in Industry, 39(1), pp. 27-33.

[10] Yamasaki, H., 2000, "Applying laminated die to manufacture automobile part in large size," Die Mould Technol, 15(7), pp. 36-45.

[11] Himmer, T., Techel, A., Nowotny, S., and Beyer, E. “Metal laminated tooling–a quick and flexible tooling concept,” Proceedings of the solid freeform fabrication symposium, Austin, TX. 2004.

[12] Yi, S.P., Liu, F., Zhang, J., and Xiong, S.Q., 2004, "Study of the key technologies of LOM for functional metal parts," Journal of Materials Processing Technology, 150(1-2), pp. 175-181.

[13] George, J. and Stucker, B., 2006, "Fabrication of lightweight structural panels through ultrasonic consolidation," Virtual and Physical Prototyping, 1(4), pp. 227-241.

[14] Friel, R.J. and Harris, R.A., 2013, "Ultrasonic additive manufacturing - A hybrid production process for novel functional products," Proceedings of the Seventeenth Cirp Conference on Electro Physical and Chemical Machining (Isem), 6, pp. 35-40.

[15] Gibson, I., Rosen, D.W., and Stucker, B., Additive manufacturing technologies. Vol. 238. 2010: Springer.

[16] Janaki Ram, G.D., Yang, Y., and Stucker, B.E., 2006, "Effect of process parameters on bond formation during ultrasonic consolidation of aluminum alloy 3003," Journal of Manufacturing Systems, 25(3), pp. 221-238.

[17] Stucker, B. and Gabbita, D., Surface roughness reduction for improving bonding in ultrasonic consolidation rapid manufacturing. 2007, Google Patents.

[18] Svenungsson, J., Choquet, I., and Kaplan, A.F.H., 2015, "Laser welding process – a review of keyhole welding modelling," Physics Procedia, 78, pp. 182-191.

[19] Tokarev, V.N., Wilson, J.I.B., Jubber, M.G., John, P., and Milne, D.K., 1995, "Modeling of self-limiting laser-ablation of rough surfaces - application to the polishing of diamond films," Diamond and Related Materials, 4(3), pp. 169-176.

[20] Kim, Y.G., Ryu, J.K., Kim, D.J., Kim, H.J., Lee, S., Cha, B.H., Cha, H., and Kim, C.J., 2004, "Microroughness reduction of tungsten films by laser polishing technology with a line beam," Japanese Journal of Applied Physics Part 1-Regular Papers Short Notes & Review Papers, 43(4a), pp. 1315-1322.

[21] Mai, T.A. and Lim, G.C., 2004, "Micromelting and its effects on surface topography and properties in laser polishing of stainless steel," Journal of Laser Applications, 16(4), pp. 221-228.

[22] Ramos-Grez, J.A. and Bourell, D.L., 2004, "Reducing surface roughness of metallic freeform-fabricated parts using non-tactile finishing methods," International Journal of Materials & Product Technology, 21(4), pp. 297-316.

[23] Heng, Q., Tao, C., and Zuo, T.C., 2006, "Surface roughness analysis and improvement of micro-fluidic channel with excimer laser," Microfluidics and Nanofluidics, 2(4), pp. 357-360.

[24] Ukar, E., Lamikiz, A., de Lacalle, L.N.L., del Pozo, D., and Arana, J.L., 2010, "Laser polishing of tool steel with CO2 laser and high-power diode laser," International Journal of Machine Tools & Manufacture, 50(1), pp. 115-125.

[25] Temmler, A., Willenborg, E., and Wissenbach, K. Laser polishing. in Proc. SPIE. 2012.

[26] Poprawe, R., Tailored Light. 2012: Springer.

[27] Lamikiz, A., Sanchez, J.A., de Lacalle, L.N.L., and Arana, J.L., 2007, "Laser polishing of parts built up by selective laser sintering," International Journal of Machine Tools & Manufacture, 47(12-13), pp. 2040-2050.

[28] Dadbakhsh, S., Hao, L., and Kong, C.Y., 2010, "Surface finish improvement of LMD samples using laser polishing," Virtual and Physical Prototyping, 5(4), pp. 215-221.

[29] Rosa, B., Mognol, P., and Hascoet, J.Y., 2015, "Laser polishing of additive laser manufacturing surfaces," Journal of Laser Applications, 27.

[30] Yasa, E., Poyraz, O., Solakoglu, E.U., Akbulut, G., and Oren, S., 2016, "A study on the stair stepping effect in direct metal laser sintering of a Nickel-based superalloy," Procedia CIRP, 45, pp. 175-178.

[31] Yasa, E., Deckers, J., and Kruth, J.P., 2011, "The investigation of the influence of laser re-melting on density, surface quality and microstructure of selective laser melting parts," Rapid Prototyping Journal, 17(5), pp. 312-327.

[32] Alfieri, V., Argenio, P., Caiazzo, F., and Sergi, V., 2017, "Reduction of surface roughness by means of laser processing over additive manufacturing metal parts," Materials, 10(1).

[33] Ma, C., Vadali, M., Duffie, N.A., Pfefferkorn, F.E., and Li, X.C., 2013, "Melt pool flow and surface evolution during pulsed laser micro polishing of Ti6Al4V," Journal of Manufacturing Science and Engineering-Transactions of the Asme, 135(6).

[34] Pfefferkorn, F.E., Duffie, N.A., Li, X.C., Vadali, M., and Ma, C., 2013, "Improving surface finish in pulsed laser micro polishing using thermocapillary flow," Cirp Annals-Manufacturing Technology, 62(1), pp. 203-206.

[35] Nusser, C., Kumstel, J., Kiedrowski, T., Diatlov, A., and Willenborg, E., 2015, "Process-and material-induced surface structures during laser polishing," Advanced Engineering Materials, 17(3), pp. 268-277.

VITA

Chen Chen was born in January 1989 in Jiangsu Province China. He received his Bachelor of Engineering degree in Electrical Engineering in 2010 from the Nanjing University of Science and Technology. From 2010 to 2012, he studied in the Science School of Nanjing University of Science and Technology as a graduate student, and worked as a visiting scholar in Missouri University of Science and Technology in 2013. In May 2018, he received his Ph.D. under the direction of Dr. Hai-Lung Tsai in Mechanical Engineering from Missouri University of Science and Technology, Rolla, Missouri, USA.